



WILLIAM & MARY

CHARTERED 1693

W&M ScholarWorks

---

Reports

---

2-2018

## Anthropocene Sea Level Change: A History of Recent Trends Observed in the U.S. East, Gulf, and West Coast Regions

John D. Boon

*Virginia Institute of Marine Science*

Molly Mitchell

*Virginia Institute of Marine Science*

Jon Derek Loftis

*Virginia Institute of Marine Science*

David M. Malmquist

*Virginia Institute of Marine Science*

Follow this and additional works at: <https://scholarworks.wm.edu/reports>

 Part of the Environmental Indicators and Impact Assessment Commons, Environmental Monitoring Commons, and the Oceanography Commons

---

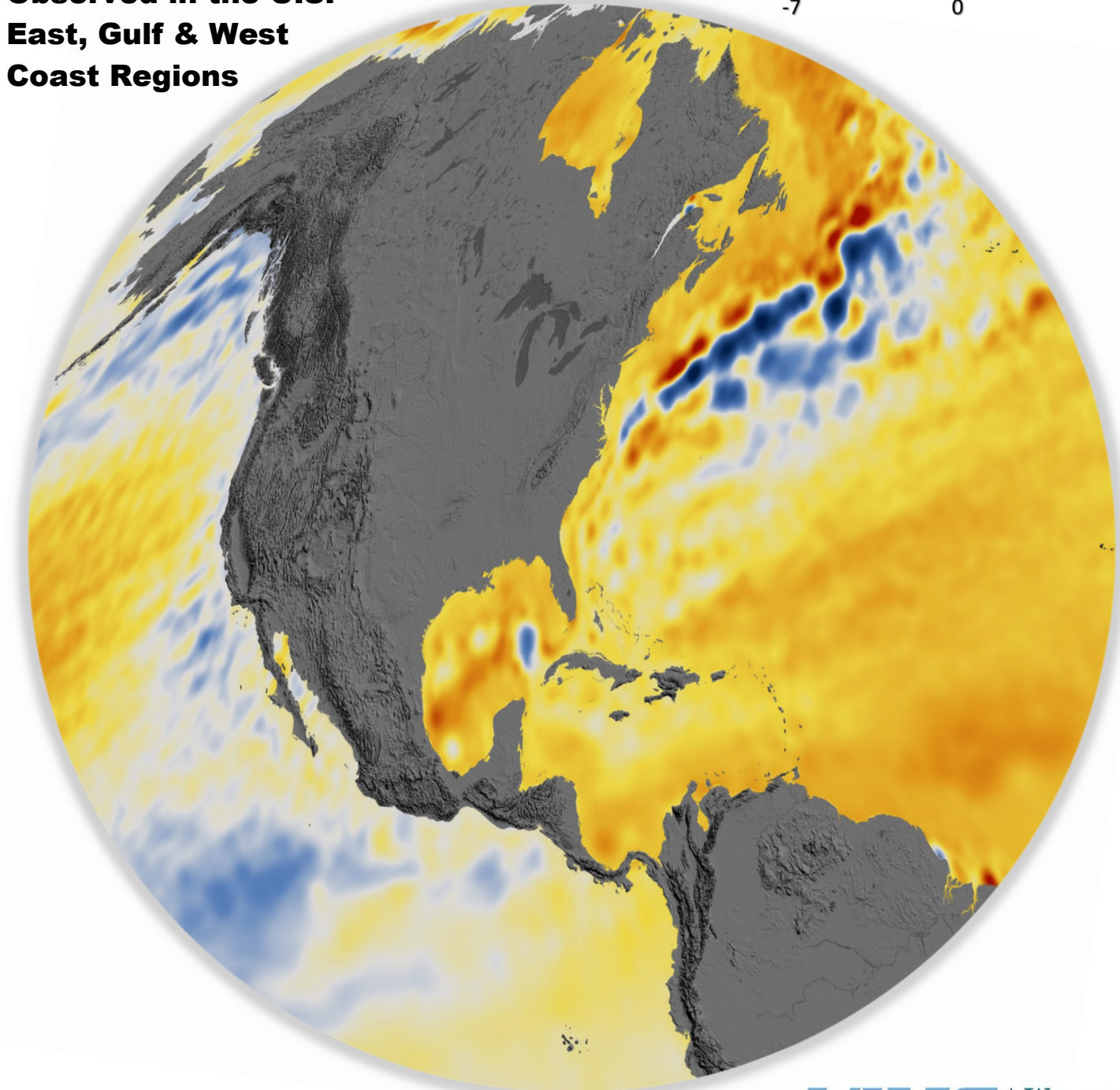
### Recommended Citation

Boon, J. D., Mitchell, M., Loftis, J. D., & Malmquist, D. M. (2018) Anthropocene Sea Level Change: A History of Recent Trends Observed in the U.S. East, Gulf, and West Coast Regions. Special Report in Applied Marine Science and Ocean Engineering (SRAMSOE) No. 467. Virginia Institute of Marine Science, College of William and Mary. <https://doi.org/10.21220/V5T17T>

This Report is brought to you for free and open access by W&M ScholarWorks. It has been accepted for inclusion in Reports by an authorized administrator of W&M ScholarWorks. For more information, please contact [scholarworks@wm.edu](mailto:scholarworks@wm.edu).

# Anthropocene Sea Level Change

**A History of Recent Trends  
Observed in the U.S.  
East, Gulf & West  
Coast Regions**



**John D. Boon**

**Molly Mitchell**

**Jon Derek Loftis**

**David L. Malmquist**

**VIMS** | WILLIAM  
& MARY  
VIRGINIA INSTITUTE OF MARINE SCIENCE

**Special Report No. 467 in Applied  
Marine Science and Ocean Engineering  
March 2018**

Cover graphic depicts satellite-observed changes in sea surface height in centimeters over a 22-year period from 1992 to 2014, featured in: <https://earthobservatory.nasa.gov/IOTD/view.php?id=91746&src=eoaeiotd>. Original satellite data from TOPEX / Poseidon, Jason-1, -2, and -3 missions are featured in an article published in the *Proceedings of the National Academy of Sciences*: R. S. Nerem, B. D. Beckley, J. T. Fasullo, B. D. Hamlington, D. Masters and G. T. Mitchum. *PNAS* 2018 February, 115 (9) 2022-2025.

<https://doi.org/10.1073/pnas.1717312115>.

# ANTHROPOCENE SEA LEVEL CHANGE

A History of Recent Trends Observed in the U.S.  
East, Gulf and West Coast Regions

John D. Boon  
Molly Mitchell  
Jon Derek Loftis  
David L. Malmquist

Special Report No. 467 in  
Applied Marine Science and Ocean Engineering

Virginia Institute of Marine Science  
Gloucester Point, Virginia 23062

John T. Wells  
Director

March 2018

## ANTHROPOCENE SEA LEVEL CHANGE

### A History of Recent Trends Observed in the U.S. East, Gulf and West Coast Regions including Alaska

#### Key Points

- Relative sea level (RSL) observations at selected U.S. tide stations since 1969 exhibit trends in RSL rise rate and acceleration that vary in response to both global and regional processes. Trend histories display a high degree of similarity among locations within coastal regions that are experiencing similar processes.
- With the exception of the U.S. Northeast Coast and Alaska, every other coastal location in the continental U.S. has experienced an upturn in RSL rise rate since 2013-2014 despite wide differences in the magnitude and trending direction of RSL acceleration.
- High RSL acceleration along the U.S. Northeast Coast has trended downward since 2011, while low RSL acceleration along the U.S. Southeast Coast has recently trended upward in response to changes likely associated with ocean dynamics and ice sheet loss.
- RSL change in the sedimentary basins of the central U.S. Gulf Coast region is highly dependent on local rates of vertical land movement (VLM). VLM here varies over relatively short time scales amid changing patterns of subsurface water and hydrocarbons extraction.
- RSL rise rates of 5 mm/year or more aided by weak acceleration in Louisiana and Texas project a total RSL rise of between 0.4 and 0.5 meter above 1992 Mean Sea Level (MSL) by the year 2050; other Gulf and East Coast locations will experience equal or greater rise if upward trends in acceleration continue.
- Low and mostly downward trends in RSL rise rate at central U.S. West Coast locations have recently reverted to a pattern of upward trends with higher rise rates. Rise rates prior to 2013 appear to have been restrained by deceleration now trending toward acceleration.
- A combination of tectonic plate convergence and glacial isostatic adjustment makes the non-contiguous U.S. coastal state of Alaska unique with regard to RSL trends. Land emergence, rather than subsidence, produces consistent trends of falling RSL in Alaska.

## EXECUTIVE SUMMARY

This report examines mounting evidence of human influence on the earth and its environmental processes as measured by a suite of water level sensors in operation throughout the U.S. during the Anthropocene, a proposed new geologic epoch following the Holocene, the latest interglacial epoch that began nearly 12,000 years ago. A review of recent relative sea level (RSL) observations at U.S. tide stations since 1969 examines trends in RSL rise rate and acceleration that vary in response to both global and regional processes. Trend histories at 32 coastal locations selected for study display a high degree of similarity between locations in regions that are experiencing similar processes. With the exception of the U.S. Northeast Coast and Alaska, every other location in the continental U.S. has experienced an upturn in RSL rise rate since 2014 despite wide differences in the magnitude and trending direction of RSL acceleration. High RSL acceleration along the U.S. Northeast Coast has trended downward since 2011 while low RSL acceleration along the U.S. Southeast Coast has recently trended upward in response to changes likely associated with ocean dynamics and ice sheet loss.

RSL change in the sedimentary basins of the central U.S. Gulf Coast region is highly dependent on local rates of vertical land movement (VLM). VLM here varies over relatively short time scales amid changing patterns of subsurface water and hydrocarbon extraction. RSL rise rates of 5 mm/year or more aided by weak acceleration in Louisiana and Texas project a total RSL rise of between 0.4 and 0.5 meters above 1992 MSL by the year 2050; other Gulf and East Coast locations will experience equal or greater rise if upward trends in acceleration continue.

Low and mostly downward trends in RSL rise rate at central U.S. West Coast locations have recently reverted to a pattern of upward trends with higher rise rates. Rise rates prior to 2013 appear to have been restrained by deceleration now trending toward acceleration. A combination of tectonic plate convergence and glacial isostatic adjustment makes the non-contiguous U.S. coastal state of Alaska unique with regard to RSL trends. Land emergence, rather than subsidence, produces consistent trends of falling RSL in Alaska.

With these observed trends in mind, RSL rise rate and acceleration patterns elucidated within the proposed Anthropocene epoch (here 1969 through 2017) are presented for U.S. coastal locations with analogous ‘report cards’ displaying nearly fifty years of RSL heights projected forward to the mid-point of the present century. Factors contributing to RSL acceleration include: 1) steric expansion, 2) ocean dynamics, 3) Greenland and Antarctic ice sheet melting, 4) glacial isostatic adjustment, 5) groundwater and hydrocarbon storage changes, 6) inverted barometer, and 7) atmospheric cycles. With these contributing factors in mind, the report concludes with a broad summary of management recommendations applicable in regions experiencing the effects of these change-producing factors, as human populations look to better understand, quantify, and mitigate adverse effects on the increasingly inhabited coastal zone.

## TABLE OF CONTENTS

- I. The Anthropocene: New Trends in a Warmer World?
- II. Measuring Local Change in Sea Level
- III. Linear and Non-linear Trend Components
- IV. Anthropocene Sea Level Histories in the U.S.
- V. Processes Affecting Regional Trends
- VI. Implications for Risk Management
- VII. References
- VIII. Acknowledgements

## APPENDICES

Appendix A – Estimating the Seasonal Cycle and Decadal Signal

Appendix B – Confidence Intervals for Sea Level Time Series

Appendix C – Linear and Quadratic Trends with Year 2050 Projections

Appendix D – Application of Q-mode Factor Analysis to Sea Level Histories

## LIST OF ACRONYMS AND BRIEF DEFINITIONS

GIA	<u>Glacial Isostatic Adjustment</u> : ongoing movement of land once burdened by ice-age glaciers. Vertical land movement of other origins are also recognized.
GMSL	<u>Global Mean Sea Level</u> : world-wide average sea level measured relative to the center of the earth or a reference ellipsoid.
GT	<u>Great Diurnal Range</u> : the difference in height between the tidal datums of mean higher high water (MHHW) and mean lower low water (MLLW).
IPCC	<u>Intergovernmental Panel on Climate Change</u> : a scientific and intergovernmental body under the auspices of the United Nations.
MMSL	<u>Monthly Mean Sea Level</u> : the average water level observed over a calendar month at U.S. tide stations.
MSL	<u>Mean Sea Level</u> : tidal datum defined by NOAA for a specific tidal datum epoch.
NOAA	<u>National Oceanographic and Atmospheric Administration</u> : U.S. federal agency that includes the National Ocean Service (NOS) charged with the collection of U.S. oceanographic and meteorological data.
NWLON	<u>National Water Level Observation Network</u> : a permanent system operated by NOAA/NOS for observing, assessing, and archiving water levels nationwide.
NTDE	<u>National Tidal Datum Epoch</u> : 19-year period used for averaging water levels to determine tidal datum elevations at U.S. tide stations, currently 1983-2001.
RSL	<u>Relative Sea Level</u> : sea level measured relative to a fixed vertical datum on land.
VLM	<u>Vertical Land Movement</u> : due to various causes including subsurface extraction of water and hydrocarbons, regional tectonics and faulting, in addition to GIA.
YMSL	<u>Yearly Mean Sea Level</u> : average water level observed over a calendar year at U.S. tide stations.

## I. THE ANTHROPOCENE: NEW TRENDS IN A WARMER WORLD?

In recent years, geoscientists viewing mounting evidence of human influence on the earth and its environmental processes have begun to consider a revision of the geologic time scale. A revision not of an earlier period but of the present bringing closure to the Holocene, the latest interglacial epoch that began nearly 12,000 years ago, to be followed by a new epoch - the *Anthropocene*. This compound word combining ‘anthropo’ (human) and ‘cene’ (recent) was first popularized by Nobel laureate P.J. Crutzen (Crutzen and Stoermer, 2000; Crutzen, 2005), who introduced it following his research on the destruction of stratospheric ozone by man-made halogen compounds, principally chlorofluorocarbons.

In the time between the industrial revolution in the late eighteenth century and the new millennium, human activities had not only produced an alarming hole in the ozone layer above Antarctica but also doubled the amount of methane in the atmosphere and increased carbon dioxide to levels higher than any found over the last 400,000 years (Monastersky, 2015). Increases in these and other greenhouse gases have led to dramatic changes in earth’s climate system since the 1950s: the atmosphere and oceans have warmed, snow and ice have been lost and global sea level has risen at increasingly higher rates. These facts have been clearly established by the observational data presented in the Fifth Assessment Report by the Intergovernmental Panel on Climate Change (IPCC, 2013) as illustrated in Figure I-1.

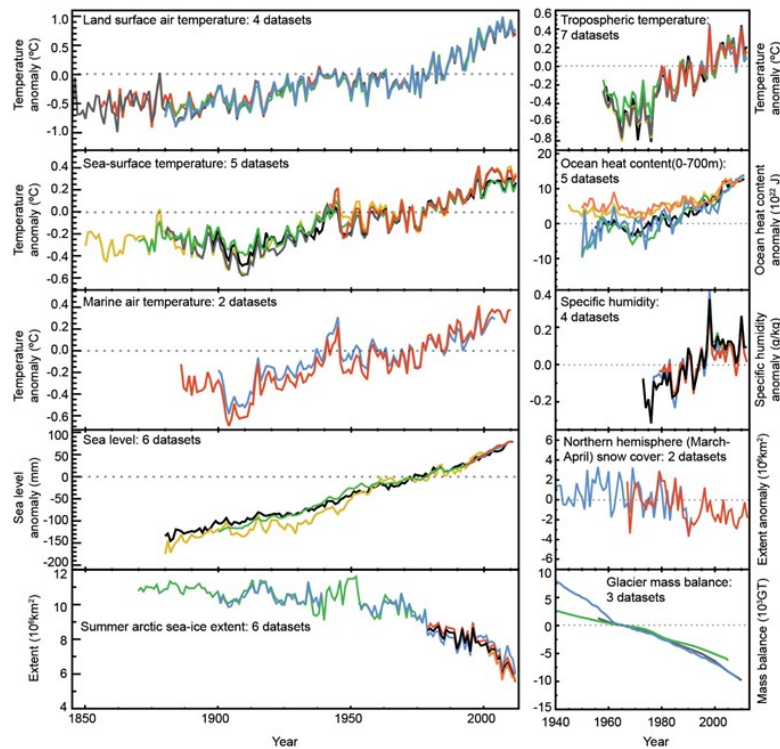


Figure I-1. Multiple complementary indicators of a changing global climate. Each line represents an independently derived estimate of change in the climate element (Figure TS-1 from WGIAR5 Technical Summary).

Although man's impact on the global environment is now unmistakable, it is difficult to assign a definite starting point in time; exactly when the Anthropocene epoch may have begun has been a matter of debate (Monastersky, 2015). However, from an observational viewpoint, most of the processes depicted in Fig. I-1 suggest that a change in many of earth's environmental systems was underway by the mid-point of the twentieth century, including sea level whose world-wide rate of increase over time has accelerated, although with no clear inflection point.

While the *global* sea level anomaly as presented in Fig. I-1 offers muted support for a precise mid-century origin for the Anthropocene epoch, sea level rise rates starting earlier are clearly less than those starting later in the twentieth century. In its Fourth Assessment Summary, IPCC Working Group I (WGIAR4) reported that global mean sea level (GMSL) rose at an average rate of 1.8 [1.3 to 2.3] mm/year over 1961-2003 and 3.1 [2.4 to 3.8] mm/year over 1993-2003 (IPCC, 2007). An updated rise rate of 3.2 [2.8 to 3.6] mm/year over 1993-2010 (IPCC, 2013) is only marginally greater. Other assessments include government study scenarios that project a GMSL rise as high as 2.0 m above 1992 levels by 2100 (Parris et al., 2012). Sweet et al. (2017) suggest increasing this upper-end limit to 2.5 m by 2100, citing recent observational and modeling literature on the potential for more rapid ice melt in Greenland and Antarctica.

Local Sea Level - A different assessment is found when investigating *local* sea level, particularly in certain regions along the U.S. coastline. Here, sea level rise rates relative to the land are usually calculated in one of two ways: either by applying a local correction for vertical land movement to an accepted globally-averaged rise rate, or directly as trends derived from a time series of water level measurements from tide gauges. Only the second method permits a data-driven evaluation of rise rate variations over time and between locations, but questions have been raised concerning record length.

Some investigators have argued that tide gauge records 75 years or more in length are required to obtain a valid estimation of sea level trends (Douglas, 1997, 2001; Houston and Dean, 2011). However, this presupposes that an underlying trend exists in the data that is completely stationary, even for records exceeding a century in length. From a purely physical standpoint, an underlying sea level trend that remains at all stationary in the presence of rapidly rising tropospheric temperatures and ocean heat content from the mid-twentieth century onward (right side of Fig. I-1) is hardly immune to challenge.

One of the first challenges came from Sallenger, Doran, and Howd (2012) who found post-1950s 'hot-spots' on the U.S. NE Atlantic coast with rise rate increases 3-4 times higher than the global average. They attributed higher rates observed at tide stations north of Cape Hatteras, North Carolina, to local forcing by dynamic processes involving changes in ocean circulation, variations in water temperature and salinity, and re-distribution of ocean water mass. Using a new analytical technique, empirical mode decomposition, Ezer and Corlett (2012) found sea level acceleration in Chesapeake Bay. Boon (2012) noted a coherent pattern of increasing rise rates beginning in 1987 north of Cape Hatteras as shown in Fig. I-2. The serial trends shown in this figure are derived as straight-line fits to successive time series windows, each 36 years in length shifted forward a year at a time. The trend value applies at the mid-point or median year of each moving window; thus the 1987 inflection shown occurs in a window whose starting point began 18 years earlier in 1969.

Very recently, East Coast tide station data analyses by Davis and Vinogradova (2017) found post-1990 sea level accelerations ranging from near-zero to about  $0.3 \text{ mm/year}^2$  due to ice-mass loss in Greenland and Antarctica, as well as ocean dynamics, in agreement with physical models.

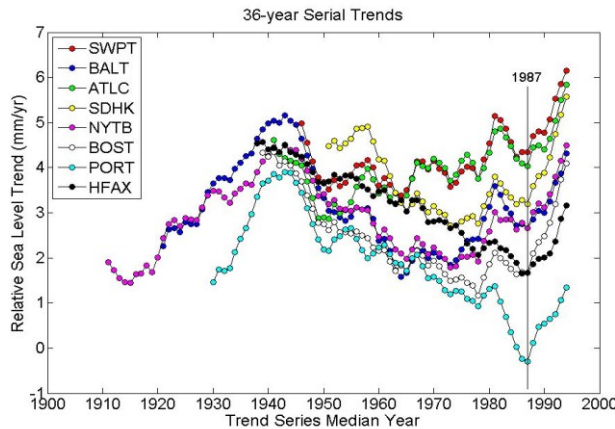


Figure I-2. Serial trends derived from 36-year sliding windows advancing one year at a time at eight U.S. Atlantic tide stations from Norfolk (SWPT), Virginia to Halifax (HFAX), Nova Scotia.  
Note that a 36-year time series starting in 1969 has 1987 as its median year.

The term ‘epoch’ can be used to describe any distinctive development that persists for a time as part of earth’s history. There is now almost certainly a new sea level epoch in existence marked by accelerations in the rate of sea level rise. However, like the Anthropocene epoch itself, some uncertainty exists over what time of origin to assign. Ezer, Haigh and Woodworth (2016) applying two different methods of analysis, conventional quadratic curve fitting and empirical mode decomposition, to long-term sea level records from western Europe found accelerations of  $0.014 \pm 0.003$  and  $0.012 \pm 0.004 \text{ mm/year}^2$ , respectively, over the past 150 years, rates which they noted as being close to the global average during this period. Boon and Mitchell (2015) applied Bayesian analysis to quadratic trend parameters derived from post-1969 tide gauge records and found much higher accelerations over the most recent 46-year period (1969-2014) at a number of U.S. East and Gulf Coast locations; e.g.,  $0.271 \pm 0.087 \text{ mm/year}^2$  at Eastport, Maine and  $0.157 \pm 0.094 \text{ mm/year}^2$  at Naples, Florida.

The question that remains is whether any period of analysis adopted at present will faithfully characterize the future behavior of changing sea level trends. The past is not always the key to the future. Both studies cited above addressed the uncertainty introduced by cyclical components present at interannual to multidecadal time scales, a consequence of ocean-atmosphere exchange. In a discussion article, Boon and Mitchell (2016) pointed to a controlling effect by spatially coherent, low-frequency variations in *monthly mean sea level* (MMSL) in modulating quadratic projections of sea level height forward to the year 2050. These quasi-periodic MMSL variations, herein referred to as the *decadal signal* (Hong, Sturges and Clark, 2000; Sturges and Hong, 2001), appear to account for a high percentage of the variance noted in 2050 sea level projections made over an extended series of years starting in 1969 and updated annually since 2004. To the extent future observations bear this out, there is a compelling reason to study the history of post-1969 trends in sea level rise rate and acceleration. In this report, sea level observations described in Section II are used as the basis for linear and non-linear trends derived using a quadratic model of sea level change as described in Section III.

## II. MEASURING LOCAL CHANGE IN SEA LEVEL

Space-based technology has offered many benefits and advantages in present day monitoring of the physical, chemical and biological processes of the world's oceans. By comparison, the task of measuring water level with an electromechanical device mounted on a dock or pier appears mundane. But in past centuries some of the best scientific and technological minds were occupied with this task and with understanding the data it produced. Today's efforts toward understanding sea level change owe more than a little gratitude for the perseverance of those who kept, and still keep, many years of meticulous records from the water level monitoring device commonly known as a *tide gauge*. This name is somewhat misleading, as changing water levels are driven by many other factors besides the astronomical tides, including varying surface winds, changes in atmospheric pressure, changes in ocean water temperature and salinity, fresh water storage and discharge from land, vertical land movement – and sea level rise.

Relative Sea Level - A tide gauge measures water level relative to the land at one location. For coastal residents concerned with flooding at or near that location in real-time, this is the measurement that counts as compared to a global metric referencing the center of the earth or a reference ellipsoid. At such times a further breakdown is unnecessary; to be told that part of the water entering a home during a storm event may be attributed to land subsidence over time offers no immediate benefit. At other times an evaluation of contributing factors is clearly worthwhile, and this frequently calls for processing treatments that strip tide gauge records of unwanted components – starting with the tide itself through averaging! The smoothing that results leads to what may be more properly termed a sea level height. In this report, trends in sea level height are examined after removing day-to-day variations and some month-to-month variations that are unrelated to longer-term patterns of change in sea level.

Monthly Mean Sea Level (MMSL) - Averaging water levels over a calendar month removes much of the so-called ‘weather’ tide in addition to the regular cycles of the astronomical or predicted tide that repeat at intervals ranging from a solar day to a lunar month. Averaging over the calendar year (YMSL) further removes a less-regular, cyclical component called the *seasonal cycle* that has both an astronomical and a meteorological origin. However, the seasonal cycle can also be isolated and removed from a time series of MMSL heights using an analytical method (harmonic analysis). Subsequent numerical filtering can then be used to obtain the *decadal signal*, the low-frequency component introduced in Section I and a key factor in interpreting the sea level trend analyses presented later in this report. A more detailed description of the analytical methods employed in treating the seasonal cycle and the decadal signal in MMSL time series is given in Appendix A.

Where to Find MMSL Data - The primary source for sea level observations worldwide is the Permanent Service for Mean Sea Level located in Liverpool, England ([www.psmsl.org](http://www.psmsl.org)). Here monthly and annual mean values of sea level are available from nearly 2,000 tide gauge stations at locations around the world. The original source of observations made in the United States and its territories is the National Water Level Observation Network (NWLON) operated by the National Oceanic and Atmospheric Administration (NOAA). These observations can be obtained from NOAA’s website ([www.tidesandcurrents.noaa.gov](http://www.tidesandcurrents.noaa.gov)) under products/water levels.

Selecting a Reference Datum for MMSL Heights - Although the PSMSL in Great Britain is widely recognized as the preferred data source for international studies on changing sea level, the MMSL time series heights used in this report are taken from the abovementioned NOAA site. The NOAA site is preferred here for two reasons: The latest MMSL heights recorded at U.S. tide stations, and verified for their accuracy through rigorous NWLON quality control procedures, are available much sooner than the corresponding heights from the PSMSL site – an important consideration when examining very recent trends. Secondly, NOAA MMSL heights are available referenced to *Mean Sea Level* (MSL), a tidal datum that is specifically defined in and for the United States in accordance with Federal law (Gill and Schultz, 2001; Parker, 2007). MSL and other U.S. tidal datums are computed as water level averages over a specific 19-year period known as the National Tidal Datum Epoch (NTDE). As sea level continues to change, the NTDE is updated as needed, or roughly every twenty-five years, to keep abreast of this change. The current NTDE is based on the series 1983-2001 whose median year is 1992. Thus, the MSL vertical reference approximates where sea level stood in 1992 at the center of the current epoch.

Datum Origin - Associating a vertical datum with a time origin is not always a consideration. As stated on its website, the foremost PSMSL objective is the establishment of a world-wide common datum for referencing water levels. Tide station data provided to the PSMSL are reduced (using datum information from submitting authorities) to heights above *Revised Local Reference*, a vertical datum set exactly 7 meters (m), or about 23 feet, below an arbitrarily fixed mean sea level whose epoch is unspecified. Often, it is simply the *rate* of sea level change that is of interest, the only requirement being that the vertical reference in use must remain unchanged over an unlimited span of time, past and present. But when investigating nascent trends over a limited span, specifically one conforming to the proposed Anthropocene epoch, it is important to be able to answer the question: The amount of rise since when? Since the year 1992 in this case.

Trends Derived from Observations - Unlike the very predictable astronomical tide, accurate prediction of sea level far into the future is a nearly impossible task, especially at individual locations. That said, trends that appear in a ‘scatter plot’ of MMSL heights over a sufficient period of time can serve as useful guides in the near-term. Most often the trend shown is a linear one defined by a straight line fitted to the data. Many U.S. examples can be found at the NOAA website ([www.tidesandcurrents.noaa.gov](http://www.tidesandcurrents.noaa.gov)) under products/sea level trends. However, as in most situations where analytical results are presented, a careful reading of the text describing the underlying data, and how they are being interpreted, is important.

For example, a recent online NOAA graphic employing colored arrows on a map to compare and contrast sea level trends at a glance presently identifies Eugene Island, Louisiana, as the U.S. locality where sea level is rising most rapidly at  $9.65 \pm 1.24$  mm/year. A statement is added that this is the equivalent of 3.17 feet (0.966 m) of rise in 100 years; an additional footnote lists a 36-year series from 1939 through 1974 as the basis for this trend. Supposing that another location also has a 36-year series but from 1969 through 2004; would a comparison between these locations whose record origins differ by thirty years still be valid? Is it misleading to make any inference at all regarding a century of sea level rise based on a single tide gauge record? To compare trends from different locations over the same period of time is the more reasonable choice along with qualified statements regarding future trends and projections.

### III. LINEAR AND NON-LINEAR TREND COMPONENTS

Various ways exist to perceive trends in *time series* data, a set of measurements ordered in time. Simply looking at a data plot may suggest upward or downward movement. When background noise makes this difficult, a smoothing procedure is often applied to bring out the hidden features of a trend – assuming there is one. But to both identify and enumerate a specific trend requires a mathematical model with a statistical component. The most basic of these is the general linear model that fits a straight line to the data using the method of least squares. Its next level extension is the quadratic model, which fits a curve defined by the quadratic equation.

Trends derived from the quadratic model are represented by a pair of parameters that give the user two important pieces of information: These are the *rate* of change, up or down, and the *acceleration* (or deceleration – a decrease) in the rate of change with time. However, the information has limits. Whether a linear or quadratic model is chosen to represent these aspects of *relative sea level* (RSL) change, there is one fundamental requirement: Even as sea level changes with time, both rate and acceleration are assumed constant as applied in the model – an assumption often difficult to justify in practice. Model estimates are made with the aid of statistical confidence intervals (see Appendix B).

Quadratic Model of RSL Change - In this model, sea level height  $h$  is represented at time  $t$  by a quadratic equation of the form

$$h = \beta_0 + \beta_1 t + \frac{1}{2} \beta_2 t^2 + \varepsilon \quad (\text{III-1})$$

In the present application, time is measured in years relative to 1992, and height is measured in millimeters (mm) relative to the tidal datum of mean sea level (MSL) as computed by NOAA for the current NTDE (1983-2001). Given a time series of observed MMSL heights with the seasonal cycle removed (as noted in Section II), estimates of the three parameters  $\beta_0$ ,  $\beta_1$ ,  $\beta_2$  are obtained using the method of least squares, a ‘best fit’ technique that minimizes the square of the error term

$$\varepsilon = h - \hat{h} \quad (\text{III-2})$$

where  $h$  is an observed height and  $\hat{h}$  is the corresponding height predicted by the model using the first three terms on the right side of Eq. III-1. Assuming random error,  $\varepsilon$  can be either positive or negative following a normal distribution with zero mean. It follows that the parameter  $\beta_0$  in Eq. III-1 representing the predicted height  $\hat{h}$  for 1992 ( $t = 0$ ), may deviate from MSL datum ( $h = 0$ ).

The *rate* of RSL change is found as the derivative of Eq. III-1,

$$\frac{dh}{dt} = \beta_1 + \beta_2 t + \varepsilon \quad (\text{III-3})$$

Eq. III-3 shows rate has two components: A linear rate of change in mm/year given by parameter  $\beta_1$  and a non-linear rate of change in mm/year<sup>2</sup> given by parameter  $\beta_2$ . The second parameter, if positive in value, is the *acceleration* (deceleration, if negative) as represented by the model.

**Model Application** - Two examples of the quadratic model applied to MMSL observations (with seasonal cycle removed) for Norfolk, Virginia, are shown below using a 36-year series from 1969 through 2004 (Fig. III-3) and a 49-year series from 1969 through 2017 (Fig. III-4).

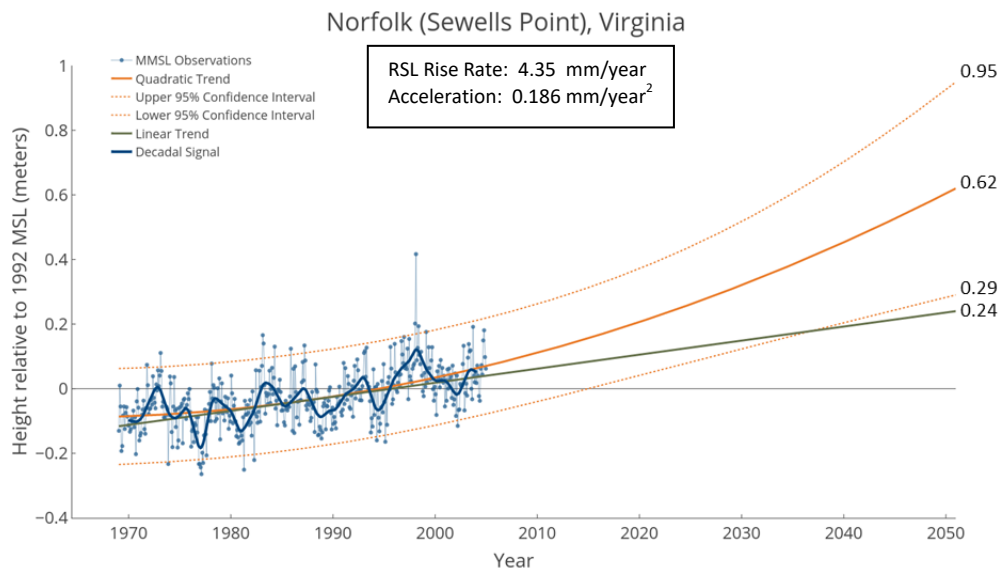


Figure III-3. Relative sea level trends, Norfolk, Virginia, 1969-2004 series

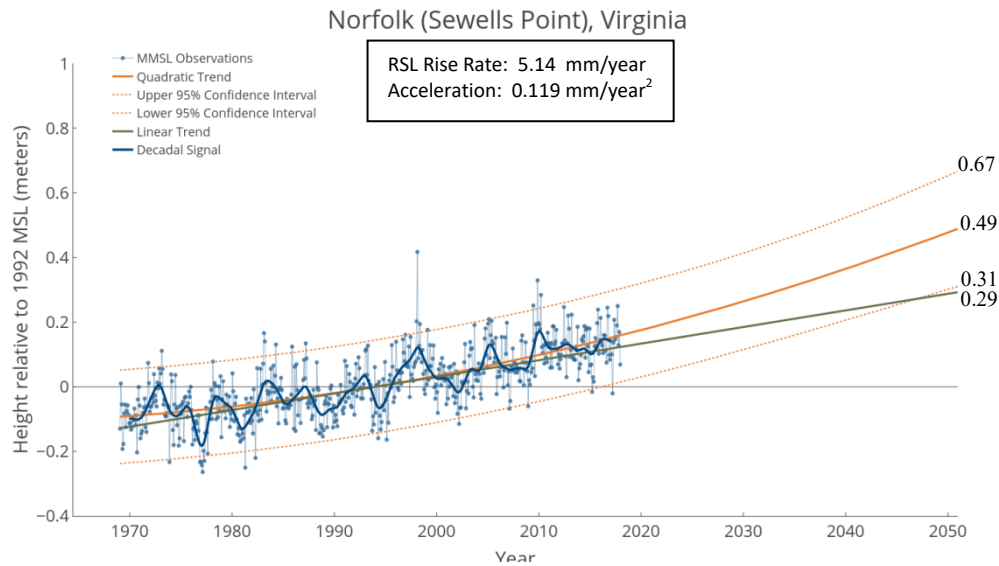


Figure III-4. Relative sea level trends, Norfolk, Virginia, 1969-2017 series

Both of the above graphs show linear and quadratic trends derived from least-squares estimates of  $\beta_1$  and  $\beta_2$  in Eq. III-1. Although both trends are shown extending through the year 2050, the widening 95% confidence intervals apparent in Fig. III-3 are a clear sign that a 2050 projection is unwarranted for the 36-year series. In Fig. III-4, the projected width of the 95% confidence intervals is almost the same all the way out to 2050. As explained in Appendix B, the intervals will include approximately 95% of the MMSL observations in any one year; counting the total number of observations that do fall between the dotted bands confirms this to be true on average. The bands therefore provide a useful guiding principle when making near-term projections: Look for the vertical interval between bands to remain roughly the same going forward in time. Further guidance is given by changes in the amplitude and phase of the decadal signal described in Section I and Appendix A, specifically whether the signal is trending high or low during the most recent MMSL observations as it modulates the projected RSL trends.

Changing Rates - As an empirical model applied to a series of observations, Eq. III-1 relies on the assumption that both the linear rate of rise (fall) represented by  $\beta_1$  and the acceleration (deceleration) represented by  $\beta_2$  remain constant throughout the model's applied time domain. Comparing the RSL rise rate and acceleration values given in Figs. III-3 and III-4 suggests that this assumption is not entirely justified (not unusual for a time series), but it conforms to our belief that neither rise rate nor acceleration are static expressions of an underlying trend. Using the full 90-year record available for Norfolk (Appendix B, Fig. B-1C) produces a lower linear trend estimate ( $\beta_1 = 4.61$  mm/year) and a much lower quadratic trend estimate ( $\beta_2 = 0.017$  mm/year<sup>2</sup>). Observations going forward would have to overcome the considerable weight of these older trends before they could possibly detect new ones.

Over geologic time, global sea level has experienced numerous successions of high stands and low stands that could not have occurred without intervening periods of acceleration and deceleration. Evidence supporting the designation of a new geologic epoch with faster rising sea levels underscores the potential for acceleration that has only become evident over the last few decades, not centuries. In that context, the quadratic model given by Eq. III-1 can be tailored to properly search for significant acceleration, evaluate its short-term history, and make limited projections for the near-term future – considering that acceleration need not be long-lasting in order to have a significant impact on sea level heights within the present century.

Relative Sea Level Report Cards - Repeated application of the quadratic model as each new year of MMSL observations become available further describes the short-term history in a way that may reveal the progress of relative sea level change – a type of *sea level report card*. Imagine a student presently failing a subject in school, yet a series of recent report cards shows steady improvement in the student's grades, inferring that a likely transition from failure to success lies ahead. Likewise, a downward linear trend presently marked by RSL deceleration may show less and less deceleration with time until the trend eventually reverses. Success here may mean that a coastal community receiving these reports will be able to use the information to its advantage when revising or updating its flood defense plans.

Sequential representation of linear and quadratic trends – sea level report cards – for a selection of NOAA tide stations with post-1969 MMSL records on the continental U.S. coastline are introduced in section IV and presented in Appendix C.

#### IV. ANTHROPOCENE SEA LEVEL HISTORIES IN THE CONTINENTAL U.S.

It is difficult to make a sensible assessment of sea level change when comparing relative sea level (RSL) trends derived from tide gauge records with different starting points. Just as a starting point is required to define the Anthropocene epoch, one is also needed for the start of an RSL record. A common beginning year enables not only a valid comparison of trends across locations within and between coastal regions but, by adding new observations as they become available, permits the development of a *sea level history* lending progressive insight into regional similarities and the direction of the most recent change. Here, the year 1969 is chosen as the starting point based on previous studies by Boon (2012) and Boon and Mitchell (2015). A comparatively large number of NOAA tide stations across the U.S. have complete or nearly complete records since 1969.

Sea level histories for the Anthropocene epoch are presented in this section for 32 U.S. tide stations with monthly mean sea level (MMSL) records from 1969 through 2017, including twelve East Coast locations, eight Gulf Coast locations, and twelve West Coast locations (Fig. IV-1). The latest graphical records (report cards) for the period 1969-2017 are presented for each coastal region in Appendix C with a summary of 1969-2017 trend and projection values given in Table IV-1.

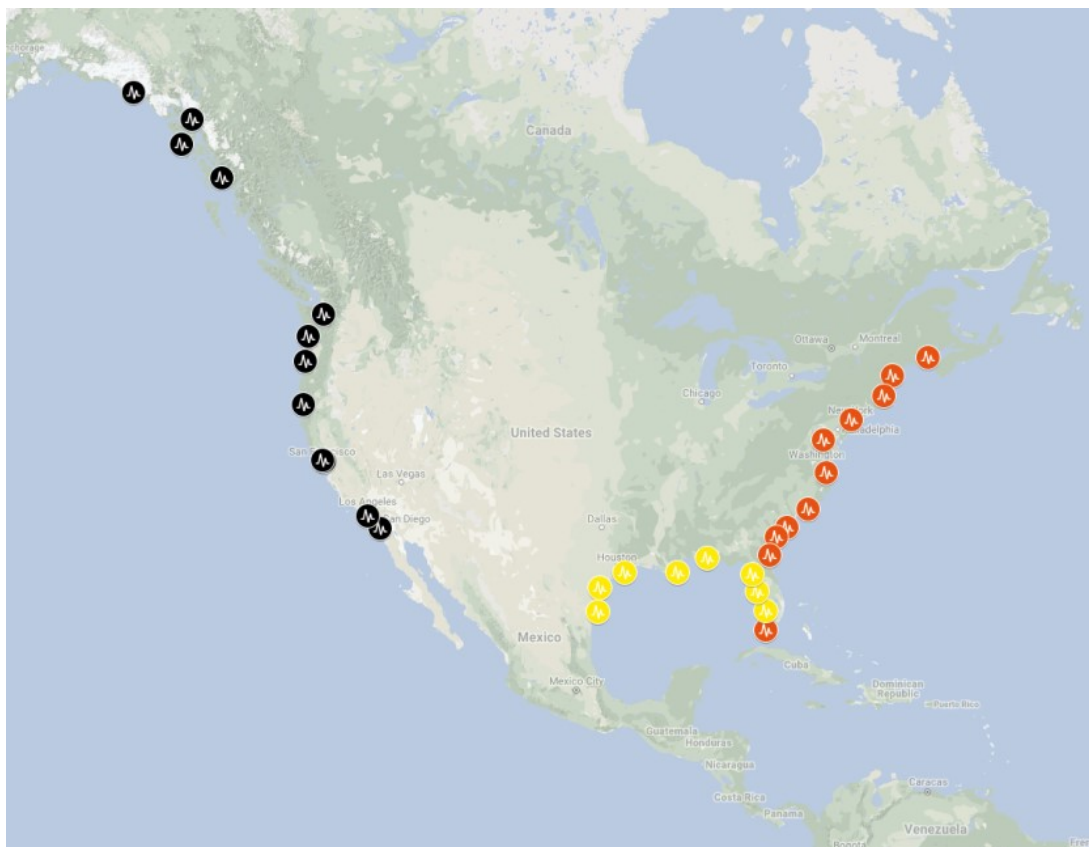


Figure IV-1. Location of NOAA tide stations listed in Table IV-1 from Maine to Alaska.

Table IV- 1. RSL trend values and year 2050 projections inferred from 1969-2017 observations.  
Confidence intervals include 95% of MMSL observations expected in year 2050.

Location	Rise Rate (mm/year)	Acceleration (mm/year <sup>2</sup> )	Linear Projection Year 2050 (m)	Quadratic Projection Year 2050 (m)
Eastport ME	1.79	0.208	0.10	0.44 ± 0.10
Portland ME	1.20	0.177	0.07	0.36 ± 0.12
Boston MA	3.11	0.186	0.18	0.48 ± 0.13
New York NY <sup>1</sup>	3.39	0.094	0.19	0.35 ± 0.15
Sandy Hook NJ	4.22	0.140	0.24	0.47 ± 0.15
Baltimore MD	3.43	0.109	0.19	0.37 ± 0.15
Norfolk VA <sup>2</sup>	5.14	0.119	0.29	0.49 ± 0.18
Wilmington NC	2.44	0.166	0.13	0.40 ± 0.19
Charleston SC	3.34	0.137	0.18	0.41 ± 0.17
Savannah GA <sup>3</sup>	3.68	0.111	0.20	0.38 ± 0.18
Jacksonville FL <sup>4</sup>	2.52	0.067	0.13	0.24 ± 0.20
Key West FL	2.99	0.102	0.17	0.34 ± 0.12
Naples FL	2.75	0.180	0.15	0.45 ± 0.11
St Petersburg FL	3.19	0.087	0.18	0.32 ± 0.11
Cedar Key FL	2.69	0.172	0.15	0.43 ± 0.14
Pensacola FL	2.72	0.201	0.15	0.49 ± 0.14
Grand Isle LA	7.72	0.017	0.44	0.47 ± 0.15
Galveston TX <sup>5</sup>	6.17	0.058	0.35	0.45 ± 0.20
Rockport TX <sup>6</sup>	6.71	0.259	0.39	0.82 ± 0.19
Port Isabel TX	4.60	0.125	0.26	0.46 ± 0.16
San Diego CA	2.54	0.037	0.14	0.20 ± 0.13
Los Angeles CA	1.61	0.032	0.09	0.14 ± 0.12
Alameda CA	0.90	0.017	0.04	0.07 ± 0.17
San Francisco CA	1.75	0.000	0.09	0.09 ± 0.17
Crescent City CA	- 0.76	-0.035	- 0.05	-0.11 ± 0.19
South Beach OR	1.90	0.088	0.10	0.25 ± 0.20
Astoria OR	0.39	0.118	0.01	0.21 ± 0.22
Seattle WA	1.93	0.043	0.11	0.18 ± 0.18
Ketchikan AK	-0.68	-0.107	-0.04	-0.21 ± 0.19
Sitka AK	-2.83	-0.074	-0.16	-0.28 ± 0.18
Juneau AK	-14.0	-0.089	-0.57	-0.71 ± 0.20
Yakutat AK	-11.8	-0.348	-0.42	-1.00 ± 0.20

<sup>1</sup> The Battery <sup>2</sup> Sewells Point <sup>3</sup> Fort Pulaski <sup>4</sup> Fernandina Beach <sup>5</sup> Pier 21 <sup>6</sup> 2017 Port Aransas TX

It is well-known that RSL change varies over geographic regions (Sallenger, Doran and Howd, 2012; Kopp et al., 2015; Valle-Levinson, Dutton and Martin, 2017). In the following subsections we annotate Anthropocene sea level history in three U.S. coastal regions with derived estimates of RSL rise rate and acceleration starting with the 1969-2004 period followed by annual updates ending with the period 1969-2017. The succession of analytical results that follow each year, from the starting period to the present period, constitutes an RSL history. As will become apparent, RSL histories across coastal regions and sub-regions frequently show a high degree of similarity in their trends, even though the magnitude of RSL rise rate and acceleration at adjacent locations may differ substantially. Similarity among locations increases confidence in the direction of apparent trends within a given region.

**U.S. East Coast Comparisons** – In the years 2012 and 2013 several researchers reported sharp contrasts in RSL behavior in the coastal regions north and south of Cape Hatteras, North Carolina [e.g., Sallenger, Doran, and Howd (2012); Boon (2012); Ezer et al. (2013); Kopp (2013); Yin and Goddard (2013)] and most recently, Valle-Levinson, Dutton and Martin (2017). An illustration is readily provided by two sea level histories of RSL rise rate (Fig. IV-2A) and acceleration (Fig. IV-2B) recorded at Norfolk, Virginia, and Wilmington, North Carolina.

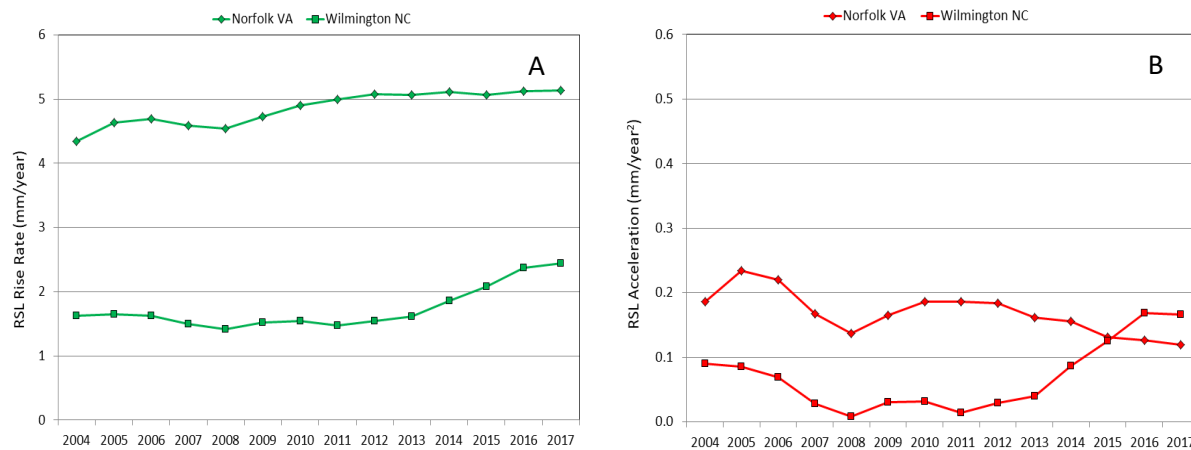


Figure IV-2. RSL rise rate (A) and acceleration (B) histories at Norfolk, Virginia and Wilmington, North Carolina. Each data point represents rise rate/acceleration from 1969 through the year indicated. Note factor of ten difference in vertical scales for plots A and B.

Norfolk has maintained a substantially higher RSL rise rate than Wilmington and other locations farther south along the U.S. East Coast. However, since 2012, Norfolk's rise rate has remained flat at around 5 mm/year, whereas the rate at Wilmington has increased from about 1.5 mm/year to slightly more than 2.5 mm/year as seen in Fig. IV-2A. The increase coincides with renewed acceleration at Wilmington – from almost no acceleration to 0.17 mm/year<sup>2</sup> in the six years since 2011 (Fig. IV-2B). In contrast, Norfolk's previously high acceleration has steadily declined over the same six-year period.

An important feature that emerges from the Norfolk-Wilmington comparison is the cyclical element evident in their RSL acceleration histories (Fig. IV-2B). Although the histories cover only a little more than a decade, the interval between highs and lows in acceleration correspond roughly to highs and lows in their respective decadal signals (Figs. IV-3,4). Particularly striking is the fact that these quasi-cyclic variations appear out of phase: RSL acceleration is decreasing at Norfolk while increasing at Wilmington. Comparisons between other East Coast locations show that this pattern is not at all unique to these two stations.

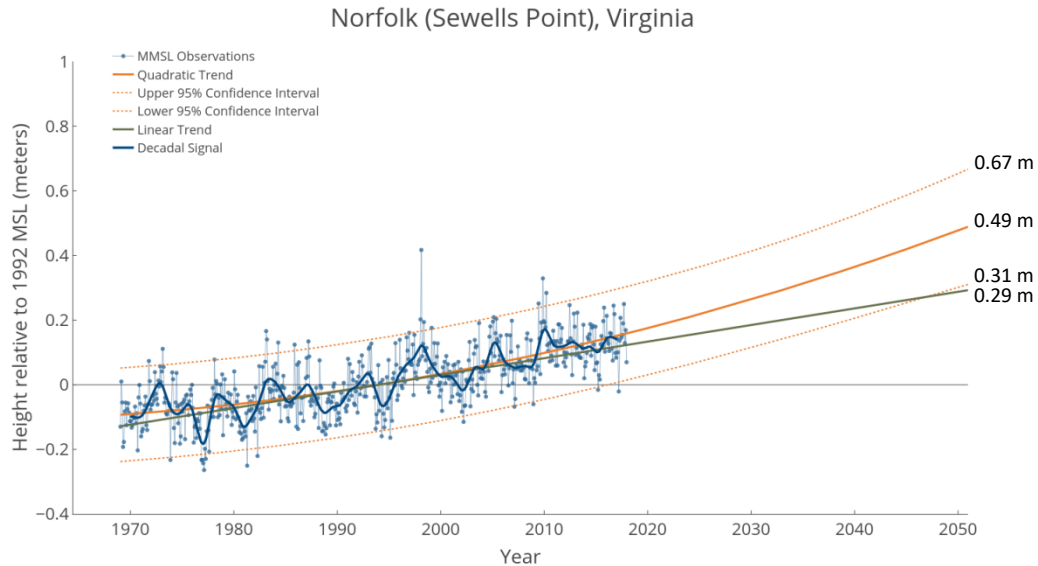


Figure IV-3. Plot of 1969-2017 MMSL, decadal signal, linear and quadratic trends, Norfolk, Virginia.

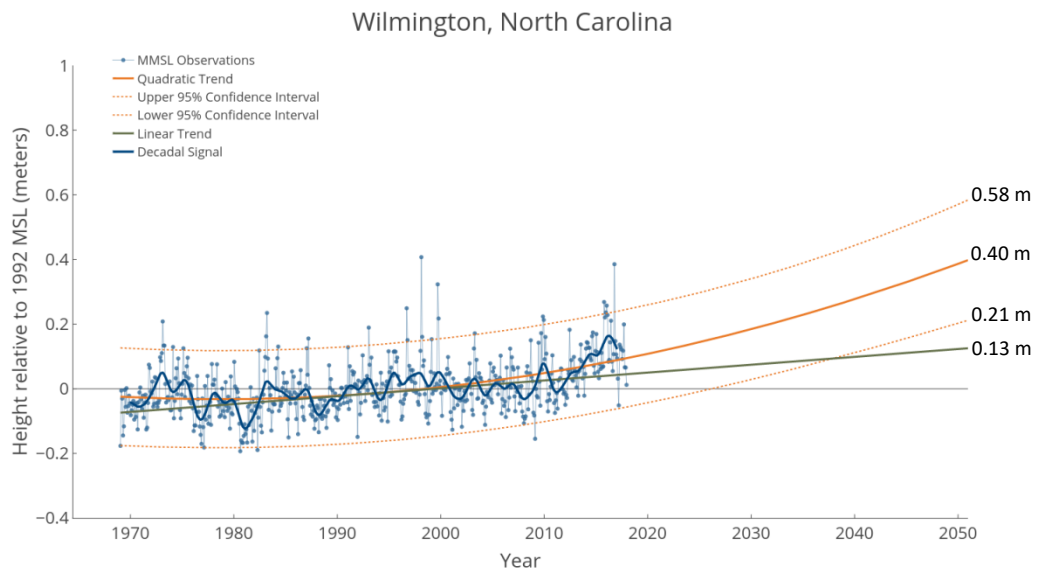


Figure IV-4. Plot of 1969-2017 MMSL, decadal signal, linear and quadratic trends, Wilmington, North Carolina.

Further insight into the nature of the relationship between locations and their RSL experiences may be gained through an analysis of the *similarity* in RSL rise rate and acceleration histories. Figures IV-5 and IV-6 demonstrate the approach by comparing rise rate and acceleration at twelve East Coast locations without regard to the *magnitude* of either; i.e., by employing an arbitrary origin on the vertical axis. Data points have the same reference periods as shown in Fig. IV-2.

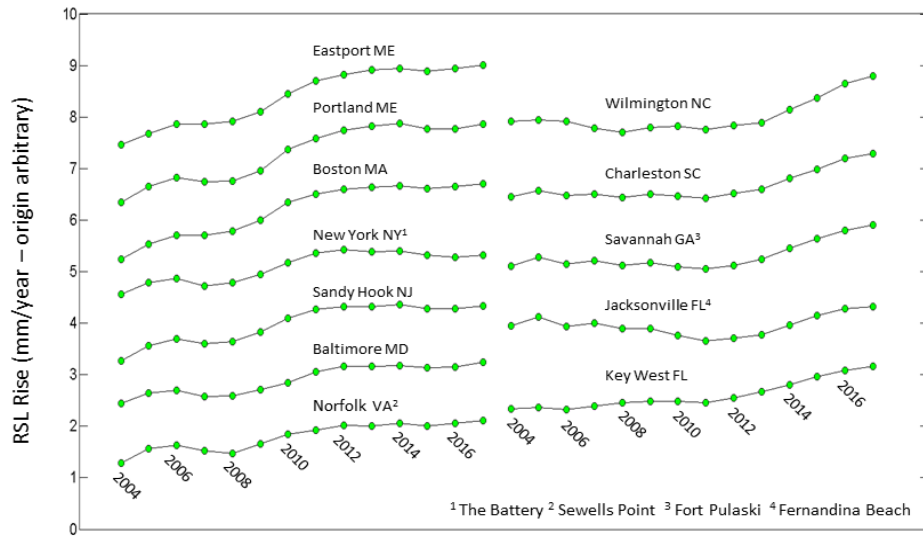


Figure IV-5. RSL rise rate histories at twelve U.S. East Coast locations from 1969-2004 to 1969-2017. Arbitrary origin compares rate similarity rather than magnitude.

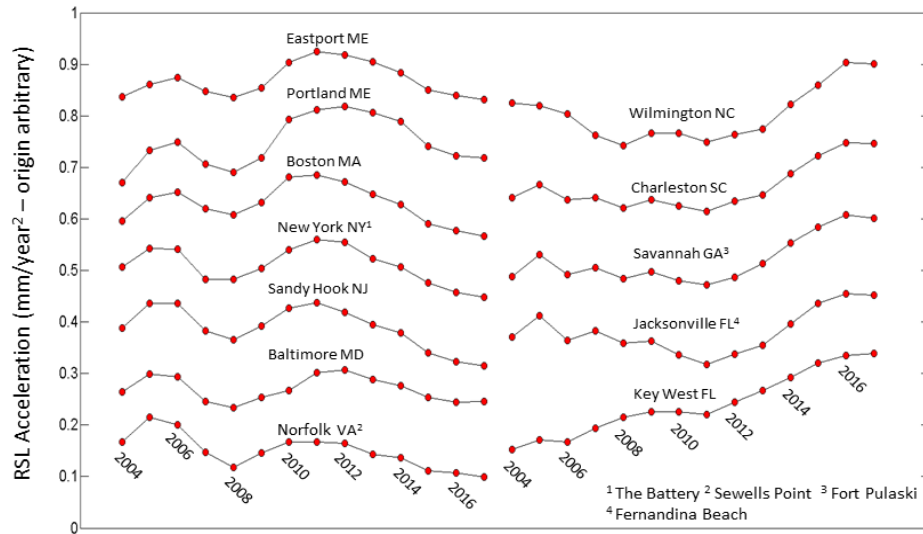


Figure IV-6. RSL acceleration histories at twelve U.S. East Coast locations from 1969-2004 to 1969-2017. Arbitrary origin compares acceleration similarity rather than magnitude.

Figure IV-6 highlights the strong similarity among RSL acceleration histories within the northeast and southeast sub-regions of the U.S. East Coast while underscoring the dissimilarity between sub-regions. The exception in this case is Key West, which lies at the boundary between the East and Gulf Coast regions at the southern tip of Florida (for test purposes we also include Key West in the Gulf Coast region). The boundary between East Coast sub-regions is found at Cape Hatteras between Norfolk, Virginia, and Wilmington, North Carolina, a location that has been noted before in connection with regional variations in coastal sea level and related oceanographic and atmospheric features. These are discussed in Section V of the report.

U.S. Gulf Coast Comparisons - RSL rise rate histories for the U.S. Gulf Coast region (Fig. IV-7) show a high degree of similarity among Florida's west coast locations where rise rates underwent very little change until 2011 when rates began trending steadily upward. Locations farther west in Louisiana and Texas have histories that are less similar but also seem to be trending upward after 2014, including Rockport, Texas, whose tide station was destroyed during Hurricane Harvey in August, 2017. RSL acceleration histories (Fig. IV-8) are likewise trending upward at most locations, several since 2006, with the exception of Rockport and Port Isabel in Texas, which have each experienced a strong downward trend in acceleration until very recently.

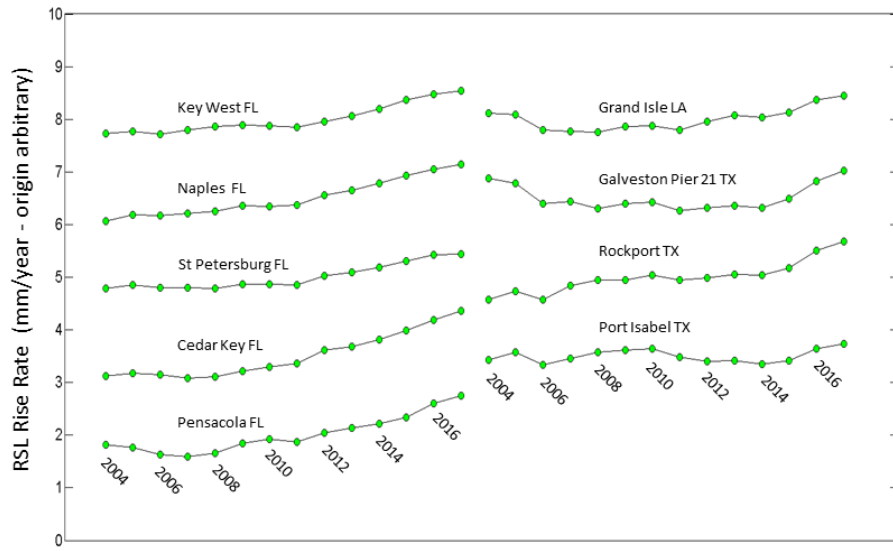


Figure IV-7. RSL rise rate histories at eight U.S. Gulf Coast locations plus Key West FL from 1969-2004 to 1969-2017. Arbitrary origin compares rise rate similarity rather than magnitude.

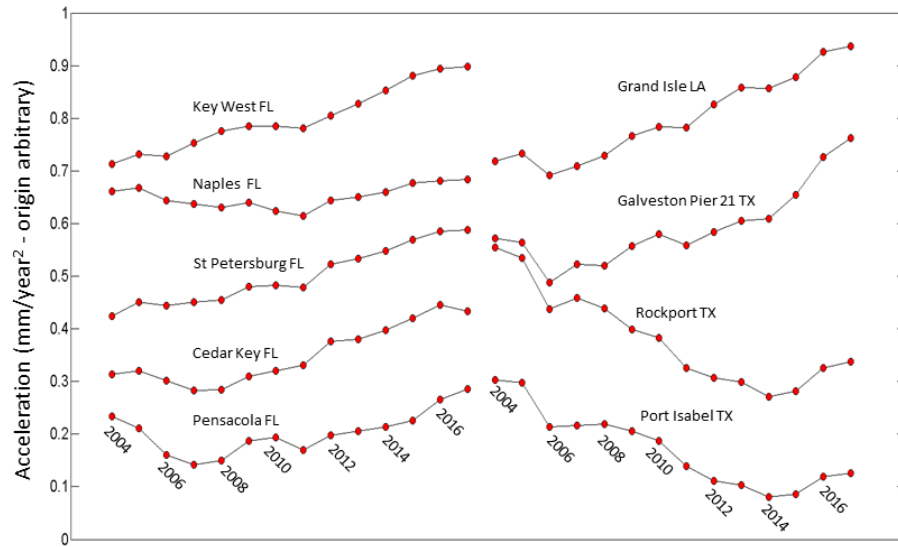


Figure IV-8. RSL acceleration histories at eight U.S. Gulf Coast locations plus Key West FL from 1969-2004 to 1969-2017. Arbitrary origin compares acceleration similarity rather than magnitude.

The central Gulf Coast is a sub-region known for its high rates of subsidence. As noted in Boon and Mitchell (2015), the Houston-Galveston area in southern Texas was a prime example of high subsidence rates until the mid-seventies when municipal and industrial ground water extraction were widely restricted and replaced by overland supplies. The RSL rise rate at Galveston decreased thereafter and remained steady at about 5.5 mm/year until the year 2014 when it began an upward trend (Fig. IV-9A). A similar history is found at Grand Isle, Louisiana, although its upward trend appears to have begun earlier in 2011. However, Fig. IV-9A shows very different histories for Rockport and Port Isabel, Texas, further west. The rise rate increased initially at Rockport before leveling off at 6 mm/year then resuming an upward track in 2014; Port Isabel has similar but more uniform rise rates varying between 4 mm/year and 5 mm/year.

The acceleration histories for the above four locations testify to the complexity of the central and western Gulf Coast sub-regions. In contrast to the U.S. East Coast region, changes in vertical land movement (VLM) here are heavily influenced by subsurface water and minerals extractions within coastal sedimentary basins as explained in Section V. Consequently, the time scale of VLM change is likely to be more variable, and this is reflected in the widely divergent acceleration histories beginning with the 1969-2004 period in Fig. IV-9B – extremely high acceleration at almost 5 mm/year<sup>2</sup> is seen at Rockport simultaneous with high *deceleration* of around -0.2 mm/year<sup>2</sup> at Galveston and Grand Isle. As acceleration trends downward at Rockport to the west, an upward trend in RSL rise rate diminishes there; as deceleration trends upward (progressively *less* deceleration) at Galveston and Grand Isle to the east, downward trends in RSL rise rate level off after 2006 before resuming an upward trend in 2014.

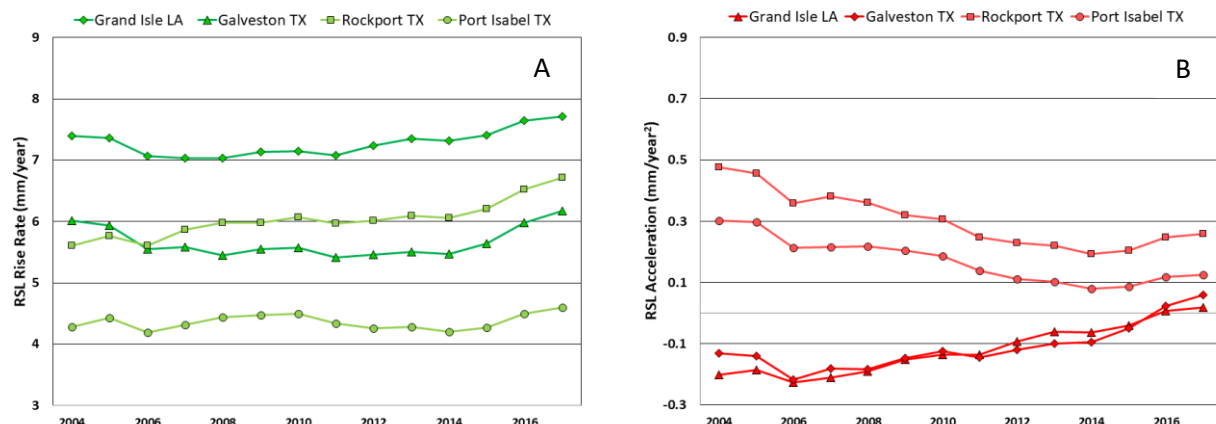


Figure IV-9. RSL rise rate (A) and acceleration (B) histories at Grand Isle LA, Galveston Pier 21 TX, Rockport TX and Port Isabel TX. Rockport TX replaced by Port Aransas TX in mid-2017. Each data point represents rise rate/acceleration from 1969 through the year indicated.

At least three locations in Louisiana and Texas now have RSL rise rates in excess of 6 mm/year. If present trends continue, these rates will result in RSL gains of more than 0.30 m (1 foot) above 1992 levels by the year 2050 without acceleration. Along the U.S. East Coast, only Norfolk, Virginia, comes close to this mark (Table IV-1). After RSL acceleration is taken into account, year 2050 projections increase significantly – except at Grand Isle, Louisiana, and Galveston, Texas, where acceleration accompanying their higher rise rates is presently near zero.

But if past history is any guide, this could change: note the durable upward trend in acceleration at Grand Isle and Galveston and the 2014 trend reversal at Rockport. Quadratic projections based on 1969-2017 observations (Table IV-1) show a year 2050 high of 0.49 m at Pensacola, Florida (Fig. IV-10) and 0.82 m at Rockport (Fig. IV-11) above 1992 MSL. Otherwise, no other tide station in the Gulf region presently exceeds the 0.49 m projection for Norfolk, Virginia taking acceleration into account. Considering the decadal signal, the Rockport-Pensacola projections will likely decrease moving beyond their respective 2016 signal peaks whereas Norfolk's 2017 mid-level signal position (Fig. IV-7) suggests its present projection may see an increase going forward.

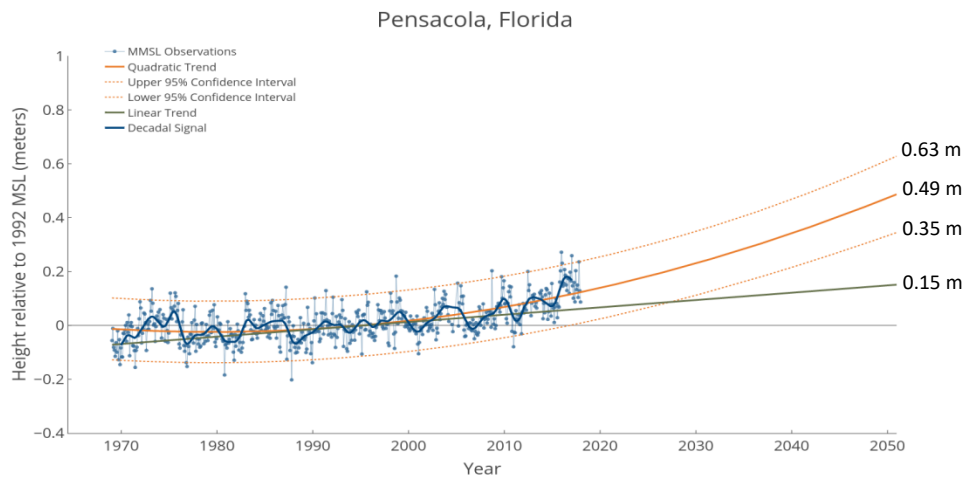


Figure IV-10. Plot of 1969-2017 MMSL, decadal signal, linear and quadratic trends, Pensacola, Florida.

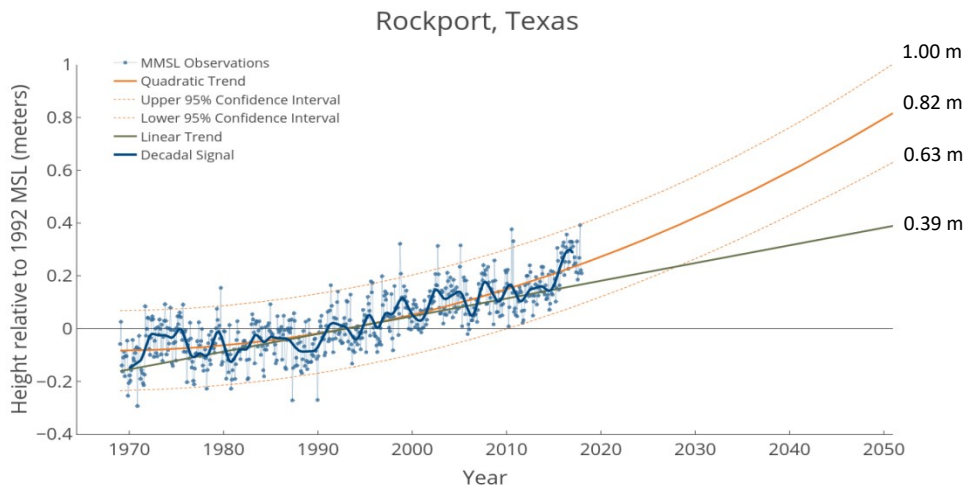


Figure IV-11. Plot of 1969-2016 MMSL, decadal signal, linear and quadratic trends, Rockport, Texas.

Of the three U.S. coastal regions examined, none has a greater deficit of tide stations with adequate post-1969 water level records than the Gulf Coast – or a greater history of losing them to coastal storms. It will be important to follow carefully the future RSL history provided by the ones remaining, including Galveston and Grand Isle, for signs of increasing RSL acceleration.

U.S. West Coast Comparisons - RSL change along the western boundary of the U.S., including Alaska, is influenced by a number of factors associated with an active continental margin – one characterized by converging tectonic plates. In addition to its convergence with the major Pacific plate near the coastline from California to Alaska, the North American plate also converges with the smaller Juan de Fuca plate (the remnant of an older, largely subducted plate) off Washington state and western Canada. Both vertical and horizontal land movement occurs sporadically in fault zones in and around plate boundaries; e.g., the San Andreas transform fault in California. San Diego, California (on the Pacific plate) presently has the highest RSL rise rate on the U.S. West Coast while Crescent City, California (on the North American plate) has the lowest (Fig. IV-12A).

The history of RSL change in Alaska is defined by an emergent coast, a consequence of both plate convergence and post-glacial rebound. In contrast to the contiguous U.S. coastal regions, sea level in Alaska is either near-zero or falling relative to the land – falling at a very high rate at Juneau and Yakutat, Alaska (Fig. 12B).

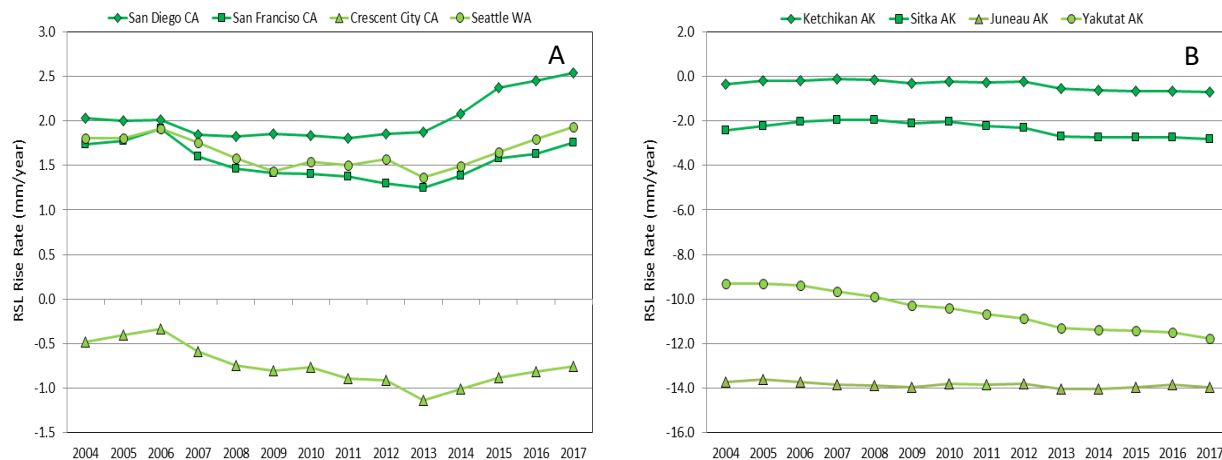


Figure IV-12. RSL rise rate histories at four U.S. West Coast locations in California and Washington (A) and four locations in Alaska to the north (B). Each data point represents rise rate from 1969 through the year indicated.

While negative RSL rise rates characterize much of Alaska, the central West Coast region from California to Washington state has experienced both rise and fall rates of relatively low magnitude (Fig. IV-12A). With the GMSL rise rate reported as 2.8 to 3.6 mm/year over 1993-2010 (IPCC, 2013) this raises the question: What has prevented a similar RSL rate of rise in the region during this time? Aside from coastal emergence as a possible factor at some locations (e.g., Crescent City, California), the long-lived Pacific Decadal Oscillation (PDO) appears to have a role here through its connection with the earth's foremost climate driver, the El Niño Southern Oscillation (ENSO), as described by Newman, Compo, and Alexander (2003). Bromirski et al. (2011) cite a dramatic change in wind stress patterns following a mid-seventies regime shift from the cool to the warm phase of the PDO as a factor contributing to West Coast sea level suppression, noting that acceleration and a resurgent RSL rise could soon occur following an expected shift to the PDO cool phase.

Figure IV-13A suggests that Bromirski et al. (2011) may be correct in their prediction of renewed RSL rise given recent trends toward acceleration. The figure shows persistent RSL deceleration up until a slight RSL acceleration is found in the 1969-2015 record at San Diego, California, followed by Seattle, Washington, whose 1969-2016 data point crosses the zero threshold. These minor crossing points by themselves, it should be noted, are statistically not different from zero. However, taking all points together the upward trends shown in Fig. IV-13A are revealing – especially at San Diego (highlighted in blue) where a trend toward acceleration beginning at slightly less than  $-0.3 \text{ mm/year}^2$  moves upward in value toward its zero-crossing point in an almost straight line. After 2013, the remaining three stations north of San Diego do the same in a highly coherent pattern. Much less coherent are the trends shown for the four locations in Alaska, three of which are now converging to about  $-0.1 \text{ mm/year}^2$  with one (Yakutat, Alaska, highlighted in blue) oscillating around  $-0.4 \text{ mm/year}^2$  (Fig. IV-13B).

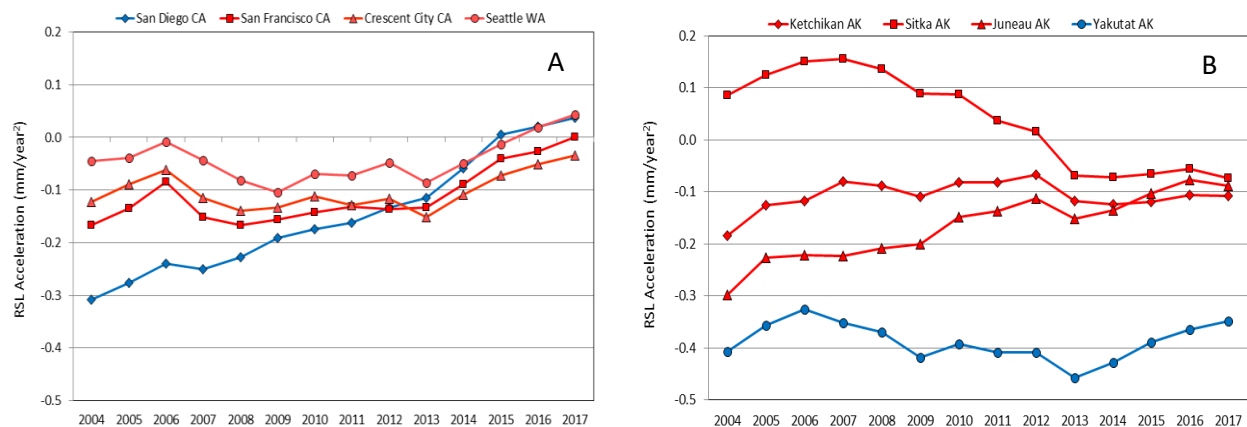


Figure IV-13. RSL acceleration histories at four U.S. West Coast locations in California and Washington (A) and four locations in Alaska to the north (B). Each data point represents acceleration from 1969 through the year indicated.

RSL rise rate histories for the central U.S. West Coast are very similar from San Diego, California, to Seattle Washington, ignoring rise rate magnitude (Fig. IV-14). Their common pattern, flatness or gentle decline followed by a synchronous upturn in 2013, suggests decadal signal modulation but may also reflect a more persistent upward trend based on the strength of the rise in acceleration after 2013 (Fig. IV-15). If so, this implies that, except for Alaska, West Coast RSL acceleration may soon see a shift in magnitude from mostly negative to mostly positive, which will further enhanced the magnitude of RSL rise rates. As for Alaska, its history of RSL fall will no doubt continue for compelling tectonic reasons as well as glacial isostatic adjustments.

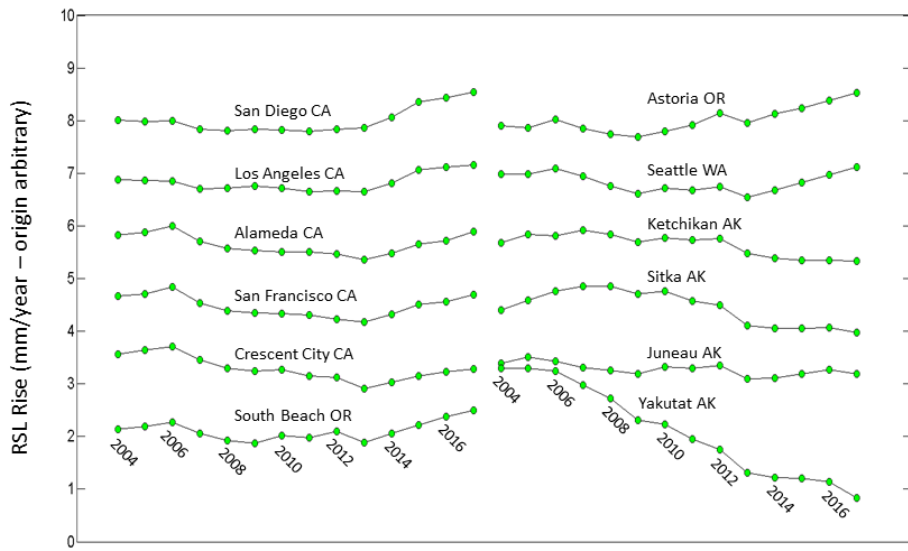


Figure IV-14. RSL rise rate histories at twelve U.S. West Coast locations from 1969-2004 to 1969-2017. Arbitrary origin compares acceleration similarity rather than magnitude.

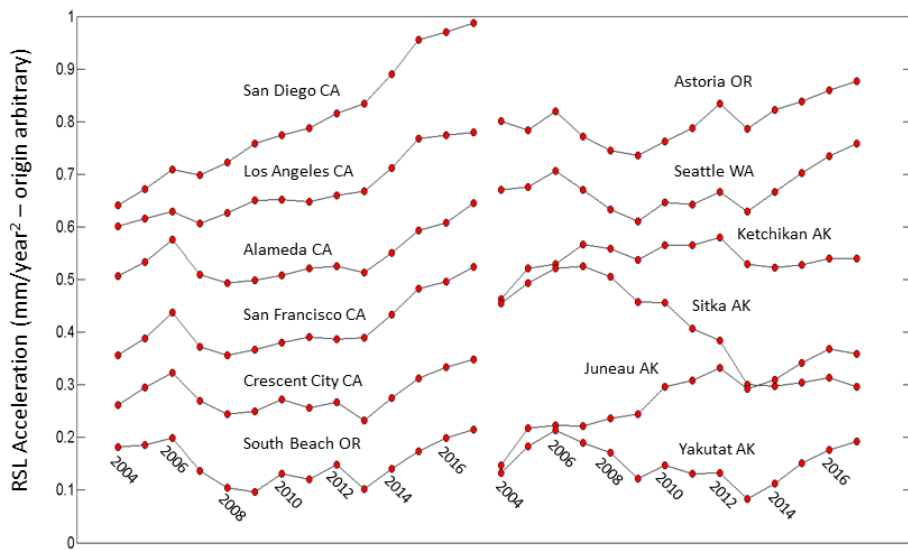


Figure IV-15. RSL acceleration histories at twelve U.S. West Coast locations from 1969-2004 to 1969-2017. Arbitrary origin compares acceleration similarity rather than magnitude.

Factor Analysis of Trend Similarity - Varying degrees of compositional similarity are noted in the sea level histories introduced in this section. Where a high degree of similarity is found between locations within a given coastal region – or sub-region – it may be assumed that the geophysical processes governing sea level change there are correspondingly uniform. Moreover, considering MMSL observations from each location to be a random sample of sea level change in the region, greater compositional similarity lends added confidence in the overall pattern of RSL trends revealed by the observations. These patterns can be compared and contrasted using factor analysis.

The type of factor analysis employed here, termed Q-mode, examines the structure of a data matrix using eigenvectors to determine the relationship between locations based on their sea level histories. The analysis permits each location to be represented graphically as a vector positioned by *factor loadings* on a limited set (usually two or three) of independent (mutually-orthogonal) vectors – the factors that best explain the variation in the data. A detailed description of the analytical methods employed, including factor rotation, is presented in Appendix D.

East Coast Rise Rates: Figure IV-16 shows the relationship between U.S. East Coast locations based on rotated factor loadings derived from an analysis of their respective RSL rise rate histories using a three-factor solution. In Fig. IV-16A Jacksonville, Florida, ‘loads’ highest on factor 1 whereas Portland, Maine, projects highest on factor 2. Very little variation among locations is shown by the loadings on factor 3, all of which occur near the factor origin (Fig. IV-16B).

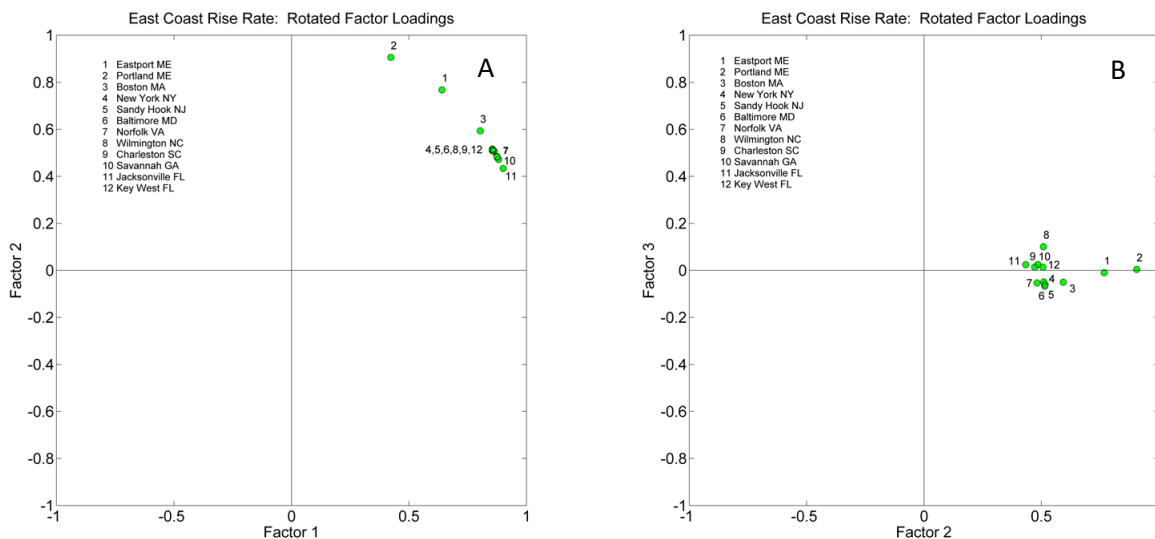


Figure IV-16. Plot of rotated loadings on factors 1-2 (A) and factors 2-3 (B) for RSL rise rate histories observed at twelve East Coast locations.

As explained in Appendix D, the factors used here are orthogonal vectors positioned within a multi-dimensional coordinate system in which the coordinates are the set of variables measured at each location; i.e., the fourteen RSL rise rates or *scores* comprising a sea level history.

Figure IV-17 contains a plot of the scores for the first two factors in Fig. IV-16B. Known as *end-members*, they are seen to be a pair of hypothetical sea level rise rate histories with the further attribute of being completely independent of one another as well as the third factor (not shown). Comparing these end-member histories, Fig. IV-5 shows the similarity between Jacksonville and factor 1, Portland and factor 2, is readily apparent – similar but not identical unless and until the location vector has a loading of one (1) on the factor in question.

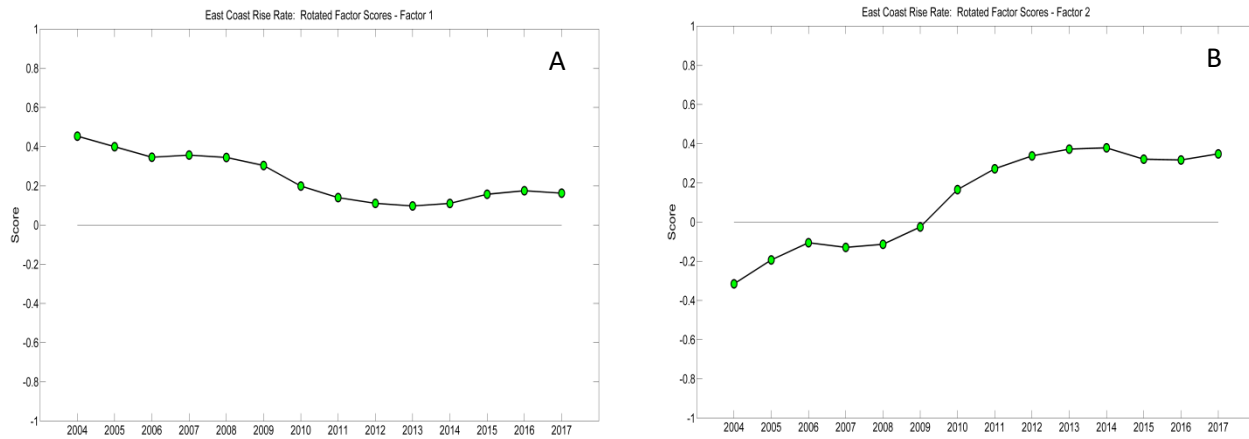


Figure IV-17. Rotated scores for factor 1 (A) and factor 2 (B) derived from RSL rise rate histories at U.S. East Coast locations using MMSL observations from 1969 through the year indicated.

East Coast Acceleration: Factor loadings for East Coast RSL acceleration histories (Fig. IV-18) reveal a very high degree of similarity as well as a loading of almost 1 (on factor 1) for the seven locations north of Cape Hatteras (Fig. IV-1). Locations 8 through 11 are less similar in their loadings on factor 2 with location 12 (Key West) loading highest on factor 3 – the outlier among the twelve locations.

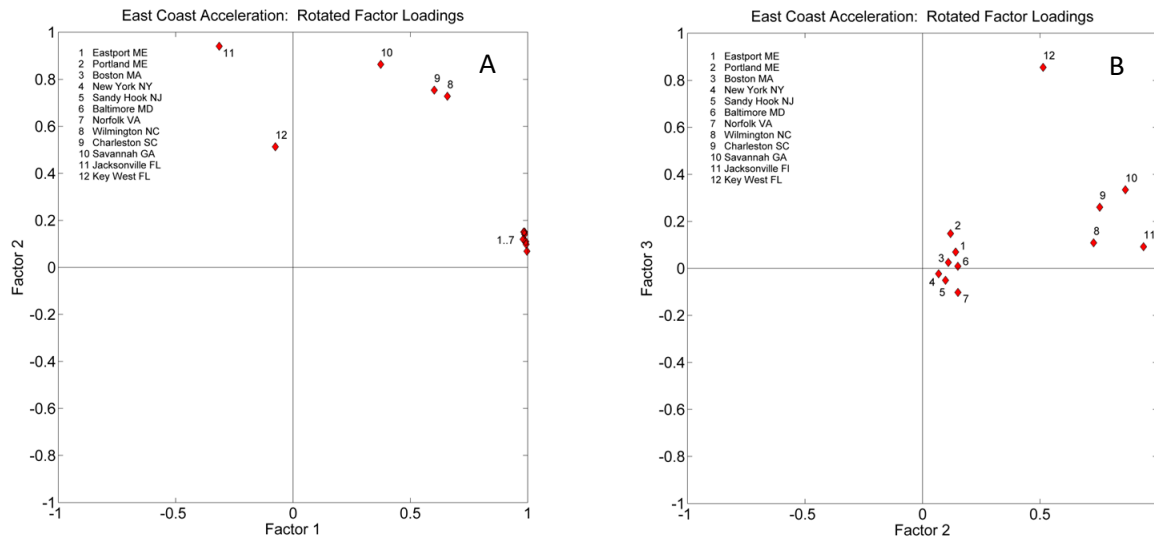


Figure IV-18. Rotated loadings for factors 1-2 (A) and factors 2-3 (B) derived from RSL acceleration histories at twelve U.S. East Coast locations.

Scores for the three factors shown in Fig. IV-18 above are presented in Fig. IV-19. In view of loadings uniformly near 1 on factor 1, the scores for factor 1 (Fig. IV-19A) could very well stand as the one RSL acceleration history best representing the entire U.S. northeast coastal sub-region from 1969 through 2017, subject to differences in magnitude. Although the loadings on factor 2 are not as high, the scores for factor 2 yield a reasonable characterization of the RSL acceleration history at all U.S. southeast locations except for Key West, Florida – a location that, as will be shown, properly belongs to the U.S. Gulf Coast region in terms of its history of sea level change.

In sum, the factor analysis just presented supports the hypothesis that U.S. East Coast rise rate and corresponding acceleration histories since 1969 have been modulated over time but with a  $180^\circ$  difference in phase between the northeast and southeast sub-regions, respectively, north and south of Cape Hatteras, North Carolina. This is most evident in the factor scores for RSL acceleration presented in Figs. IV-19A and IV-19B.

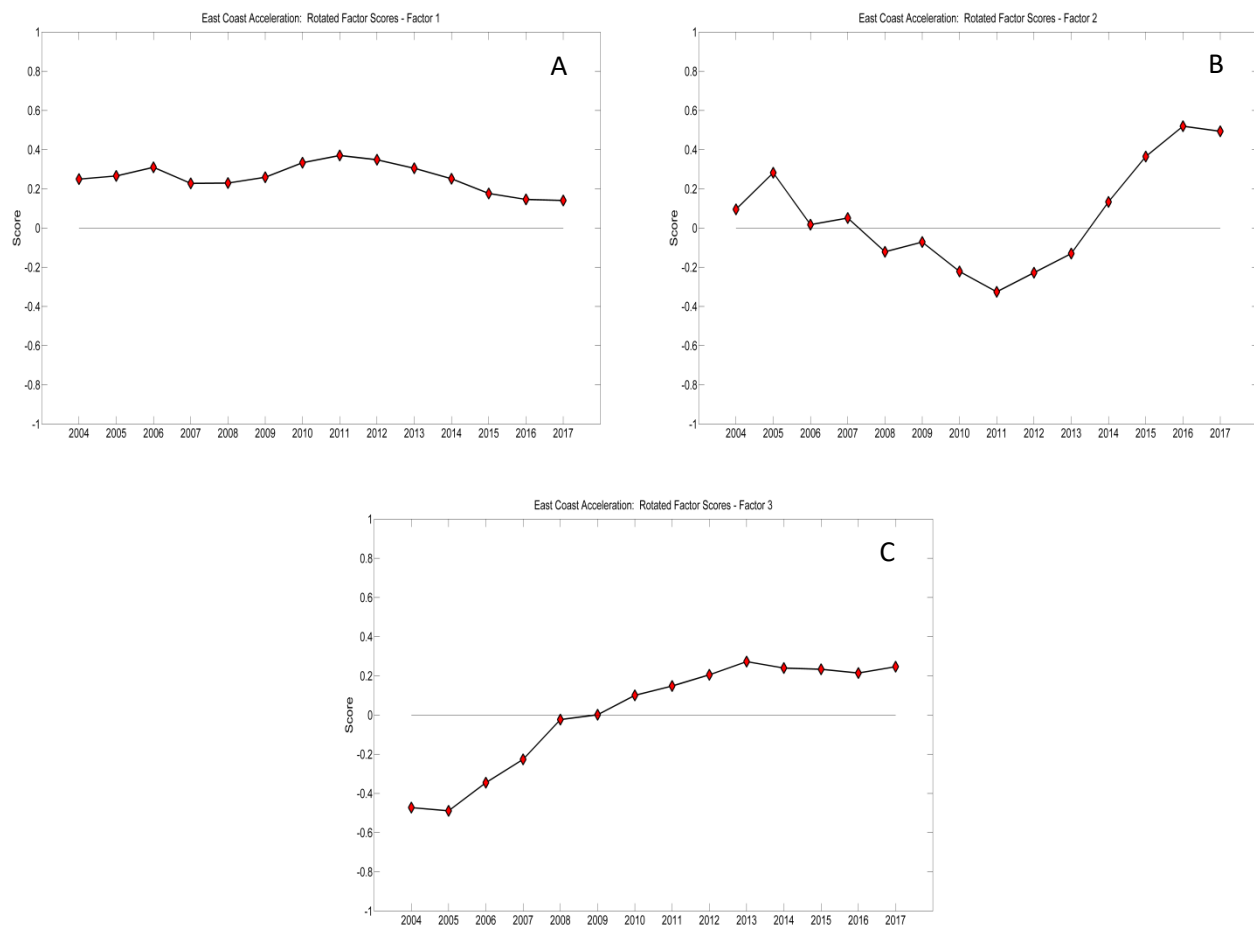


Figure IV-19. Rotated scores for factor 1 (A), factor 2 (B) and factor 3 (C) derived from RSL acceleration histories at U.S. East Coast locations using MMSL observations from 1969 through the year indicated.

**Gulf Coast Rise Rates:** Sea level change along the U.S. Gulf Coast is somewhat unique. Q-mode factor analysis applied to RSL rise rate histories at the nine locations selected for the present study fails to effectively distinguish more than one factor (the reason for this is discussed in Appendix D). The factor loadings shown in Fig. IV-20 nevertheless provide useful information about the order of similitude among locations – the contrast between Cedar Key-Pensacola-Naples and Grand Isle-Galveston-Port Isabel is noticeable in both Fig. IV-7 and Fig. IV-20.

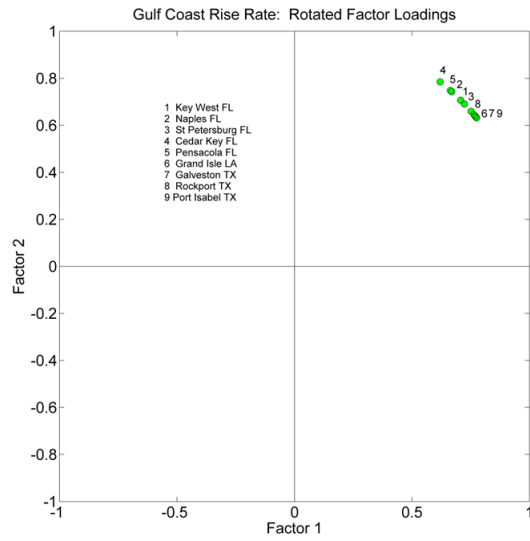


Figure IV-20. Rotated loadings for factors 1-2 derived from RSL rise rate histories at eight U.S. Gulf Coast locations plus Key West.

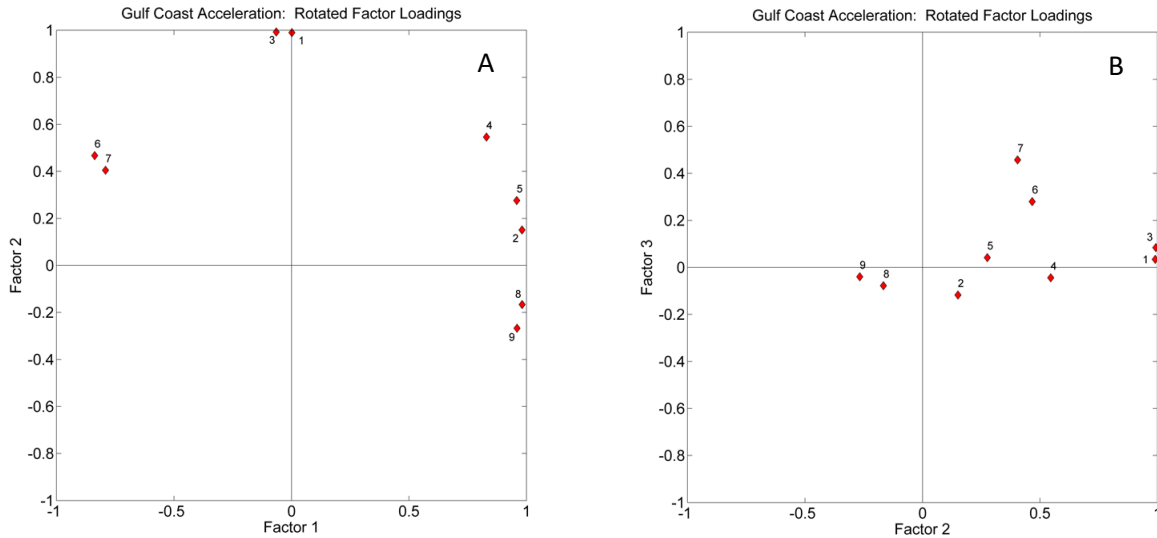


Figure IV-21. Rotated loadings for factors 1-2 (A) and factors 2-3 (B) derived from RSL acceleration histories at eight U.S. Gulf Coast locations plus Key West FL using MMSL observations from 1969 through the year indicated.

**Gulf Coast Acceleration:** More than one factor is found in the analysis of Gulf Coast RSL acceleration histories. As seen in Fig. IV-21B above, Key West, Florida, has a loading of 1 on factor 2, which implies that the scores for factor 2 (Fig. IV-22B) should be identical, except for scaling, to the RSL acceleration history for Key West shown in Fig. IV-8. This is in fact the case, making Key West an end-member for Gulf Coast acceleration history with St. Petersburg, Florida, a close second. Both of these locations on the eastern side of the Gulf exhibit steadily increasing acceleration. Other locations in Fig. IV-21 have high loadings on factor 1 whose scores (Fig. IV-22A) indicate an initial decrease followed by steady acceleration increasing only in the last three years – in sharp contrast to Key West and St. Petersburg. These include nearby Naples, Cedar Key and Pensacola on Florida’s west coast as well as Rockport and Port Isabel on the south Texas coast, attesting to the complexity of vertical land movement (VLM) in this region.

A more pronounced drop-and-rise is seen in the scores for factor 3 (Fig. IV-22C). Of the nine Gulf Coast locations in Fig. IV-21, only Grand Isle, Louisiana, and Galveston, Texas, show a tendency toward this end-member. As previously shown in Fig. IV-9B, these two locations, in addition to Rockport and Port Isabel in Texas, have near-zero RSL acceleration at present.

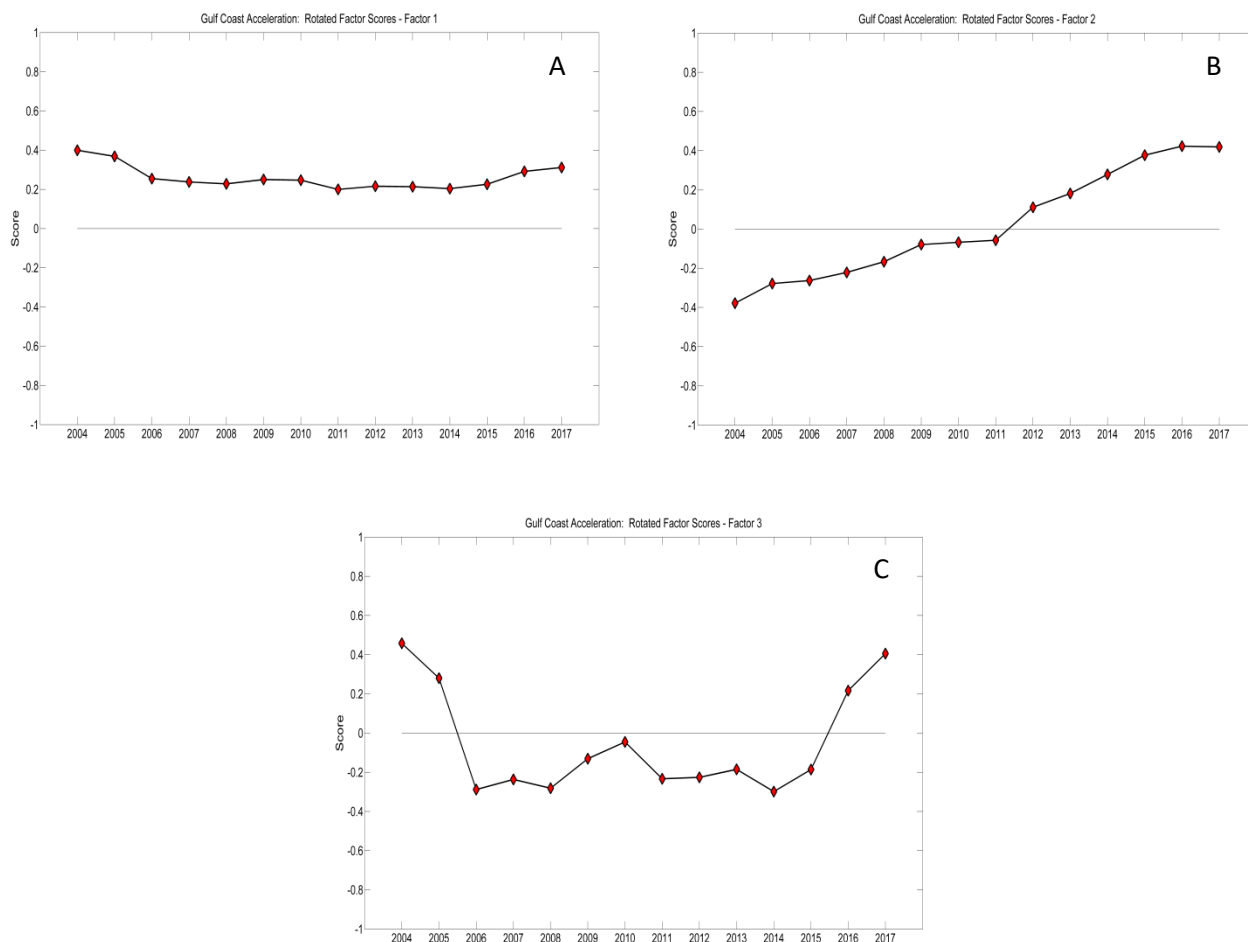


Figure IV-22. Rotated scores for factor 1 (A), factor 2 (B) and factor 3 (C) derived from RSL acceleration histories at U.S. Gulf Coast locations.

**West Coast Rise Rates:** Factor analysis of West Coast RSL rise rates separates locations into two distinct groups with one obvious outlier as shown in Fig. IV-23. The outlier (Astoria, Oregon) has a high loading on factor 2 whereas the other eleven locations are separated into two groups by factors 1 and 3. The first group, with loadings highest on factor 1 and intermediate (negative) loadings on factor 3, include west coast locations from San Diego, California, to Seattle, Washington, with one exception: Crescent City, California. Crescent City falls into the second group that includes four locations on the emergent coast of Alaska, suggesting that Crescent City also has experienced significant uplift. Scores for factors 1-3 (Fig. IV-24) emphasize the upturn and near-linear increase in RSL rise rates since 2013, a feature previously noted on p. IV-10.

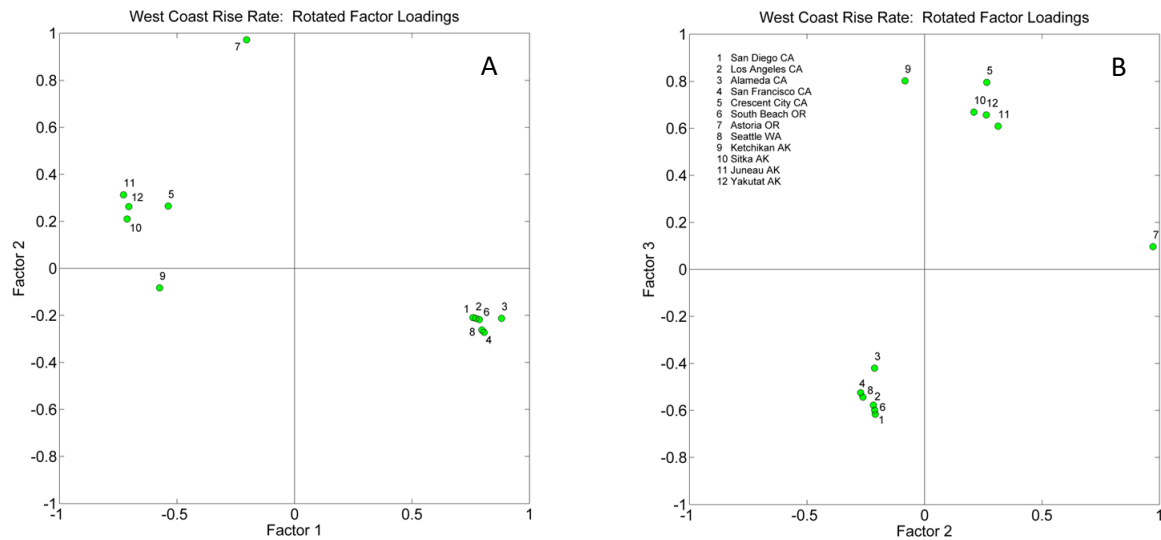


Figure IV-23. Plot of rotated loadings on factors 1-2 (A) and factors 2-3 (B) derived from RSL rise rate histories at twelve West Coast locations.

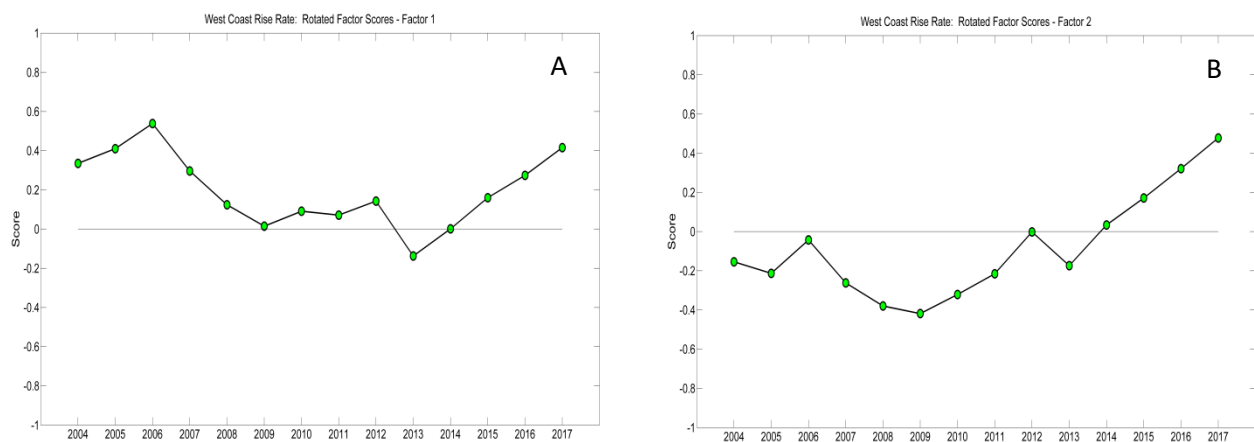


Figure IV-24. Rotated scores for factor 1 (A), factor 2 (B) and factor 3 (C) derived from RSL rise rate histories at U.S. West Coast locations using MMSL observations from 1969 through the year indicated.

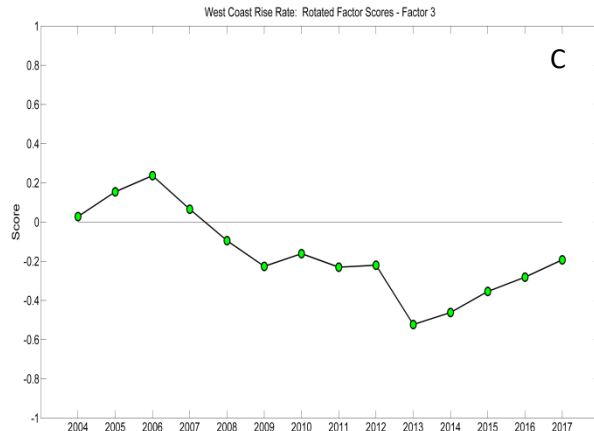


Figure IV-24. West Coast rise rate rotated factor scores (continued)

West Coast Acceleration: Unlike rise rates, factor loadings for acceleration at West Coast locations are not as tightly clustered – or divided into groups that hint at alignment with a particular sub-region. Nine locations have their highest loadings on factor 1, combined with low-to-intermediate negative loadings on factors 2 and 3; two locations in Oregon (South Beach and Astoria) have high loadings on factor 2 with Sitka, Alaska, displaying a high loading on factor 3.

Scores for West Coast acceleration factors (Fig. IV-26) also highlight a ubiquitous 2013 upturn – even at Sitka, Alaska, where RSL acceleration was in sharp decline from 2006 to 2013 before beginning a modest rise, a trend captured by factor 3. Factors 1 and 2, though compositionally independent (their vectors in variable space are orthogonal), nevertheless display a resemblance in the position of highs and lows in the sequence of their respective scores – a sign that nearby locations (as vectors in factor space) are a mixture mostly of factors 1 and 2.

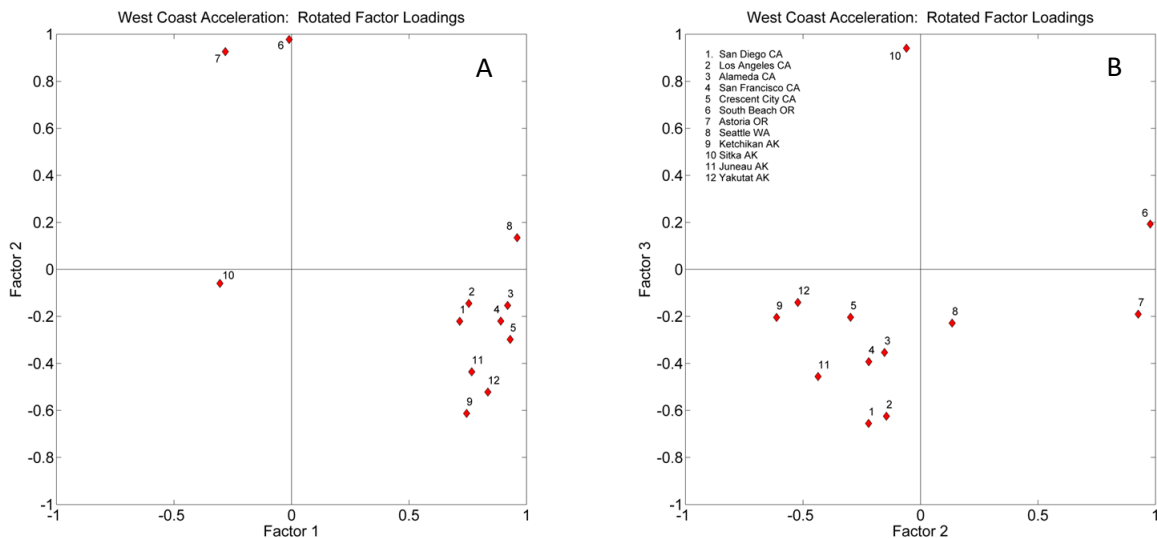


Figure IV-25. Plot of rotated loadings on factors 1-2 (A) and factors 2-3 (B) for RSL acceleration histories observed at twelve U.S. West Coast locations.

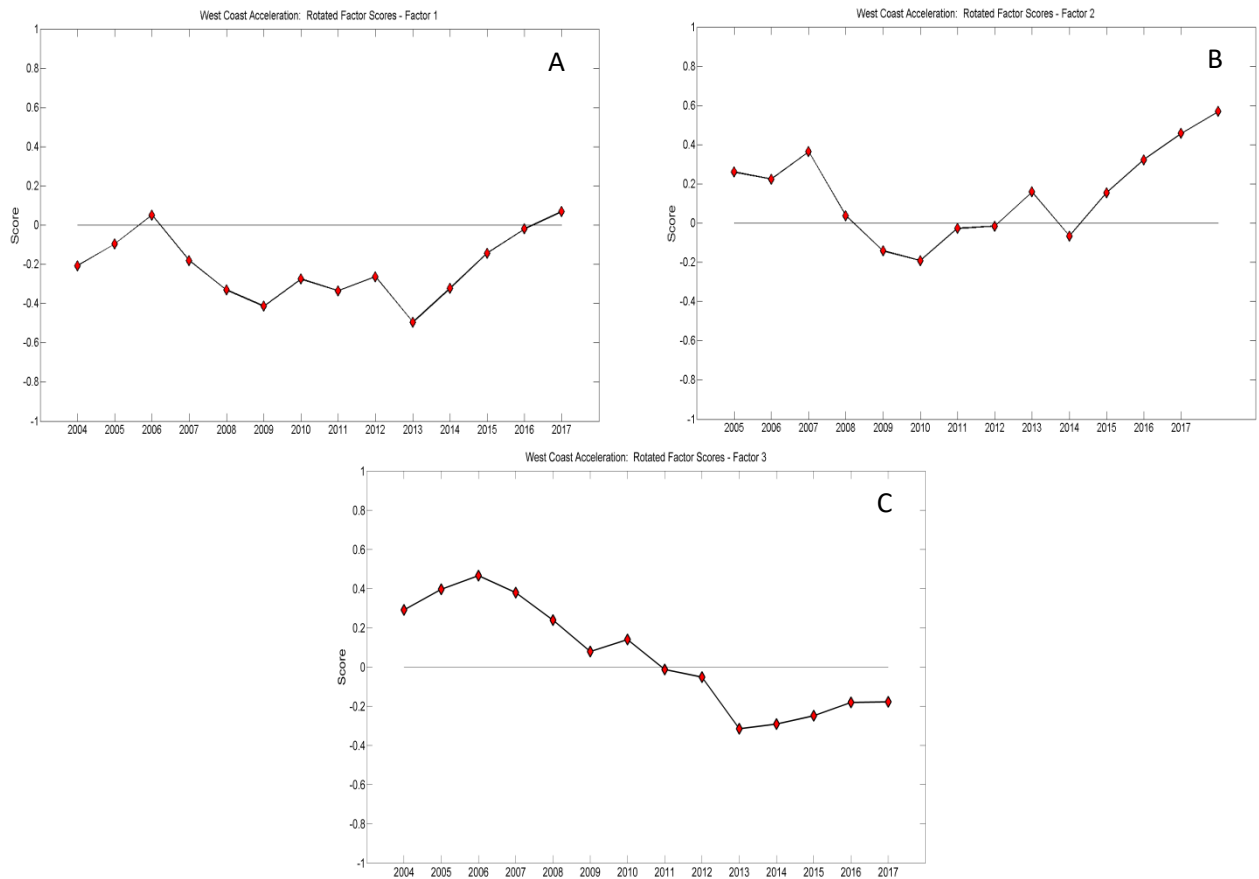


Figure IV-26. Rotated scores for factor 1 (A), factor 2 (B) and factor 3 (C) derived from RSL acceleration histories at U.S. West Coast locations using MMSL observations from 1969 through the year indicated

Summation: Q-mode factor analysis, a computational technique used here to explore the relationship between U.S. coastal locations by means of their respective relative sea level (RSL) rise rate and acceleration histories, offers new insight into trends unfolding in the Anthropocene epoch based on recent observations. Far from a display of randomness, similar groups are found within each coastal regional that mirror the geophysical processes governing RSL trends locally. One of the most obvious groupings is found between the sub-regions of the U.S. East Coast north and south of Cape Hatteras, North Carolina; despite differences in magnitude, RSL acceleration histories at seven locations from Maine to Virginia are extremely uniform and therefore offer valuable guidance and insight on near-term RSL projections within this sub-region. Sub-regions are also found on the U.S. Gulf Coast that reflect the complex task of evaluating the likely contribution of acceleration to observed rise rates, and consequent near-term RSL projections, due to ongoing vertical land movement (VLM) resulting from mineral extractions (ground water and hydrocarbons) and associated faulting. On the U.S. West Coast, very recent trends away from RSL deceleration toward RSL acceleration appear likely to initiate a new phase of RSL rise in locations where sea level trends have been flat until now. Compositional end-members derived as factors through Q-mode factor analysis will continue to serve as references against which future sea level histories can be compared as new observations become available.

## V. PROCESSES AFFECTING REGIONAL TRENDS

### Background of processes that affect rates of sea-level rise and acceleration

A number of processes have been linked to long-term variations in sea level rise. These vary in spatial scale, with some processes acting on a very local level, while others affect global rise rates.

Two main processes explain global sea level rise: steric and eustatic. Steric sea-level changes are changes in ocean volume resulting from thermal expansion (thermosteric) and salinity (halosteric) changes. One study suggests that geographic variations in these processes are responsible for some of the variation in relative sea level rise seen globally (Cazenave and Nerem, 2004). Eustatic sea level change results from the addition of water mass to the oceans from melting ice sheets and glaciers, as well as atmospheric exchange from land storage. Gravitational and rotational processes can cause this additional water to distribute unevenly (Mitrovica et al., 2009), also contributing to the variation in relative sea level rise seen globally. These steric and eustatic variations suggest that different water bodies may have different rates of sea level rise; therefore, in this report we examine each coastline separately and compare only between stations in the same body of water.

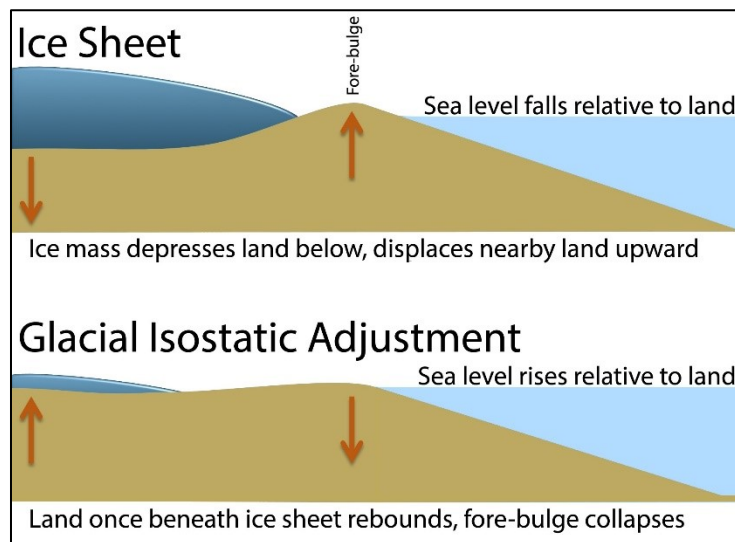


Figure V-1. Glacial isostatic adjustment.

Regional processes affect sea level rise rates on portions of a coastline and can lead to sea level variability on interannual-to-decadal time scales. These processes include vertical land movement (VLM) due to glacial isostatic adjustment (GIA), inverted barometer effects, and ocean dynamics, frequently related to atmospheric shifts. GIA is the response of the earth's surface to the unloading of ice sheet and glacial mass, resulting in upward motion (rebounding) in areas previously covered by ice and subsidence of the land surface in adjoining areas (glacial forebulge collapse, Figure V-1). The inverted barometer effect is the response of ocean height to atmospheric pressure. Consistent wind stress patterns can produce a similar effect. Both effects are more related to temporal variability than long-term sea level changes, but they may affect the

trends seen in historic gauge analyses and therefore need to be considered. Ocean dynamics can also contribute to temporal variability, but some shifts, such as changes in the Atlantic Meridional Overturning Circulation, are hypothesized to be trajectory responses to climate change rather than temporal variations (Jackson et al., 2015).

Relative sea level (RSL) rise can also be affected by local subsidence due to groundwater/hydrocarbon withdrawal or tectonic faulting and uplift (other VLM processes). These processes are likely to affect only one or two tide stations in the same way, and therefore, contribute greatly to variation in RSL rise along a coast. Understanding the magnitude and impact of this process is critical for adaptation and management efforts, since it can be relatively easily controlled. Past subsidence can also greatly impact RSL trends and must be carefully considered when choosing the appropriate length of record to analyze. Important processes are summarized in Table V-1.

Table V-1. RSL trends, acceleration patterns, variability, and relative scale charted for important processes of:  
 1) steric expansion, 2) ocean dynamics, 3) Greenland and Antarctic ice sheet melting, 4) glacial isostatic adjustment, 5) groundwater and hydrocarbon storage changes, 6) inverted barometer, and  
 7) atmospheric cycles.

Processes	Dominant signal			Scale
	Rise/Fall	Acceleration	Variability	
Steric	◊			Global
Ocean dynamics		◊	◊	Regional
Greenland/Antarctic ice sheet melting		◊		Global
Glacial isostatic adjustment	◊			Regional
Groundwater/hydrocarbon storage changes		◊		Local
Inverted barometer		?	◊	Regional
Atmospheric cycles			◊	Regional/Global

## A. East Coast Stations

In addition to steric changes, dominant processes affecting sea level rise variability along the U.S. East Coast are GIA (Karegar et al., 2017; Sella et al., 2007), Greenland ice sheet (GIS)/Antarctic ice sheet (AIS) (Davis and Vinogradova, 2017; Mitrovica et al., 2001), groundwater storage/withdrawal, (Karegar et al., 2017; Karegar et al., 2016) and circulation patterns (Park and Sweet, 2015; Yin and Goddard, 2013; Ezer et al., 2013). Of these processes, all but GIA have undergone recent changes in magnitude and are considered to be contributing to Anthropocene RSL acceleration. GIA has been contributing to subsidence/uplift at steady rate throughout the Anthropocene.

The table below shows the variability in magnitude of each process along the coast that results in varying rates of RSL rise. Many of these rates are difficult to measure, and different assessments of their contribution to RSL rise can be found in the literature. Therefore, we are identifying the

trends in the processes as reflected in the primary literature but not attempting to quantify their contribution. Impacts of these processes to East Coast tide gauge records are summarized in Table V-2 and explicitly discussed in the following sub-sections.

Table V-2. Variability in magnitude of important processes to RSL along the U.S. East Coast. The asterisk (\*) indicates that no specific information can be found.

Stations	Steric	Ocean dynamics	Greenland ice sheet melting	Antarctic ice sheet melting	Vertical Land Movement		
					Glacial isostatic adjustment	Groundwater /hydrocarbon storage changes	Other factors
<b>Eastport, ME</b>	rising	unimportant	low accelerating	accelerating	near zero	bulging?	minor IB?
<b>Portland, ME</b>	rising	unimportant	low accelerating	accelerating	near zero	bulging	minor IB
<b>Boston, MA</b>	rising	unimportant	low accelerating	accelerating	near zero	unimportant	minor IB
<b>New York, NY</b>	rising	unimportant	low-moderate accelerating	accelerating	rising	unimportant	minor IB
<b>Sandy Hook, NJ</b>	rising	unimportant	moderate accelerating	accelerating	rising	current impact?	minor IB
<b>Baltimore, MD</b>	rising	moderate accelerating	moderate accelerating	accelerating	GIA max?	not impt	unimportant
<b>Norfolk, VA</b>	rising	high accelerating	moderate accelerating	accelerating	GIA max?	withdrawal recovery	unimportant
<b>Wilmington, NC</b>	rising	high accelerating	moderate accelerating	accelerating	rising	withdrawal recovery	unimportant
<b>Charleston, SC</b>	rising	moderate accelerating	mod-high accelerating	accelerating	rising	withdrawal recovery	unimportant
<b>Fort Pulaski, GA</b>	rising	unimportant	mod-high accelerating	accelerating	rising	unimportant	unimportant
<b>Fernandina Beach, FL</b>	rising	unimportant	high accelerating	accelerating	*	unimportant	unimportant
<b>Key West, FL</b>	rising	unimportant	high accelerating	accelerating	*	unimportant	unimportant

### Ocean dynamics

For stations south of Chesapeake Bay, variations in the Gulf Stream have been cited as an important control of coastal sea level, with a weaker current resulting in higher sea levels (Ezer et al., 2013). The magnitude of the impact is greatest for Cape Hatteras (between Norfolk, Virginia and Wilmington, North Carolina) and decreases northward (Ezer et al., 2013). Acceleration in this area has also been linked to the Atlantic Multidecadal Oscillation, North Atlantic Oscillation, and Gulf Stream North Wall indices (Kopp, 2013). The long-term prognosis for changes in these dynamic processes are yet unresolved, hampering projections.

### Greenland and Antarctic ice-sheet melting

Mass loss from ice sheets results in an increase in sea level due to the conversion of ice to water. It also affects sea level because the melted, smaller ice sheet exerts less gravitational attraction

on adjacent waters. The Gravity Recovery and Climate Experiment (GRACE) measures changes in ice sheet mass that show significant acceleration of loss in both the GIS and AIS (Velicogna et al., 2014). Results of GRACE-based modeling show the joint contribution of ice sheet melting as 0.07–0.15 mm/year along the East Coast stations, decreasing steadily from Florida to Maine (Davis and Vinogradova, 2017). The AIS contribution is distributed evenly across the East Coast stations, affecting acceleration but not contributing to spatial variability in trends of sea level rise (Davis and Vinogradova, 2017). In contrast, GIS sea level contributions vary spatially along the East Coast from -0.03 mm/year in the north to 0.1 mm/year in Florida (Davis and Vinogradova, 2017) due to combined effects of self-attraction and gravitational loading from the loss of mass (Mitrovica et al., 2001). Combined GIS and AIS contributions are suggested to exceed contributions to sea level acceleration from ocean dynamics (including steric) and inverted barometer effects at all stations south of Sandy Hook, New Jersey and become relatively more important south of Norfolk, Virginia (Davis and Vinogradova, 2017). In addition, the originating location of the glacial melt may affect the distribution of its contribution to relative sea level rise. For example, GIS contributions to sea level rise at the New York gauge are connected to melting at Petermann Glacier, Humboldt Glacier, and North-East Greenland Ice Stream (Larour et al., 2017).

#### Vertical land movement: Glacial isostatic adjustment (GIA)

Vertical land movement is measured through both geologic records (giving long-term averages) and GPS (giving Anthropocene movements). GIA is a long-term process and therefore is captured in both datasets, although the GPS record also captures shorter VLM processes (see next section). According to analyses of these records, all East Coast tide stations are in areas of subsidence that has been attributed in part to GIA, except for Eastport, Maine, Portland, Maine, and Boston, Massachusetts, which fall near the zero line of subsidence, and Fernandina Beach, Florida, which vertical GPS suggests is slightly uplifting but not necessarily due to GIA (Sella et al., 2007). Models of GIA recovery, based on GPS measurements suggest that maximum subsidence due to GIA is found around 39°N and is estimated to be 1.5 mm/year (Karegar et al., 2017).

#### Vertical land movement: Changes from water storage/withdrawal

According to Karegar et al. (2017), there are two anomalies in the VLM record (based on geological and GPS records) that suggest an influence of water storage and withdrawal practices. A ‘southern anomaly’ is found between 37.5°N and 32.5°N, where Anthropocene subsidence exceeds geologic subsidence rates, resulting in the highest rates of GPS-measured subsidence for stations in Norfolk, Virginia, Wilmington, North Carolina, and Charleston, South Carolina. This is attributed to excessive groundwater withdrawal between the late 1970s and early 2000, followed by a recovery trajectory. The ‘northern anomaly’ is between 45°N and 43°N where Anthropocene uplift is found in an area with geologic subsidence. This impacts stations in Eastport, Maine and Portland Maine and is attributed to geologic loading from water storage above a dam. Johnson et al. (2018) hypothesize that groundwater withdrawal (from a pumping station ~2 km away) is the second most important process (after GIA) affecting RSL rates at Sandy Hook, New Jersey.

#### Other factors

The inverted barometer effect (IB) has been put forward as an important control of inter-annual sea level variation along the East Coast (Piecuch and Ponte, 2015). There is some implication that it may be affecting sea level rise projections due to recent low-pressure systems that resulted in extreme sea level rise events. Piecuch and Ponte (2015) suggest that IB may be responsible for ~50% of sea level rise in New England during 2008 and 2010 and 10–30% of multidecadal sea level accelerations in the mid-Atlantic “hot spot” (Boon, 2012; Ezer and Corlett, 2012; Sallenger et al., 2012). However, when the IB contribution to Anthropocene sea level rise acceleration was evaluated, both its contribution and variability were small (0.0–0.05 mm/year rising from south to north; Davis and Vinogradova, 2017). Therefore, we consider this to be a more important control of temporal variability than sea level rise.

## B. Gulf Coast Stations

In addition to steric changes, the dominant process affecting sea level rise variability along the Gulf Coast of the United States is groundwater and hydrocarbon withdrawal (Gabrysch and Coplin, 1990; White and Tremblay, 1995; Morton et al., 2006; Kolker et al., 2011). Groundwater and hydrocarbon withdrawal rates have undergone multiple shifts in magnitude between 1969 and 2017, affecting measured changes in sea level rise acceleration.

Table V-3 shows that variability in magnitude of each process along the coast results in varying rates of RSL rise. Many of these rates are difficult to measure, and different assessments of their contribution to RSL rise can be found in the literature. Therefore, we are identifying the trends in the processes as reflected in the primary literature but not attempting to quantify their contribution. Impacts of each process to Gulf Coast tide gauge records are summarized in Table V-3 and explicitly discussed in the following sub-sections.

Table V-3. Variability in magnitude of important processes to RSL along the U.S. Gulf Coast. The asterisk (\*) indicates that no specific information can be found.

Stations	Vertical land motion						
	Steric	Ocean dynamics	Greenland ice sheet melting	Antarctic ice sheet melting	Glacial isostatic adjustment	Groundwater/hydrocarbon storage changes	Other factors
Key West, FL	rising	unimportant	accelerating	accelerating	*	*	*
Naples, FL	rising	unimportant	accelerating	accelerating	minimal	*	*
St. Petersburg, FL	rising	unimportant	accelerating	accelerating	minimal	*	*
Pensacola, FL	rising	unimportant	accelerating	accelerating	minimal	unimportant	*
Grand Isle, LA	rising	unimportant	accelerating	accelerating	minimal	withdrawal recovery	thick Holocene sediment
Galveston Pier 21, TX	rising	unimportant	accelerating	accelerating	minimal	withdrawal recovery	seismic?
Rockport, TX	rising	unimportant	accelerating	accelerating	minimal	minimal impact	seismic?
Port Isabel, TX	rising	unimportant	accelerating	accelerating	minimal	minimal impact	seismic?

## Ocean dynamics

Global models suggest that ocean dynamics will contribute little to variability in sea level trends along the Gulf Coast stations (Kopp et al., 2014). While the along-shore currents in the Gulf are unlikely to contribute much to variability among Gulf Coast stations, it is worth noting that analysis of past trends will be unable to fully capture the dynamics changes incurred after aperiodic anomalies (such as hurricanes). Hurricanes are likely to impact the land–water interface due to the warmer waters of the Gulf increasing the intensity of land-falling storms in this region. This potentially could shift the currently-projected minimal variability between Gulf Coast stations to observe a greater perceived rate of RSL rise in areas frequented by future storm systems, such as Texas and Louisiana.

In a Gulf Coast Analysis of National Estuarine Research Reserves, it was noted that a 2-m increase in sea level would result in tidal inundation from Mississippi through the Florida Panhandle to increase by 1472 km<sup>2</sup> (Kidwell et al., 2017). This is equivalent to 20% of the present-day total surface area of the bays within the Eastern Gulf region. Thus, barrier islands in this region are projected to have increased shoreline and dune erosion under higher rates of sea-level rise, suggesting that storm surge response to sea level rise will be an increasingly non-linear issue that is likely to have lasting effects on the Gulf Coast’s future RSL rates.

Kidwell et al. (2017) note in a model analysis that storm surge flooding of developed areas for the Mississippi, Alabama, and Florida Panhandle regions more than double with an overall increase of 138% from present day (282.7 km<sup>2</sup> of flooding) to a 2-m SLR (672.3 km<sup>2</sup> of flooding). In 2017, all hurricanes that made landfall in the U.S. mainland did so in the Gulf Coast, with Harvey, Irma, and Nate. In the case of Hurricane Harvey, GPS data surrounding Houston, Texas, detected a widespread decrease in vertical land movement of more than 2 cm over a 5-day period (van Oldenborgh et al., 2017). This rapid subsidence under the massive weight of the persistent floodwaters coupled with barrier island erosion during Harvey’s passage may affect perceived impacts of RSL at Galveston, Texas differently than other stations along the Gulf in the future, thereby causing ocean dynamics to indirectly contribute to future variability in RSL trends.

## Greenland and Antarctic ice sheet melting

Global models suggest that contributions of the GIS and AIS to sea level rise should not vary along the Gulf Coast stations (Kopp et al., 2014).

## Vertical land movement: Glacial isostatic adjustment (GIA)

The role of GIA along the Gulf Coast has not been well defined. Minimal GIA contribution (0.4 mm/year) has been documented for Pensacola, Florida (Gonzalez and Tornqvist, 2006). Models suggest that GIA may still be a contributor to subsidence along the north central Gulf Coast, making a minimal contribution to most stations in this analysis (Mitrovica and Milne, 2002).

## Vertical land movement: Changes from water storage/withdrawal

Historically, both groundwater withdrawal and hydrocarbon withdrawal have been associated with subsidence in Louisiana and Texas. Groundwater withdrawal in the Galveston, Texas area

resulted in excessive subsidence rates (120 mm/year, 1964–1973; Gabrysich and Coplin, 1990). These rates slowed dramatically following the reduction of groundwater pumping in the early 1970s (Gabrysich and Coplin, 1990). However, those high rates are still captured in the beginning of the sea-level-rise histories presented here.

Continual subsidence was derived from tide gauge records from both Galveston, Texas and Grand Isle, Louisiana from 1950–1990 but with steadily declining subsidence rates following 1970. By 1990, subsidence appears to have effectively stopped (Kolker et al., 2011). This subsidence was linked to oil production for Grand Isle, Louisiana, which began to decline in the 1970s and was minimal by the 1990s, and to groundwater withdrawal for Galveston, Texas (Kolker et al., 2011). Subsidence rates near the points of withdrawal are substantially higher than surrounding areas (Morton et al., 2006), suggesting that Rockport, Texas and Port Isabel, Texas probably did not experience the high levels of subsidence at any point in their history.

#### Other factors

The Texas Gulf coastline has significant faulting, and periodic shifts occur along these faults (White and Tremblay, 1995). The effect of these seismic shifts on tide gauge records has not been examined but potentially could affect acceleration rates. In Galveston, Texas slippage was most active during the period 1960–1970 of the records studied (Kolker et al., 2011). In contrast, the tide gauge station at Pensacola, Florida sits on a stable carbonate platform and is considered to be tectonically stable (Gonzalez and Tornqvist, 2006; Kolker et al., 2011).

Barometric anomalies affect sea levels at Gulf Coast stations. During years of high pressure, resulting wind fields drive water towards the northern Gulf, while in years of low pressure, winds are driven to the south (Kolker et al., 2011).

Sediment loading can affect subsidence. Grand Isle, Louisiana has higher rates of sea level rise than the surrounding Gulf Coast stations, which has been attributed in part to its thick Holocene sediment layer that is thinner in Texas and completely absent in Florida (Penland and Ramsey, 1990).

### **C. West Coast Stations**

In addition to steric changes, the dominant processes affecting sea level rise variability along the West Coast of the United States are GIA (Elliot et al., 2010), tectonic processes (Elliot et al., 2010), and possible suppression of ocean dynamics (Bromirski et al., 2011).

Table V-4 shows that the variability in magnitude of each process along the coast results in varying rates of RSL rise. Many of these rates are difficult to quantify, and different assessments of their contribution to RSL rise can be found in the literature. Therefore, we are identifying the trends in the processes as reflected in the primary literature but not attempting to quantify their contribution. Impacts of each process to West Coast tide gauge records are summarized in the table below and explicitly discussed in the following sub-sections.

Table V-4. Variability in magnitude of important processes to RSL along the U.S. West Coast. The asterisk (\*) indicates that no specific information can be found.

Stations	Steric	Ocean dynamics	Greenland ice sheet melting	Antarctic ice sheet melting	Vertical land motion		
					Glacial isostatic adjustment	Groundwater/hydrocarbon storage changes	Other factors
San Diego, CA	rising	SLR suppressed	rising	rising	unimportant	*	*
Los Angeles, CA	rising	SLR suppressed	rising	rising	unimportant	*	*
Alameda, CA	rising	SLR suppressed	rising	rising	minor subsidence	*	*
San Francisco, CA	rising	SLR suppressed	rising	rising	minor subsidence	*	*
Crescent City, CA	rising	SLR suppressed	rising	rising	minor subsidence	*	*
South Beach, OR	rising	SLR suppressed	rising	rising	minor subsidence	*	*
Astoria, OR	rising	SLR suppressed	minor rising	rising	minor subsidence	*	*
Seattle, WA	rising	SLR suppressed	minor rising	rising	minor subsidence	*	*
Ketchikan, AK	rising	*	minor rising	rising	uplift	*	tectonic
Sitka, AK	rising	*	minor rising	rising	uplift	*	tectonic
Juneau, AK	rising	*	minor rising	rising	uplift	*	tectonic
Yakutat, AK	rising	*	minor rising	rising	uplift	*	tectonic

### Ocean dynamics

A shift in wind stress patterns along the West Coast occurred in the mid-1970s, resulting in a regime shift from cold to warm phases of the Pacific Decadal Oscillation (PDO). It has been suggested that this has been dynamically suppressing sea level rise along this coast since the 1980s (Bromirski et al., 2011). A reversal in this trend would result in an acceleration of sea level rise rates.

### Greenland and Antarctic ice sheet melting

Global models suggest that contributions of the AIS to sea level rise should not vary along the West Coast stations (Mitrovica et al., 2001). However, the GIS does show some variation along the West Coast, with less contribution to Alaska, Washington, and Oregon stations than to California stations (Mitrovica et al., 2001). In addition, mountain glacial melt may contribute more to California stations than Alaska stations, with intermediate contributions in Washington and Oregon (Mitrovica et al., 2001).

### Vertical land movement: Glacial isostatic adjustment (GIA)

Models suggest that GIA may still be a contributor to subsidence along the West Coast, making a minimal contribution to most stations in this analysis and being relatively unimportant in

southern California stations (Mitrovica and Milne, 2002). In Alaska, GIA due to ice-sheet melting following the little ice age has resulted in significant, on-going uplift with peak uplift rates in the Yakutat ice field (Elliot et al., 2010).

#### Vertical land movement: Changes from water storage/withdrawal

Land subsidence associated with groundwater withdrawals was identified along large areas of central California in the 1960s. However, only two near-coast areas were specifically identified: Santa Clara (near San Francisco, California) and Wilmington (near Los Angeles, California) (Poland, 1960). The magnitude of effect (if any) that stretches from these locations to nearby tide gauges, or how that effect would have changed over time is not clear.

#### Other factors

Tectonic effects (post-earthquake deformation) contribute to uplift in parts of Alaska, although these are temporally and spatially variable in magnitude. In southeastern Alaska, tectonic deformation has been found to be less important than the GIA-induced deformation (Sato et al., 2012). In the northwestern part of Alaska, Yakutat Block is colliding with southern Alaska, causing deformation and uplift (Elliot et al., 2010). It is unclear how far-reaching the effect of this collision is along the coastline.

Locally high rates of subsidence (exceeding 10 mm/year) due to compacting of artificial landfill and Holocene mud deposits have been documented in northern California (Shirzaei and Bürgmann, 2018) near the San Francisco and Alameda tide gauges. However, there is extensive spatial variability in the subsidence rates and there has been no suggestion that high subsidence is currently affecting either tide gauge record.

## VI. IMPLICATIONS FOR RISK MANAGEMENT

Relative sea level (RSL) histories and projections can be used to inform management and reduce future flood impacts. RSL histories can be used to help understand which forcing processes are most important to the long-term record and how stations may vary from others along their coast. RSL projections can be used to anticipate future flood risks; allowing accommodation and adaptation measures to be taken. However, there are important considerations to address before using this information: 1) Some of the processes forcing the RSL history are temporally variable, 2) the further a projection reaches into the future, the more uncertainty is inherent in the projection, 3) projections are given as heights above mean sea level (MSL), but sea level varies annually and inter-annually in expected ways. These issues are discussed below, with some practical recommendations for handling them.

RSL histories - The histories show that along a coast, there are certain trends that are fairly coherent between stations, while other trend are unique to one or two stations. It is likely that the coherent trends are attributable to global and regional forcing processes. For the global and many regional forcing processes affecting RSL rise, it is reasonable to consider past trends as informing near-future trends. The local forcing processes, in particular groundwater and hydrocarbon withdrawals, tend to be locally variable and controlled through local management actions. In areas where these processes have greatly contributed to past subsidence (e.g., Grand Isle, Louisiana and Galveston, Texas) great care should be taken in extrapolating sea level histories. A regional process, the potential suppression of the Pacific Decadal Oscillation, requires that California stations also take care extrapolating past trends to the future. Although essentially flat for a long time, recent acceleration trends suggest that RSL projections at these stations may be underestimating future water levels.

Continual monitoring of RSL and comparison to the RSL histories and projections will allow for early detection of changes in the trajectory. RSL projections for 2050 should be updated annually and the history of the shifts in those projections should also be examined to see if any patterns or trends occur.

Projecting RSL - In this study, we extend almost 50 years of historical data into projections for approximately 30 years in the future. Further extension of the past trends into the future is questionable and will result in increasing uncertainty of the projections. RSL histories highlight the importance of decision-making on RSL. Water withdrawal and storage can change local vertical land motion, and these changes can be reversed through further management decisions. In addition, processes such as ice sheet melting are inherently non-linear. If there are management actions requiring longer outlooks (e.g., 2100), climate model projections such as those provided by the National Climate Assessment should be used.

Using RSL projections - The graphs shown in Appendix C give the yearly mean sea level (YMSL) expected in 2050 for both linear and quadratic RSL projections based on 1969-2017 monthly mean sea level (MMSL) observations. Of course water levels both higher and lower than YMSL in the year 2050 will likely occur during any given day; most of this variation will be due to the very predictable astronomical tide. What will not be so predictable, then as now, is the often substantial change in average water level from one month to the next due to weather. A part of this monthly variation is accounted for through the seasonal cycle, which is normally included in tidal predictions as described in Appendix A. The MMSL observations used for the RSL projections in Appendix C, however, have had the seasonal cycle removed.

High Water Vulnerability Index - What is left after the seasonal cycle is removed from an MMSL series is the *non-tidal change* – the part that cannot be predicted well in advance other than through a statistic such as a confidence interval. The *tidal* part consists entirely of water level change that occurs at known tidal frequencies, making it predictable far in advance. A ratio of the two can be formed by dividing the 95% MMSL confidence interval on quadratic projections by the *diurnal tide range* (GT) available for U.S. locations under datums at [www.tidesandcurrents.noaa.gov](http://www.tidesandcurrents.noaa.gov). The dimensionless interval/range ratio, herein called the *High Water Vulnerability Index* (or HiVI), is a measure of the weather-induced RSL change likely to occur at a location compared to a known amount of RSL change due to the astronomical tide. Index values are given for the 32 locations of the present study in Table VI-1.

Table VI-1. MMSL confidence intervals for year 2050 quadratic projections compared to diurnal tide range at selected locations. Intervals listed include 95% of MMSL heights expected in year 2050. High Water Vulnerability Index is the interval/range ratio.

Location	95% MMSL Interval (m)	Diurnal Range (m)	Interval/Range Ratio
Eastport ME	0.20	5.87	0.034
Portland ME	0.24	3.02	0.079
Boston MA	0.25	3.13	0.080
New York NY	0.29	1.59	0.182
Sandy Hook NJ	0.30	1.59	0.189
Baltimore MD	0.30	0.51	0.588
Norfolk VA	0.36	0.84	0.429
Wilmington NC	0.38	1.43	0.266
Charleston SC	0.34	1.76	0.193
Savannah GA	0.36	2.29	0.157
Jacksonville FL	0.39	2.00	0.195
Key West FL	0.24	0.55	0.436
Naples FL	0.22	0.88	0.250
St Petersburg FL	0.22	0.69	0.319
Cedar Key FL	0.27	1.16	0.233
Pensacola FL	0.28	0.38	0.737
Grand Isle LA	0.30	0.32	0.938
Galveston TX	0.39	0.43	0.907
Rockport TX	0.37*	0.31*	1.194*
Port Isabel TX	0.31	0.42	0.738
San Diego CA	0.25	1.75	0.143
Los Angeles CA	0.24	1.67	0.144
Alameda CA	0.33	2.01	0.164
San Francisco CA	0.33	1.78	0.185
Crescent City CA	0.37	2.10	0.176
South Beach OR	0.40	2.54	0.157
Astoria OR	0.44	2.62	0.168
Seattle WA	0.35	3.46	0.101
Ketchikan AK	0.37	4.71	0.079
Sitka AK	0.36	3.03	0.119
Juneau AK	0.40	4.97	0.080
Yakutat AK	0.40	3.07	0.130

\* Interval equivalent and diurnal range for Rockport TX taken from nearby Port Aransas TX.

At locations with a low vulnerability index (e.g., Eastport, Maine) it implies that coastal residents and planners there can more easily adapt to less predictable ‘weather tides’ when they are small in comparison to the astronomical tides they experience day in and day out. At Rockport, Texas, residents accustomed to building near the water’s edge in an area with a very small diurnal range were highly vulnerable to the storm surge from Hurricane Harvey in 2017.

As noted in Appendix B, the 95% confidence interval – the RSL height difference between the upper and lower confidence limits – includes approximately 95% of the MMSL heights expected relative to YMSL in any given year. MMSL observations made during the 1969-2017 period confirm this expectation. That leaves 5% on average that will be higher or lower than the limit interval, including months with an unusual storm surge adding to whatever MMSL height is present at the time. Although resistant infrastructure including roads that can take some temporary flooding may be built in the zone between YMSL and the upper confidence interval limit, it is recommended that this practice be avoided for all other construction.

The RSL trends presented in this report contribute additional value when coupled with a hydrodynamic model adding storm surge. This can be done by collecting the observation data record at a nearby tide gauge for a specific past storm event, and using the projected linear or quadratic trend (or accompanying 95% confidence intervals) from this or other studies to project the RSL trend to the desired future date to reanalyze the impact of a similar strength storm in the future. An example is illustrated in Loftis et al. (2016) at NASA Langley Research Center, in Hampton, Virginia, using a hydrodynamic model (Figure VI-1).

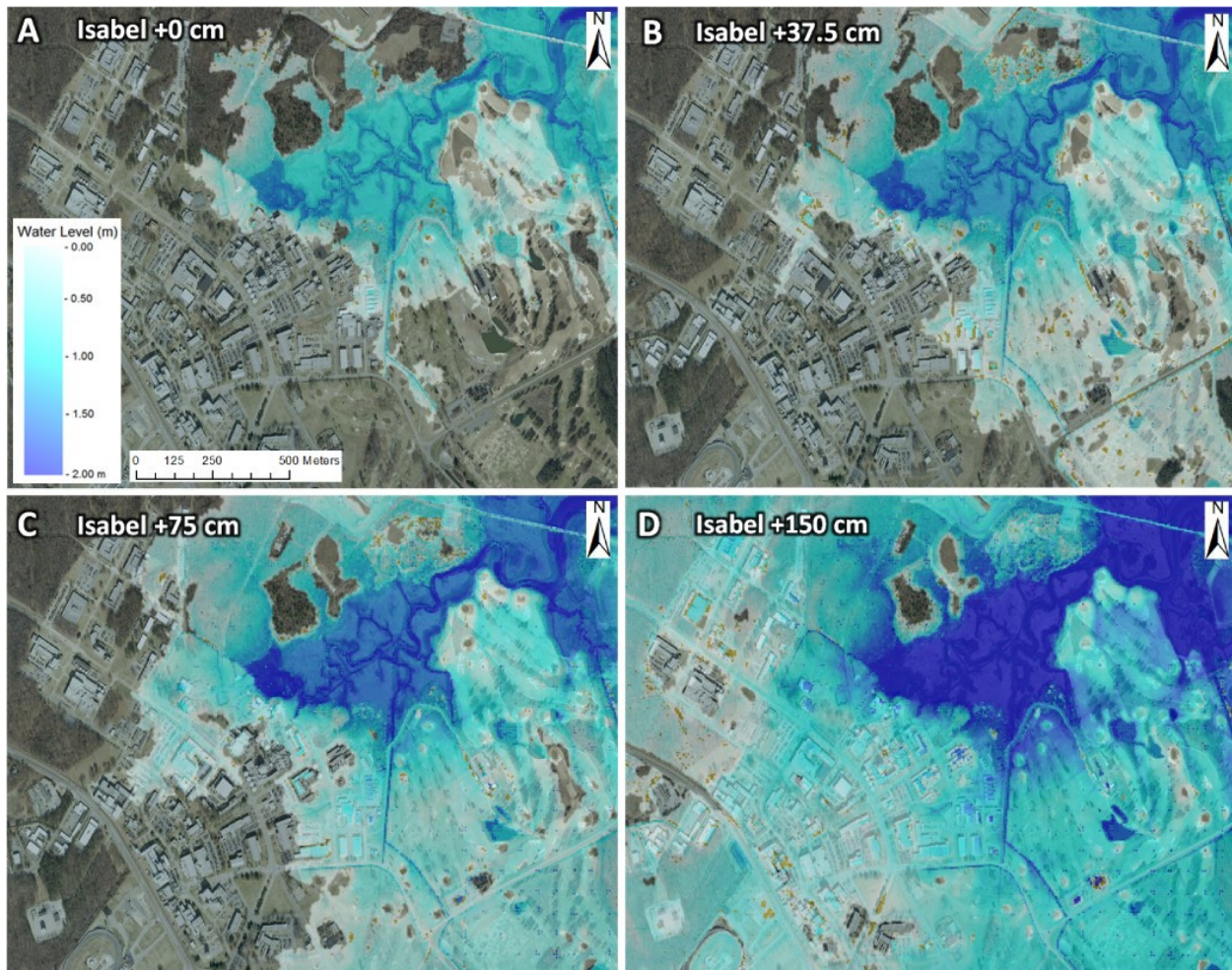


Figure VI-1. Impact of 2003 Hurricane Isabel in Hampton VA, under four RSL rise scenarios including the original storm: (A) +0 cm, (B) +37.5 cm, (C) +0.75 cm, and (D) +150 cm. These inundation maps do not account for elevation uncertainty (adapted from Loftis et al., 2016).

While bathtub models and viewers can reanalyze selected storm effects (as further discussed in the next sub-section), they do not account for wind-driven slope impacts on the free surface of the water, friction differences induced by fluid flow over variable terrain types or wind direction, rainfall flow aggregation, storm drainage infrastructure, or soil infiltration, all of which are of paramount importance for accurately modeling storm surge in urban environments (Loftis, 2014; Wang et al., 2014). One example of some hydrodynamic model-assisted guidance provided to the City of Portsmouth to advise development of their comprehensive plan using RSL rise trends uses the figure referenced in Section III, Figure 4, combined with storm surge observed in the city in 2003 during Hurricane Isabel. Hurricane Isabel resulted in a peak water level of nearly 2 m above 1992 MSL at Norfolk, Virginia. Thus, Figure VI-2 illustrates the thresholds in the RSL trend for the nearby tide gauge at Norfolk combined with the storm surge observations at the gauge in 2003 to simulate anticipated flooding extents and potentially vulnerable infrastructure in the face of a storm identical in path and strength to Isabel in 2050. Highlighted buildings and flood layers in the Figure VI-3 are color-coded using the key in Figure VI-2 and descriptions below and represent the lowest water level scenario wherein those areas or structures are inundated. For example:

- Red highlighted structures are predicted to be inundated only by an Isabel-like storm in 2050 if RSL trends hold to: the upper 95% confidence interval of the quadratic trend.
- Orange highlighted structures could be inundated by an Isabel-like storm in 2050 if RSL trends hold to: the quadratic or its upper 95% confidence interval trend.
- Yellow highlighted structures could be inundated by an Isabel-like storm in 2050 if RSL trends hold to: the lower 95%, the quadratic, or its upper 95% confidence interval trend.
- Green highlighted structures could be inundated by an Isabel-like storm in 2050 if RSL trends hold to: the linear trend, the lower 95%, the quadratic, or its upper 95% trend.
- Blue highlighted structures likely flooded during Hurricane Isabel, and are at the greatest risk of flooding now, or in the future by an Isabel-like storm in 2050 if RSL trends hold true.

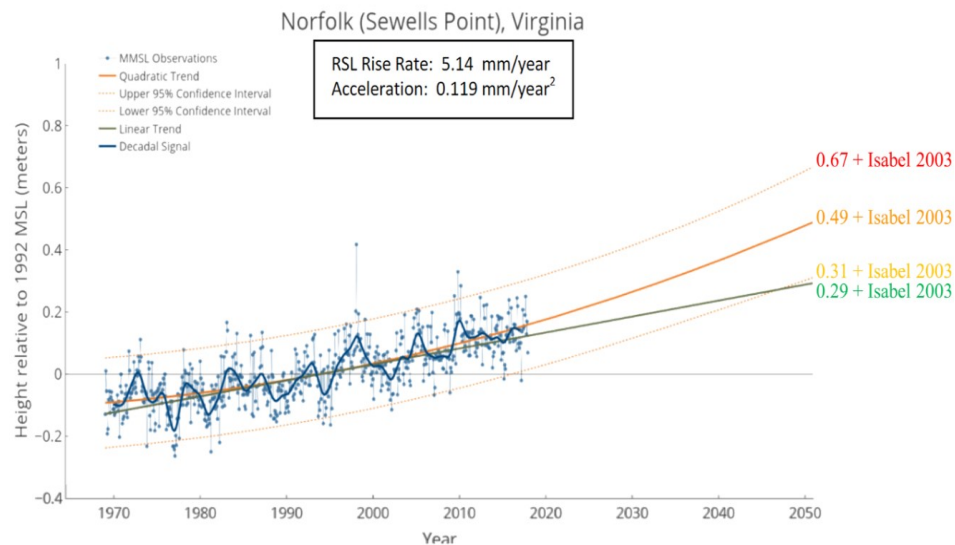


Figure VI-2. Revisiting Figure III-4 with relevance to 2003 Hurricane Isabel to project four RSL + storm surge scenarios based upon the linear trend, the quadratic trend, and the limits of its lower and upper 95% confidence intervals.

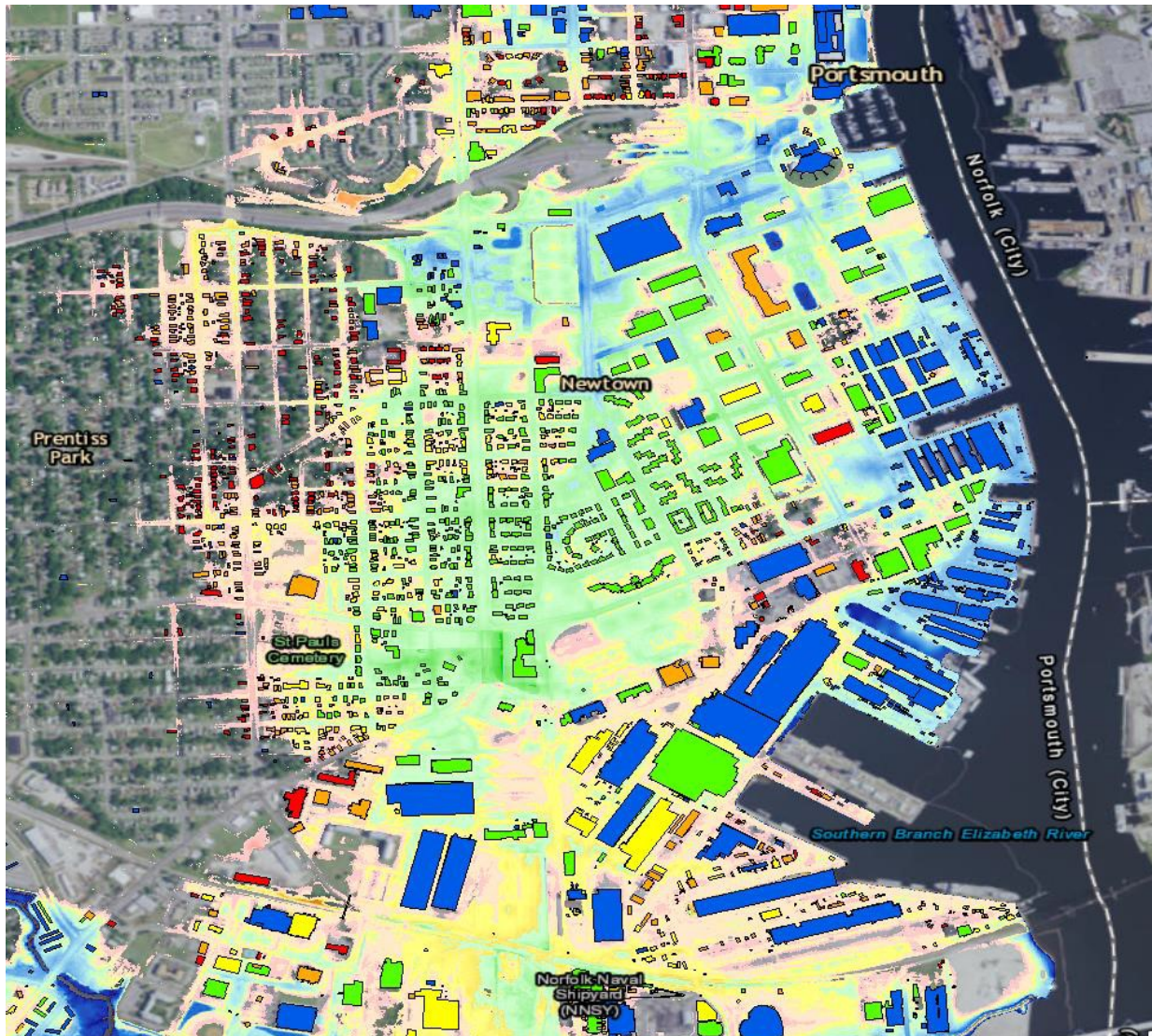


Figure VI-3. Projecting four RSL trends color coded with Figure VI-2 in combination with 2003 Hurricane Isabel driven by a street-level hydrodynamic model depicting future flood scenarios in Portsmouth, Virginia.

Communicating RSL rise impacts - Tracking and communicating water levels is one of the best ways to minimize flood impacts. Sensors installed by the U.S. Geological Survey (USGS), and the National Oceanic and Atmospheric Administration (NOAA) account for most sensors in the U.S. capable of water level observation and tidal prediction, respectively. However, there are also several regional water authorities who monitor and maintain archived records of water levels for increased density of data resources, including the California Department of Water Resources, the Iowa Flood Center, the Harris County Flood Control District (in and around Houston, Texas), and StormSense (in and around Hampton Roads, Virginia), to name some examples.

To elaborate on an ongoing example in Coastal Virginia, StormSense is an (Internet of Things) IoT-enabled inundation forecasting research initiative and an active participant in the Global City

Teams Challenge. The project aims to enhance flood preparedness in the smart cities of Hampton Roads, Virginia for flooding resulting from storm surge, rain, and tides (Loftis et al., 2017). In this study, we present the results of the new StormSense water level sensors to help establish the “regional resilience monitoring network” noted as a key recommendation from the Intergovernmental Pilot Project. To accomplish this, the Commonwealth Center for Recurrent Flooding Resiliency’s Tidewatch tidal forecast system is being used as a starting point to integrate the extant (NOAA) and new (USGS and StormSense) water level sensors throughout the region, and demonstrate replicability of the solution across the cities of Newport News, Norfolk, and Virginia Beach within Hampton Roads, Virginia (Loftis et al. 2018a). The StormSense network employs a mix of ultrasonic and radar remote sensing IoT technologies to record water levels in 6-minute intervals at 28 locations around Hampton Roads established in 2017. More details on data and locations of sensors are listed on the project’s website, <http://www.stormsense.com>.

Visualizing RSL flood risk - Based upon the availability of sensor data to communicate RSL in multiple locations throughout a region, there are a number of websites that allow mapping of sea level rise, however, flood events occur on top of sea level changes and can be harder to communicate. If sensors are densely populated in a region, it is likely that a meaningful interpolation (with shoreline barriers) could be automated for a richer interpretation of water levels in a region. Integration of data from multiple networks can be useful in the context of data viewers and portals via dynamic visualization to attempt to communicate the risks of RSL rise (Loftis et al., 2018b).

RSL data are communicated through many sea level rise viewers and most provide the ability to access different types of data through a single server. Portals are typically aimed at users who want to do their own analyses and provide information to un-synthesized data. Viewers provide mapped and synthesized data tools for resilience planning. From a nationwide perspective, three prominent portals are commonly used to address resilience planning and evaluate sea-level rise scenarios:

- NOAA’s Sea Level Rise viewer (<https://coast.noaa.gov/digitalcoast/tools/slriser>) allows the user to visualize potential impacts from sea level rise through interactive maps and photos in landmark locations that have been digitally altered to create an oblique view of flooding at thresholds up to 6 ft above mean sea level (MSL).
- Climate Central’s Surging Seas viewer (<http://sealevel.climatecentral.org/>) covers most U.S. coastal states and allows integrated mapping of social, economic, and flood risk factors. It allows for easy comparison of different scenarios to facilitate decision making related to future sea level rise scenarios up to 10 m (~32 ft) above MSL.
- U.S. Integration Ocean Observing System (U.S. IOOS) offers a number of regional portals for coastal ocean observing systems. Each aggregates data from regional universities, public data sources, and unique data through innovative partnerships. The Mid-Atlantic Coastal Ocean Observing System (<http://www.MARACOOS.org>), for example, covers the Mid-Atlantic region through the OceansMap Viewer accessible at <http://oceansmap.maracoos.org/>.

From a state-wide perspective, many states have resilience planning portals, which are used to guide informed management decision-making. For example, in Virginia, AdaptVA (<http://www.AdaptVA.org>) is a website dedicated to providing climate-related data specifically curated for adaptation efforts in Virginia (Figure VI-4). It provides both a data geo-portal and synthesized information, targeting different users with each. The geo-portal is primarily built to deliver Virginia specific data, but will also search ArcGIS.com for global data. All of the synthesized data tools are specific to Virginia (VIMS CCRM, 2017).

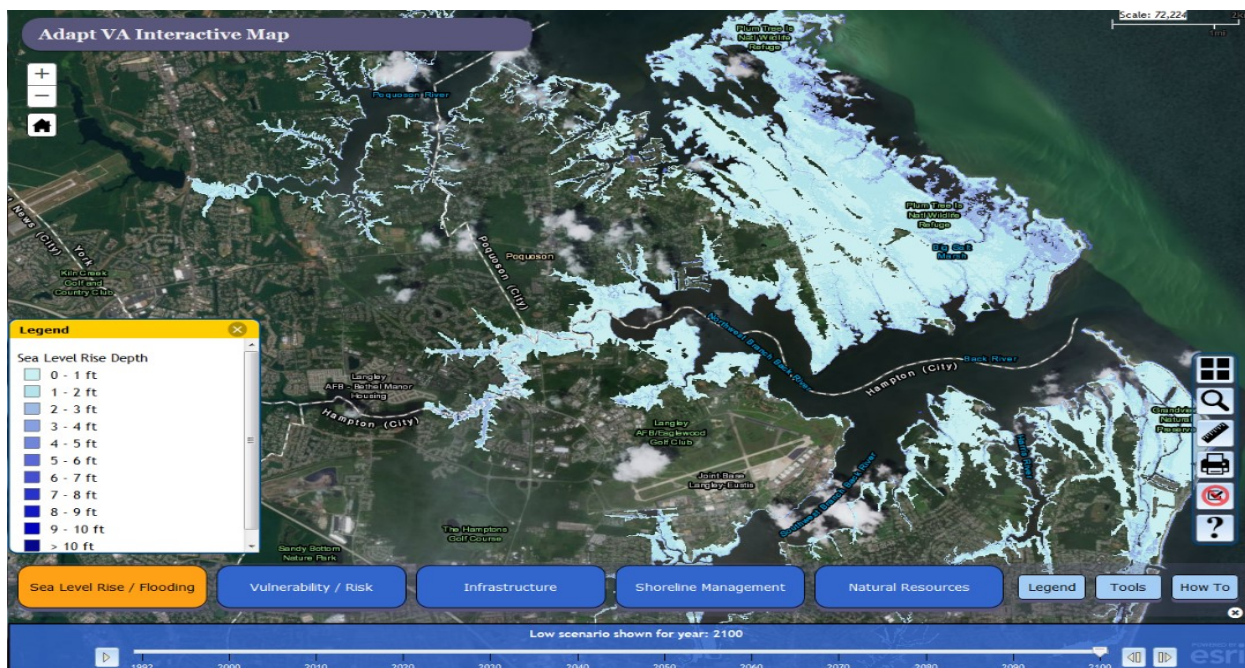


Figure VI-4. The AdaptVA portal shows projected water depths over land under RSL rise scenarios by employing a topographic bathtub model approach.

Guiding resilience efforts in the face of increasing RSL - Resiliency requires both a clear understanding of the problem posed by RSL changes and management strategies that are adaptable to those changes. In this section, we will highlight some best practices to achieving resiliency to sea level change.

The value of the data presented in this VIMS special report is that a trend analysis cannot be deciphered and interpreted to provide future predictions without a record of the past. The same applies for the flooding and inundation events that occur now and in the future. The USGS provides storm-specific data records for hurricanes that make landfall in the U.S. through their interactive mapping platform; however, little is currently being done to address a more frequent issue, tidal flooding. Often branded as simply a nuisance, the cost that frequently flooded coastal cities are incurring is considerable. Thus, around the coastal U.S., communities are striving to get a better handle on the highest of these tidal flooding events, called king tides, in hope of preparing for sea level rise. Scientists, planners, environmentalists and journalists have launched projects that involve everyday residents documenting how high the king tides rise. In one example of citizen-science community support, Hawaii Sea Grant has organized a multi-island

monitoring effort through the Hawai‘i and Pacific Islands King Tides Project (<http://ccsr.seagrant.soest.hawaii.edu/king-tides>).

In another recent example, from coastal Virginia, "Catch the King" Tide was a successful citizen-science GPS data collection effort that took place during the king tide on November 5, 2017, focusing on Hampton Roads, Virginia. Other communities in Miami, Florida, Charleston, South Carolina, Outer Banks, NC, and Cape Cod, Massachusetts, contributed data during the king tide along the U.S. East Coast. An interactive story map (<http://bit.ly/2A6xh7c>) and web application (<http://bit.ly/2zcS7Ba>) recruited interested volunteers and superposed the GPS observation data with the predicted flooding extent image services to provide cross-platform flood predictions to interested volunteers regardless of device type. Both pages resulted in more than 10,000 page views (each) within the first three months after they were released.

Over 600 volunteers mapped the king tide's maximum flooding extent to validate and improve predictive models and future forecasting of increasingly pervasive 'nuisance' flooding. Nearly 60,000 GPS high water marks and over 1200 geotagged pictures of inundation were captured using the Sea Level Rise mobile application to drop GPS breadcrumbs tracing the floodwaters. Response from the event's dedicated volunteers, fueled by constant media coverage leading up to the event, caused "Catch the King" to become the largest flood-related crowdsourcing data event in the world (Loftis, 2017). Hydrodynamic and sensor-guided tidal forecasts were provided in Hampton Roads by Tidewatch through the Commonwealth Center for Recurrent Flooding Resiliency, Virginia's State-Funded Flood Center, while outside areas consulted the National Ocean Service tidal forecast stations noted in this study.

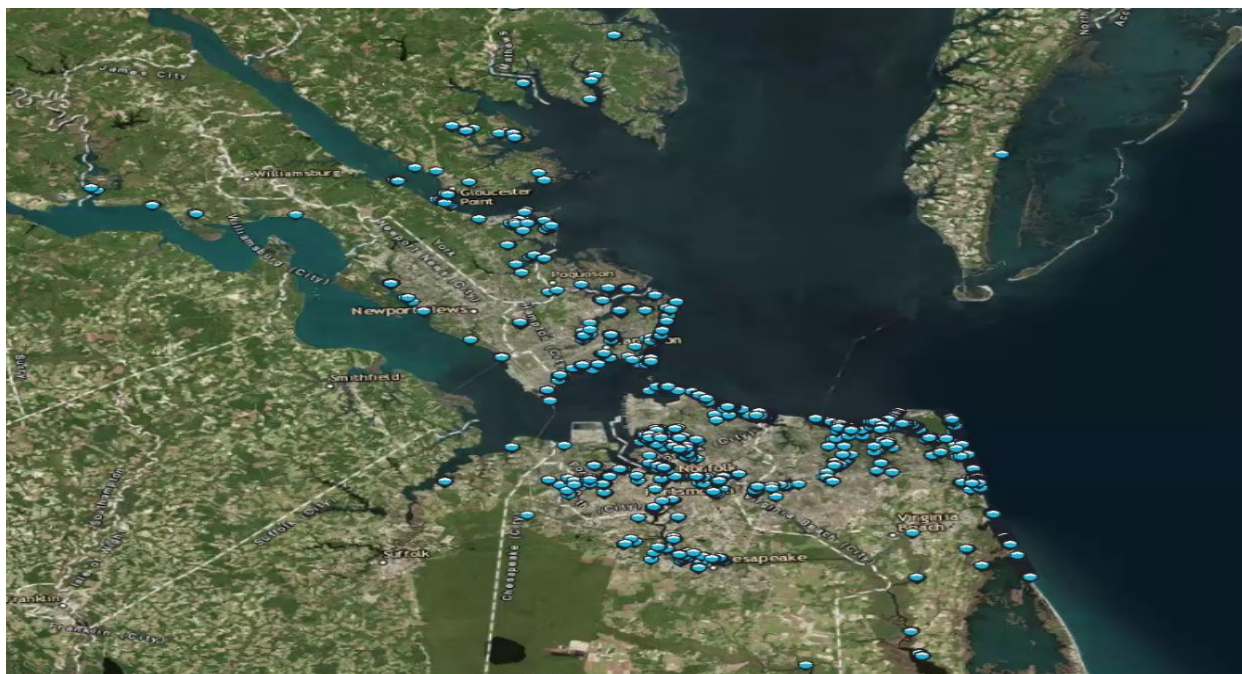


Figure VI-5. A map of volunteer-reported high water marks during from 7:50 a.m.-12:45 p.m. EST on November 5, 2017, in Hampton Roads, Virginia.

A hydrodynamic model developed by VIMS was used to predict the timing of tidal flooding, while extents were also estimated with the assistance of a topographic bathtub model in areas outside the street-level model's coverage in Hampton Roads, Virginia. The accuracy of the model forecasts for predicted tidal flood depths were found to be accurate to 1.4 in (3.5 cm) via root mean squared error (RMSE) and within an aggregate RMSE 19.3 ft (5.9 m) for tidal flooding extents measured by the nearly 60,000 GPS high water marks.

In the context of future flooding, the true value of monitoring the king tide is to improving hydro-correction in digital elevation models for areas occluded from airborne Lidar (such as those canopied by tree cover or streams under bridge overpasses or culverts). The user-reported flooding extent data provided geospatial model validation and highlighted areas where these predictions were inaccurate and could be improved.

Once the extent of the projected changes can be reasonably comprehended, it should be incorporated into coastal planning efforts through an emphasis on adaptable solutions. An example of an adaptable coastal solution is the use of natural shoreline treatments (“living shorelines” or “natural and nature-based features”) for shoreline stabilization (Figure VI-6). As a flood defense, natural shoreline strategies have been shown to be more sustainable, cost-effective, and have fewer side effects than conventional (hardening) strategies (Temmerman et al., 2013). Natural features, such as marshes, also have the capacity to move and elevate with changing water levels. Therefore, they are a recommended strategy for coping with RSL rise-driven erosion and flooding (Bilkovic et al., 2016; Bilkovic et al., 2017). Under changing conditions, natural features are considered a “low regret” option for shoreline stabilization and should be prioritized (Mitchell et al., 2013).



Figure VI-6. Natural shoreline defense in Sarah Creek, Virginia. The marsh reduces flooding impacts while adapting to RSL rise, enhancing shoreline resilience.

Summary of Management Recommendations -

1. RSL should be monitored on an annual basis and consistently compared to year 2050 RSL projections.
2. RSL rise projections should be limited to approximately 30 years in the future, since changing processes and decision making will affect longer term projections in ways not anticipated by their histories.
3. Construction will be safest when placed above the elevation of the upper 95% confidence interval, rather than above the 2050 RSL projection itself. In locations with a high HiVI score, storm activity raises water levels above yearly mean sea level (YMSL) frequently enough to warrant consideration of including these higher water levels in planning efforts. In these areas, it is important to add a storm “buffer” above the upper 95% MMSL confidence interval into future planning efforts.
4. Mapping RSL changes is critical to integrating these changes into management actions. Given limited funding, prioritization of flood issues can help localities address problems in a logical fashion.
5. Resiliency to RSL changes is dependent on communication with all stakeholders, a good understanding of the rate and direction of the change, and the incorporation of RSL change impacts into coastal planning.

## VII. REFERENCES

1. Bilkovic, D.M., Mitchell, M., Mason, P. and Duhring, K., 2016. The role of living shorelines as estuarine habitat conservation strategies. *Coastal Management*, 44(3), pp.161-174, <https://doi.org/10.1080/08920753.2016.1160201>
2. Bilkovic, D.M., Mitchell, M.M., La Peyre, M.K. and Toft, J.D. eds., 2017. Living shorelines: the science and management of nature-based coastal protection. CRC Press
3. Boon, J. D. (2012), Evidence of Sea Level Acceleration at U.S. and Canadian Tide Stations, Atlantic Coast, North America, *J Coastal Res*, 28(6), 1437-1445, <https://doi.org/10.2112/Jcoastres-D-12-00102.1>.
4. Boon, J. D., J. M. Brubaker, and D. R. Forrest (2010), *Chesapeake Bay Land Subsidence and Sea Level Change: An Evaluation of Past and Present Trends and Future Outlook*, edited, pp. 1-41, Virginia Institute of Marine Science, Gloucester Point, Virginia.
5. Boon, J. D., and M. Mitchell (2015), Nonlinear Change in Sea Level Observed at North American Tide Stations, *J Coastal Res*, 31(6), 1295-1305, <https://doi.org/10.2112/JCOASTRES-D-15-00041.1>
6. Boon, J. D., and M. Mitchell (2016), Reply to: Houston, JR, 2016. Discussion of: Boon, JD and Mitchell, M., 2015. Nonlinear Change in Sea Level Observed at North American Tide Stations, *Journal of Coastal Research*, 31(6), 1295-1305. *Journal of Coastal Research*, 32(4), 983-987. *J Coastal Res*, 32(4), 988-991, <https://doi.org/10.2112/Jcoastres-D-16a-00001.1>.
7. Boon, J. D., M. Mitchell, D. K. Loftis, and D. L. Malmquist (2018), Anthropocene Sea Level Change: A History of Recent Trends Observed in the U.S. East, Gulf and West Coast Regions, in Special Report in Applied Marine Science and Ocean Engineering (SRAMSOE) No. 467, edited, Virginia Institute of Marine Science, Gloucester Point, VA, <https://doi.org/10.21220/V5T17T>.
8. Bromirski, P. D., A. J. Miller, R. E. Flick, and G. Auad (2011), Dynamical suppression of sea level rise along the Pacific coast of North America: Indications for imminent acceleration, *J Geophys Res-Oceans*, 116, <https://doi.org/10.1029/2010jc006759>.
9. Cazenave, A., and R. S. Nerem (2004), Present-day sea level change: Observations and causes, *Rev Geophys*, 42(3), <https://doi.org/10.1029/2003rg000139>.
10. Center for Coastal Resources Management, Virginia Institute of Marine Science. 2017. Adapt Virginia: A New Web Portal about Climate Change Adaptations. *Rivers & Coast*, Summer 2017, Volume 12. Virginia Institute of Marine Science, College of William and Mary, <http://publish.wm.edu/reports/700>.
11. Crutzen, P. J. (2002), Geology of mankind, *Nature*, 415(6867), 23-23, <https://doi.org/10.1038/415023a>.
12. Crutzen, P. J., and E. F. Stoermer (2000), *The “Anthropocene”*, in IGBP Global Change Newsletter, edited.
13. Davis, J. L., and N. T. Vinogradova (2017), Causes of accelerating sea level on the East Coast of North America, *Geophys Res Lett*, 44(10), 5133-5141, <https://doi.org/10.1002/2017gl072845>.
14. Douglas, B. C. (1997), Global sea rise: A redetermination, *Surv Geophys*, 18(2-3), 279-292, <https://doi.org/10.1023/A:1006544227856>.

15. Douglas, B. C. (2001), Sea level change in the era of the recording tide gauge, in *Sea Level Rise: History and Consequences*, edited by B. C. Douglas, M. S. Kearney and S. P. Leatherman, pp. 37-64, Academic Press, San Diego, CA.
16. Elliott, J. L., C. F. Larsen, J. T. Freymueller, and R. J. Motyka (2010), Tectonic block motion and glacial isostatic adjustment in southeast Alaska and adjacent Canada constrained by GPS measurements, *J Geophys Res-Sol Ea*, 115, <https://doi.org/10.1029/2009jb007139>.
17. Ezer, T., L. P. Atkinson, W. B. Corlett, and J. L. Blanco (2013), Gulf Stream's induced sea level rise and variability along the U.S. mid-Atlantic coast, *J Geophys Res-Oceans*, 118(2), 685-697, <https://doi.org/10.1002/jgrc.20091>.
18. Ezer, T., and W. B. Corlett (2012), Is sea level rise accelerating in the Chesapeake Bay? A demonstration of a novel new approach for analyzing sea level data, *Geophys Res Lett*, 39(19), <https://doi.org/10.1029/2012GL053435>.
19. Ezer, T., I. D. Haigh, and P. L. Woodworth (2016), Nonlinear Sea-Level Trends and Long-Term Variability on Western European Coasts, *J Coastal Res*, 32(4), 744-755, <https://doi.org/10.2112/Jcoastres-D-15-00165.1>.
20. Gabrysch, R. K., and L. S. Coplin (1990), Land-Surface Subsidence in Houston-Galveston Region, Texas, edited by T. W. D. Board, p. 19, Texas Water Development Board, Austin, TX.
21. Gill, S.K., and J.R. Schultz (2001), Tidal Datums and their Applications, NOAA Special Publication NOS CO-OPS 1, 111p.
22. González, J. L., and T. E. Tornqvist (2006), Coastal Louisiana in crisis: Subsidence or sea level rise?, *Eos, Transactions American Geophysical Union*, 87(45), 493-498, <https://doi.org/10.1029/2006EO450001>.
23. Hong, B. G., W. Sturges, and A. J. Clarke (2000), Sea level on the US East Coast: Decadal variability caused by open ocean wind-curl forcing, *J Phys Oceanogr*, 30(8), 2088-2098, [https://doi.org/10.1175/1520-0485\(2000\)030<2088:Slotus>2.0.Co;2](https://doi.org/10.1175/1520-0485(2000)030<2088:Slotus>2.0.Co;2).
24. Houston, J. R., and R. G. Dean (2011), Sea-Level Acceleration Based on US Tide Gauges and Extensions of Previous Global-Gauge Analyses, *J Coastal Res*, 27(3), 409-417, <https://doi.org/10.2112/Jcoastres-D-10-00157.1>.
25. IPCC (2007), Summary for Policymakers, in *Climate Change 2007: The Physical Science Basis. Contribution of Working Group I to the Fourth Assessment Report of the Intergovernmental Panel on Climate Change*, edited by S. Solomon, D. Qin, M. Manning, Z. Chen, M. Marquis, K. B. Avery, M. Tignor and H. L. Miller, Cambridge University Press, Cambridge, United Kingdom and New York, NY, USA.
26. IPCC (2014), *Climate Change 2013: The Physical Science Basis. Contribution of Working Group I to the Fifth Assessment Report of the Intergovernmental Panel on Climate Change*, edited by T. F. Stocker, D. Qin, G.-K. Plattner, M. Tignor, S. K. Allen, J. Boschung, A. Nauels, Y. Xia, V. Bex and P. M. Midgley, p. 1535, Cambridge University Press, United Kingdom and New York, NY, USA, <https://doi.org/10.1017/CBO9781107415324>.
27. Jackson, L. C., R. Kahana, T. Graham, M. A. Ringer, T. Woollings, J. V. Mecking, and R. A. Wood (2015), Global and European climate impacts of a slowdown of the AMOC in a high resolution GCM, *Clim Dynam*, 45(11-12), 3299-3316, <https://doi.org/10.1007/s00382-015-2540-2>.

28. Johnson, C. S., K. G. Miller, J. V. Browning, R. E. Kopp, N. S. Khan, Y. Fan, S. D. Stanford, and B. P. Horton (2018), The Role of Sediment Compaction and Groundwater Withdrawal in Local Sea-Level Rise, Sandy Hook, New Jersey, USA, *Quaternary Sci Rev*, 181, 30–42, <https://doi.org/10.1016/j.quascirev.2017.11.031>.
29. Karegar, M. A., T. H. Dixon, and S. E. Engelhart (2016), Subsidence along the Atlantic Coast of North America: Insights from GPS and late Holocene relative sea level data, *Geophys Res Lett*, 43(7), 3126-3133, <https://doi.org/10.1002/2016gl068015>.
30. Karegar, M. A., T. H. Dixon, R. Malservisi, J. Kusche, and S. E. Engelhart (2017), Nuisance Flooding and Relative Sea-Level Rise: the Importance of Present-Day Land Motion, *Scientific Reports*, 7(1), 11197, <https://doi.org/10.1038/s41598-017-11544-y>.
31. Kidwell, D. M., J. C. Dietrich, S. C. Hagen, and S. C. Medeiros (2017), An Earth's Future Special Collection: Impacts of the coastal dynamics of sea level rise on low-gradient coastal landscapes, *Earths Future*, 5(1), 2-9, <https://doi.org/10.1002/2016ef000493>.
32. Kolker, A. S., M. A. Allison, and S. Hameed (2011), An evaluation of subsidence rates and sea-level variability in the northern Gulf of Mexico, *Geophys Res Lett*, 38, <https://doi.org/10.1029/2011gl049458>.
33. Kopp, R. E. (2013), Does the mid-Atlantic United States sea level acceleration hot spot reflect ocean dynamic variability?, *Geophys Res Lett*, 40(15), 3981-3985, <https://doi.org/10.1002/grl.50781>.
34. Kopp, R. E., C. C. Hay, C. M. Little, and J. X. Mitrovica (2015), Geographic Variability of Sea-Level Change, *Current Climate Change Reports*, 1(3), 192-204, <https://doi.org/10.1007/s40641-015-0015-5>.
35. Kopp, R. E., R. M. Horton, C. M. Little, J. X. Mitrovica, M. Oppenheimer, D. J. Rasmussen, B. H. Strauss, and C. Tebaldi (2014), Probabilistic 21st and 22nd century sea-level projections at a global network of tide-gauge sites, *Earths Future*, 2(8), 383-406, <https://doi.org/10.1002/2014ef000239>.
36. Larour, E., E. R. Ivins, and S. Adhikari (2017), Should coastal planners have concern over where land ice is melting?, *Sci Adv*, 3(11), <https://doi.org/10.1126/sciadv.1700537>.
37. Loftis, J.D. 2014. [Development of a Large-Scale Storm Surge and High-Resolution Sub-Grid Inundation Model for Coastal Flooding Applications: A Case Study during Hurricane Sandy](#). Ph.D. Dissertation. College of William & Mary. 229pp.
38. Loftis, J.D., Wang, H.V., DeYoung, R.J., and Ball, W.B. 2016. Using Lidar Elevation Data to Develop a Topobathymetric Digital Elevation Model for Sub-Grid Inundation Modeling at Langley Research Center, In: Brock, J.C.; Gesch, D.B.; Parrish, C.E.; Rogers, J.N., and Wright, C.W. (eds.), Advances in Topobathymetric Mapping, Models, and Applications. *Journal of Coastal Research*, Special Issue 76, 134-148. <https://doi.org/10.2112/SI76-012>
39. Loftis, J.D., Wang, H., Forrest, D., Rhee, S., Nguyen, C. (2017). Emerging Flood Model Validation Frameworks for Street-Level Inundation Modeling with StormSense. *SCOPE '17 Proceedings of the 2nd International Workshop on Science of Smart City Operations and Platforms Engineering*, 2(1), 13-18.
40. Loftis, J.D., Forrest, D.R., Katragadda, S., Spencer, K., Organski, T., Nguyen, C., and Rhee, S. 2018a. StormSense: A New Integrated Network of IoT Water Level Sensors in the Smart Cities of Hampton Roads, VA. *Marine Technology Society Journal*, 52(2): (In Press). <https://wm1693.box.com/s/j501eg525rtqnya41n2dfm6a0o4yx7gh>

41. Mitchell, M., Hershner, C., Herman, J., Schatt, D., Egginton, E., and Stiles, S. 2013. [Recurrent flooding study for Tidewater Virginia](#). Virginia senate document no. 3. Richmond, Virginia. Report.
42. Mitrovica, J. X., N. Gomez, and P. U. Clark (2009), The Sea-Level Fingerprint of West Antarctic Collapse, *Science*, 323(5915), 753-753, <https://doi.org/10.1126/science.1166510>.
43. Mitrovica, J. X., and G. A. Milne (2002), On the origin of late Holocene sea-level highstands within equatorial ocean basins, *Quaternary Sci Rev*, 21(20-22), 2179-2190, [https://doi.org/10.1016/S0277-3791\(02\)00080-X](https://doi.org/10.1016/S0277-3791(02)00080-X).
44. Mitrovica, J. X., M. E. Tamisiea, J. L. Davis, and G. A. Milne (2001), Recent mass balance of polar ice sheets inferred from patterns of global sea-level change, *Nature*, 409(6823), 1026-1029, <https://doi.org/10.1038/35059054>.
45. Monastersky, R. (2015), The human age, *Nature*, 519(7542), 144-147, <https://doi.org/10.1038/519144a>.
46. Morton, R. A., J. C. Bernier, and J. A. Barras (2006), Evidence of regional subsidence and associated interior wetland loss induced by hydrocarbon production, Gulf Coast region, USA, *Environ Geol*, 50(2), 261-274, <https://doi.org/10.1007/s00254-006-0207-3>.
47. Nerem, R. S., B. D. Beckley, J. T. Fasullo, B. D. Hamlington, D. Masters, and G. T. Mitchum (2018), Climate-change–driven accelerated sea-level rise detected in the altimeter era, *Proceedings of the National Academy of Sciences*, 115(9), 2022, <https://doi.org/10.1073/pnas.1717312115>.
48. Newman, M., G. P. Compo, and M. A. Alexander (2003), ENSO-forced variability of the Pacific decadal oscillation, *J Climate*, 16(23), 3853-3857, [https://doi.org/10.1175/1520-0442\(2003\)016<3853:Evotpd>2.0.Co;2](https://doi.org/10.1175/1520-0442(2003)016<3853:Evotpd>2.0.Co;2).
49. Park, J., and W. Sweet (2015), Accelerated sea level rise and Florida Current transport, *Ocean Sci*, 11(4), 607-615, <https://doi.org/10.5194/os-11-607-2015>.
50. Parker, B. B. (2007), Tidal Analysis and Prediction. NOAA Special Publication NOS CO-OPS 3, 378p.
51. Parris, A., et al. (2012), [Global Sea Level Rise Scenarios for the US National Climate Assessment](#), edited by N. T. Memo, p. 37, OAR CPO-1.
52. Penland, S., and K. E. Ramsey (1990), Relative Sea-Level Rise in Louisiana and the Gulf of Mexico - 1908-1988, *J Coastal Res*, 6(2), 323-342, <http://www.jstor.org/stable/4297682>.
53. Piecuch, C. G., and R. M. Ponte (2011), Mechanisms of interannual steric sea level variability, *Geophys Res Lett*, 38(15), n/a-n/a, <https://doi.org/10.1029/2011GL048440>.
54. Piecuch, C. G., and R. M. Ponte (2015), Inverted barometer contributions to recent sea level changes along the northeast coast of North America, *Geophys Res Lett*, 42(14), 5918-5925, <https://doi.org/10.1002/2015gl064580>.
55. Poland, J. F. (1960), Land subsidence in the San Joaquin Valley and its effect on estimates of ground-water resources, International Association of Scientific Hydrology, 52, 324–335.
56. Sallenger, A. H., K. S. Doran, and P. A. Howd (2012), Hotspot of accelerated sea-level rise on the Atlantic coast of North America, *Nat Clim Change*, 2(12), 884-888, <https://doi.org/10.1038/Nclimate1597>.

57. Sato, T., S. Miura, W. K. Sun, T. Sugano, J. T. Freymueller, C. F. Larsen, Y. Ohta, H. Fujimoto, D. Inazu, and R. J. Motyka (2012), Gravity and uplift rates observed in southeast Alaska and their comparison with GIA model predictions, *J Geophys Res-Sol Ea*, 117, <https://doi.org/10.1029/2011jb008485>.
58. Sella, G. F., S. Stein, T. H. Dixon, M. Craymer, T. S. James, S. Mazzotti, and R. K. Dokka (2007), Observation of glacial isostatic adjustment in "stable" North America with GPS, *Geophys Res Lett*, 34(2), <https://doi.org/10.1029/2006gl027081>.
59. Shirzaei, M., and R. Bürgmann (2018), Global climate change and local land subsidence exacerbate inundation risk to the San Francisco Bay Area, *Sci Adv*, 4(3). <https://doi.org/10.1126/sciadv.aap9234>.
60. Sturges, W., and B. G. Hong (2001), Decadal Variability of Sea Level, in *Sea Level Rise: History and Consequences*, edited by B. C. Douglas, M. S. Kearney and S. P. Leatherman, pp. 165-180, Academic Press, San Diego, CA.
61. Sweet, W., R. Kopp, C. Weaver, J. Obeysekera, R. Horton, E. Thieler, and C. Zervas (2017), [Global and Regional Sea Level Rise Scenarios for the United States](#), edited by N. T. Report, NOS CO-OPS 083.
62. Temmerman, S., Meire, P., Bouma, T.J., Herman, P.M., Ysebaert, T., and De Vriend, H.J. 2013. Ecosystem-based coastal defense in the face of global change. *Nature* 504 (7478): 79–83, <https://doi.org/10.1038/nature12859>
63. Valle-Levinson, A., A. Dutton, and J. B. Martin (2017), Spatial and temporal variability of sea level rise hot spots over the eastern United States, *Geophys Res Lett*, 44(15), 7876-7882, <https://doi.org/10.1002/2017GL073926>.
64. van Oldenborgh, G. J., K. van der Wiel, A. Sebastian, R. Singh, J. Arrighi, F. Otto, K. Haustein, S. H. Li, G. Vecchi, and H. Cullen (2017), Attribution of extreme rainfall from Hurricane Harvey, August 2017, *Environ Res Lett*, 12(12), <https://doi.org/10.1088/1748-9326/aa9ef2>.
65. Velicogna, I., T. C. Sutterley, and M. R. van den Broeke (2014), Regional acceleration in ice mass loss from Greenland and Antarctica using GRACE time-variable gravity data, *Geophys Res Lett*, 41(22), 8130-8137, <https://doi.org/10.1002/2014GL061052>.
66. Wake, L., G. Milne, and E. Leuliette (2006), 20th Century sea-level change along the eastern US: Unravelling the contributions from steric changes, Greenland ice sheet mass balance and Late Pleistocene glacial loading, *Earth and Planetary Science Letters*, 250(3), 572-580, <https://doi.org/10.1016/j.epsl.2006.08.006>.
67. Wang HV, Loftis JD, Liu Z, Forrest D, Zhang J. (2014), The Storm Surge and Sub-Grid Inundation Modeling in New York City during Hurricane Sandy. *Journal of Marine Science and Engineering*; 2(1), 226-246, <https://doi.org/10.3390/jmse2010226>
68. White, W. A., and T. A. Tremblay (1995), Submergence of Wetlands as a Result of Human-Induced Subsidence and Faulting Along the Upper Texas Gulf-Coast, *J Coastal Res*, 11(3), 788-807, <http://www.jstor.org/stable/4298381>.
69. Yin, J. J., and P. B. Goddard (2013), Oceanic control of sea level rise patterns along the East Coast of the United States, *Geophys Res Lett*, 40(20), 5514-5520, <https://doi.org/10.1002/2013gl057992>.

### VIII. ACKNOWLEDGEMENTS

The material presented in this report is based in part upon work supported by NOAA under Grant Number NA17NOS4730142, the National Science Foundation under Grant Number 1600131, and the NASA Disasters Demonstration Study: Communities at Intensive Risk. Any opinions, findings, and conclusions or recommendations expressed in this material are those of the author(s) and do not necessarily reflect the views of the National Science Foundation or the National Aeronautics and Space Administration.

Gratitude is expressed to the National Oceanic and Atmospheric Administration (NOAA) and the National Ocean Service (NOS) for providing verified water level observations and other information collected at U.S. tide stations and made available through the NOAA website [www.tidesandcurrents.noaa.gov](http://www.tidesandcurrents.noaa.gov). The analyses performed and the results presented in this report are the work of the authors and do not necessarily reflect the views of NOAA.

We are indebted to Douglas L. Dwoyer, Larry P. Atkinson, and Mark Bushnell for their critical review of the report manuscript. Special thanks are given to Helen T. Worthington for editing and communications tips toward reaching a wider audience on the subject of sea level change.

## Appendix A – Estimating The Seasonal Cycle and Decadal Signal

The Seasonal Cycle - Seasonal variations in monthly mean sea level (MMSL) recorded by tide gauges have both an astronomical and a meteorological origin. The astronomical component arises from cyclic variations in the sun's declination and distance from the Earth which have periods of half a year and one year, respectively. This component is represented in predictions of the astronomic tide by the solar annual (Sa) and solar semiannual (Ssa) tidal constituents. However, changes due to earth-sun gravitational interactions are relatively minor in comparison to weather-induced variations, principally the annual cycle in solar heating and expansion-contraction of the ocean water column. Because most of the amplitude of the Sa and Ssa constituents derives from meteorological forcing, which changes noticeably from one year to the next, an average is usually taken over several years. One way of representing the seasonal cycle uses water level averages computed separately for each calendar month of the year over a period of up to 19 years. Another method derives it by least-squares harmonic analysis applied directly to a detrended multidecadal MMSL series (Parker, 2007). The latter method was used here for the seasonal cycle, shown in Fig. A-1 as it appears over a typical decade at Norfolk, Virginia; typical except for a rare MMSL high that appears in February, 1998, coinciding with the expected low in the seasonal cycle for this month. The high noted is an example of the diverse effects of weather and the importance of averaging.

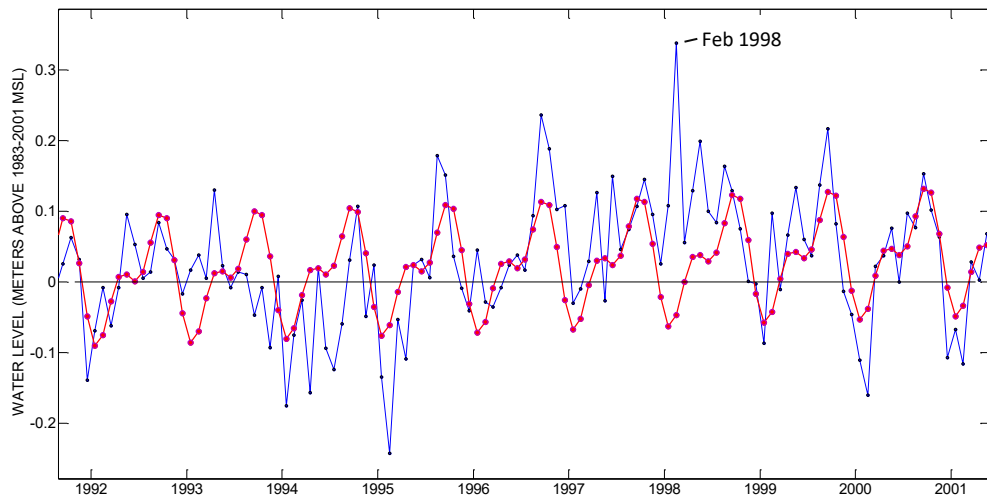


Figure A-1. Graph showing raw MMSL heights (blue) and monthly values of the predicted seasonal cycle (red) at Norfolk, Virginia. Note that the form of the cycle does not change as it gradually rises along with the sea level trend over the decade shown.

The seasonal cycle is removed by subtracting its detrended monthly values from those of a raw MMSL series downloaded from [www.tidesandcurrents.noaa.gov](http://www.tidesandcurrents.noaa.gov) referencing NOAA's MSL tidal datum for the 1983-2001 epoch. Water level variance occurring at tidal frequencies makes no net contribution to the trend itself in a MMSL time series spanning multiple decades. By removing it, one final source of variance at known tidal frequencies is eliminated. A typical example of the reduction in variance can be seen in the MMSL series comparisons presented in Fig. A-2.

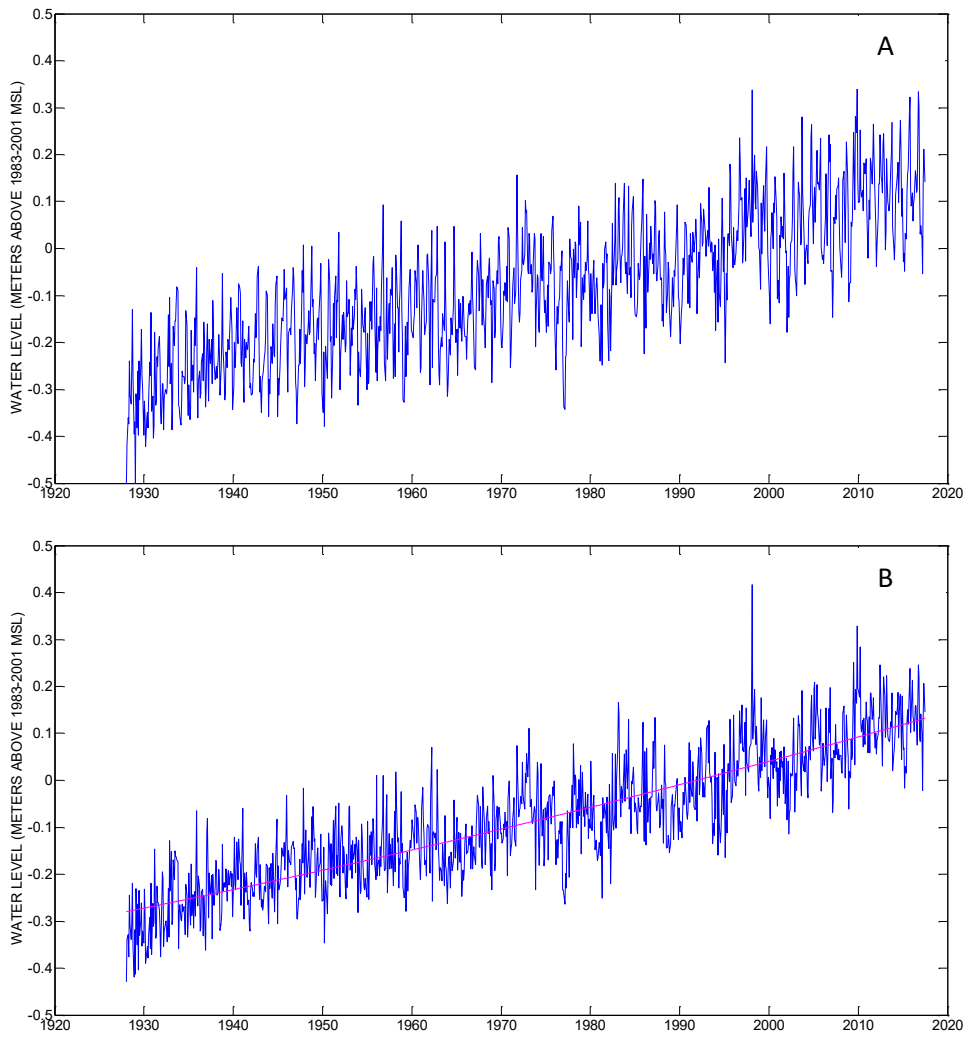


Figure A-2. Graphs comparing variance in MMSL heights (A) before and (B) after removing the seasonal cycle from 1928-2017 MMSL, Norfolk, Virginia.

The Decadal Signal - Quasi-periodic variations in sea level associated with varying surface winds and ocean-atmosphere exchange are of considerable interest here because they are often highly coherent from one coastal location to the next with amplitudes as high as 10 cm (Boon, Brubaker and Forrest, 2010). Unlike the fully periodic seasonal cycle with nearly the same amplitude, the decadal signal has no fixed interval of recurrence for its highs and lows. Sturges and Hong (2001) state that, in normal usage, the term ‘decadal’ loosely applies to spectral energy found at frequencies corresponding to periods “longer than a year out to ten years and beyond.” This precludes its derivation by least-squares harmonic analysis or similar methods dealing with fixed frequencies. It is derived in this report by applying a third-order Butterworth digital filter with cutoff period of 24 months (using MATLAB function *butter* in combination with function *filtfilt*, which performs zero-phase digital filtering by processing input data in both forward and reverse directions).

Although a decadal signal derived by filtering can be displayed superposed on a time series of MMSL heights, it is questionable whether it can be removed from the series in the same way as the seasonal cycle; i.e., without affecting the linear – and especially the quadratic – trends subsequently obtained from the reduced series. Unlike least-squares harmonic analysis deriving variance at fixed frequencies, filtering removes variance from a detrended series over a range of frequencies leaving the decadal signal in a residual form that may include part of a trend. Superposing the decadal signal provides visual clues for understanding the effect of a recent decadal high or low in modulating RSL projections in the near term (see Appendix C).

The decadal signal shown in Fig. A-3 has ten ‘zero-up’ trend crossings spread over almost 50 years, an average recurrence period of about 5 years for the decadal highs (or lows) in this segment. The digital filter used to derive the decadal signal has a 24-month cutoff period, its span being one more than the number of data points lost at the series ends. In this case, eleven months are given up at either end of the series as seen in the figure below. While this is unavoidable, enough of the signal phase (trending high or low) can be seen to judge its effect in modulating the quadratic trend projection going forward in time. For the 1969-2017 segment shown in Fig. A-3 the decadal signal begins and ends in a neutral position, neither high nor low.

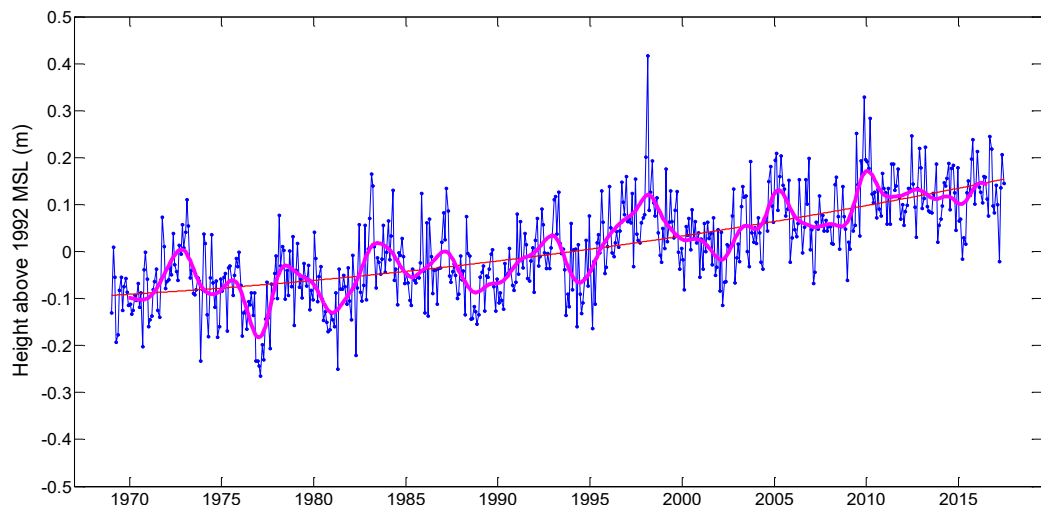


Figure A-3. Graph showing the decadal signal (magenta curve) superposed on a MMSL series segment with seasonal cycle removed at Norfolk, Virginia. The fitted quadratic trend is the thin red line also superposed on the MMSL segment.

## Appendix B – Confidence Intervals for Sea Level Time Series

Confidence Interval for  $\beta_1$  - The linear rate of sea level rise in millimeters per year is represented by the parameter  $\beta_1$  in the regression equation

$$Y_i = \beta_0 + \beta_1 X_i + \varepsilon_i \quad (\text{B-1})$$

where  $Y_i$  represents the  $i^{\text{th}}$  sea level height,  $X_i$  is the corresponding fractional year and  $\varepsilon_i$  is the  $i^{\text{th}}$  error or deviation from regression in a time series of  $n$  values. Using overbars to represent the series mean of  $Y_i$  and  $X_i$ , the unknown parameter  $\beta_1$  is estimated as

$$b_1 = \sum_i (X_i - \bar{X}) Y_i / \sum_i (X_i - \bar{X})^2 \quad (\text{B-2})$$

with  $\beta_0$  estimated as  $b_0 = \bar{Y} - b_1 \bar{X}$ . The estimated *standard error* for  $b_1$  is

$$Se(b_1) = \frac{s}{\sqrt{\sum_i (X_i - \bar{X})^2}} \quad (\text{B-3})$$

where  $s$  is the standard deviation of the series heights,  $Y_i$ , and the quantity in the denominator is computed as the root sum of squares for the series of years  $X_i$ ,  $i = 1, n$ . The confidence interval on  $b_1$  is then computed as the product of a value from the  $t$  - distribution and  $Se$ , the estimated standard error. At the 95% level of confidence,

$$b_1 \pm t_{.05} Se(b_1) \quad (\text{B-4})$$

noting that, for  $n-2$  degrees of freedom (*d.f.*)  $> 120$ ,  $t_{.05} \approx 1.97$ .

Source: Draper, N.R. and H. Smith, 1998. *Applied Regression Analysis*, 3<sup>rd</sup> Ed. John Wiley & Sons.

Example Computation for Norfolk, Virginia - The following is an illustration of the limitations of a confidence interval when applied to sea level time series trends. A 90-year record was selected beginning in 1928, the first complete year of monthly mean sea level (MMSL) available at Sewells Point in Norfolk, Virginia (from [www.tidesandcurrents.noaa.gov](http://www.tidesandcurrents.noaa.gov)). Starting with the first ten years of record ( $i = 1, 120$ ), the linear trend parameter,  $b_1$ , was calculated using Eq. B-2 with  $Y_i$  in mm above MSL datum and  $X_i$  in years relative to 1992. From Eq. B-3, the ratio of the standard deviation of  $Y_i$  (denoted as SDY) to the root sum of squares of  $X_i$  (denoted as RSSX) produces the standard error of the trend:  $Se = SDY/RSSX$ . The computations were then repeated adding new data in 10-year increments. No corrections were made for serial correlation likely to be present in a time series of sea level height.

Figure B-1(A) illustrates the apparent benefit of longer records in reducing trend standard error. Figure B-1(B) shows how that benefit is achieved; not by a reduction in SDY (it increases gradually with record length) but through a sharp increase in RSSX, recalling that trend standard error is defined as the ratio SDY/RSSX. This means there is nothing in the added measurements themselves contributing to a smaller confidence interval on sea level rise rate at Norfolk; it is simply the result of adding years independent of the data they present. Although it may be considered valid to write the  $\pm$  numbers shown in Figs. B-1(C) and B-1(D), the implication that an infinitely long record will yield high confidence in a single precise number representing sea level rise is unsettling if not obscure. Trends can and do change over time.

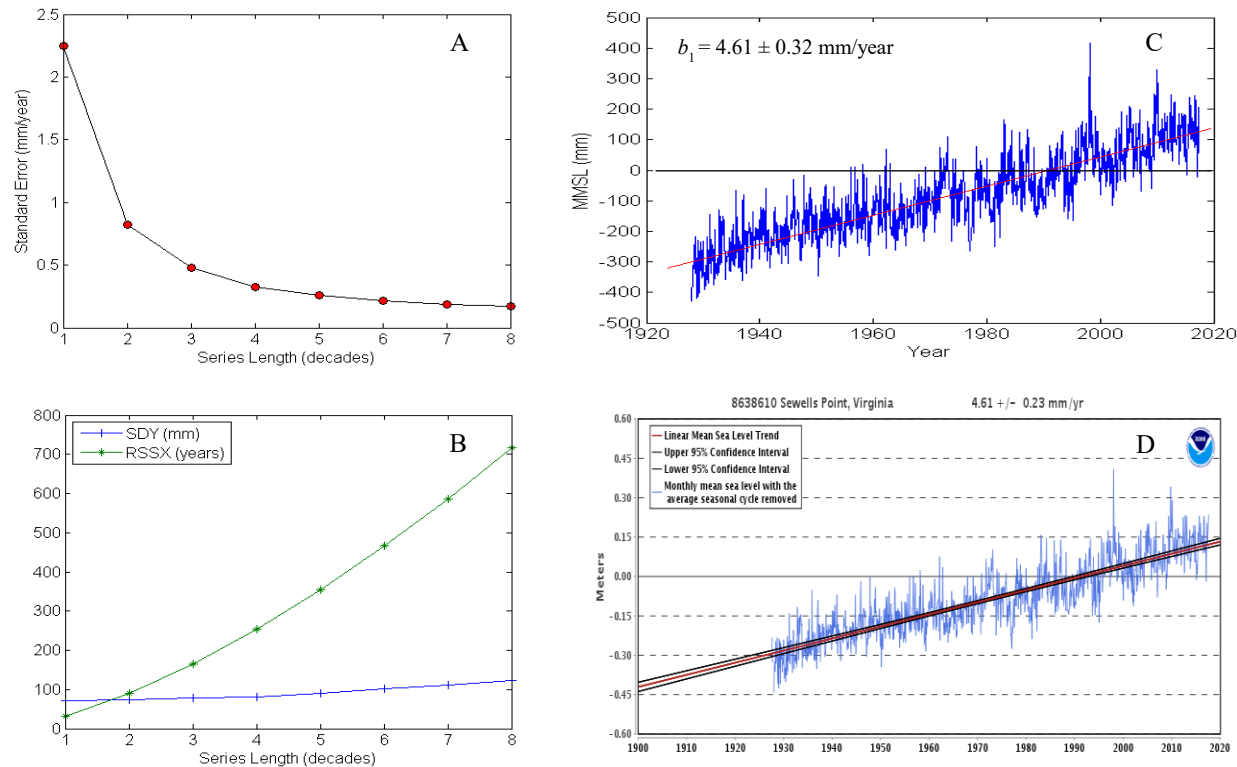


Figure B-1. Plots for Norfolk, Virginia, showing decrease in trend standard error (A) with increasing standard deviation in sea level height and root sum of squares in years (B). The trend in downloaded MMSL heights with seasonal cycle removed (C) is compared with the sea level trend published by NOAA (D).

Confidence Intervals for Predicted Heights - Not to be confused with confidence intervals on the *rate* of sea level rise, the upper and lower 95% confidence intervals shown as curving black lines above and below the red trend line in Fig. B-1D set limits on the expected range in predicted sea level height over time written as

$$\hat{Y} = b_0 + b_1 X \quad (\text{B-5})$$

Substituting  $b_0 = \bar{Y} - b_1 \bar{X}$ , the predicted height at any given time  $X_0$  is

$$\hat{Y}_0 = \bar{Y} + b_1(X_0 - \bar{X}) \quad (\text{B-6})$$

In the above form, Eq. B-6 makes clear that  $\hat{Y}_0 = \bar{Y}$  at  $X_0 = \bar{X}$  where the standard deviation of the mean height  $\bar{Y}$  is  $s/\sqrt{n}$ . But as  $X_0$  moves away from  $\bar{X}$  in either direction, additional uncertainty is contributed through the estimated trend parameter  $b_1$ . The standard error on  $\hat{Y}_0$  is then estimated as

$$Se(\hat{Y}_0) = s \left\{ \frac{1}{n} + \frac{(X_0 - \bar{X})^2}{\sum_i (X_i - \bar{X})^2} \right\}^{\frac{1}{2}} \quad (\text{B-7})$$

Substituting  $Se(\hat{Y}_0)$  for  $Se(b_1)$  in Eq. B-4 provides upper and lower 95% confidence intervals for  $\hat{Y}_0$  enabling inclusive bands to be drawn with the classic ‘bow-tie’ appearance over the full range of times  $X_i$ ; e.g., Fig. B-1D.

Confidence Intervals for MMSL observations - Confidence intervals derived with Eq. B-7 apply only to the predicted mean heights that lie on the trend line of best fit to the MMSL observations. In some situations, it may be of greater interest to know the likely range in deviation from trend of the individual observations across  $X_i$  and beyond. This can be achieved using the following equation in place of Eq. B-7,

$$Se(Y_i) = s \left\{ 1 + \frac{1}{n} + \frac{(X_0 - \bar{X})^2}{\sum_i (X_i - \bar{X})^2} \right\}^{\frac{1}{2}} \quad (\text{B-8})$$

Source: Draper, N.R. and H. Smith, 1998. *Applied Regression Analysis*, 3<sup>rd</sup> Ed. John Wiley & Sons.

The 95% confidence intervals on height derived with Eq. B-8 will thus be wider and more uniform than those obtained with Eq. B-7 and will enclose approximately 95% of the MMSL observations as shown in Fig. B-2(A). This interval can be a valuable guide where flooding is a concern as it informs the user of the amount of sea level deviation from trend to expect in any one month.

If a decision is made to project a trend forward in time beyond the latest observation, Eq. B-8 may be useful in another way. When a projection to time  $X_0$  extends too far into the future, the numerator of the third term inside the large brackets,  $(X_0 - \bar{X})^2$ , will become large in comparison to the sum of squares of  $X$ , causing the 95% confidence intervals to expand more than is reasonable. The intervals will expand even further and eventually ‘blow up’ if the span of the time series of observations is too short compared to the length of the projection. Figure B-2(B) illustrates the effect after reducing the Norfolk series length from 49 years (1969-2017) to 26 years (1969-1994).

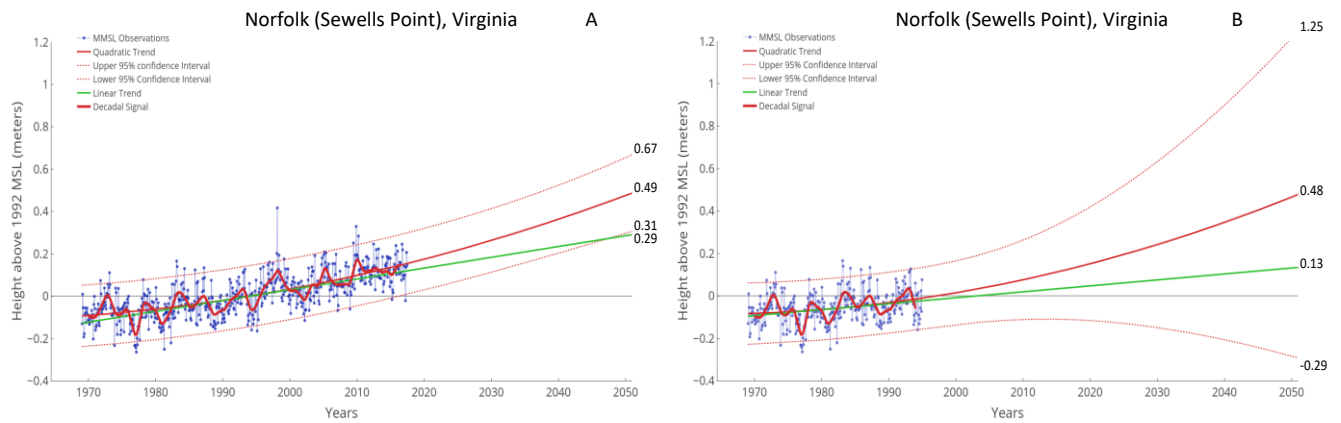


Figure B-2. Year 2050 Sea Level Projection for Norfolk, Virginia comparing (A) analysis of 1969-2016 MMSL with (B) a short record analysis of 1969-1994 MMSL. Heights are displayed in meters.

Estimates of  $\beta_1, \beta_2$  obtained using MATLAB - Both graphs in Fig. B-2 above are based on the quadratic model, a second-order polynomial equation that is usually written as

$$Y_i = \beta_0 + \beta_1 X_i + \beta_2 X_i^2 + \varepsilon_i \quad (\text{B-9})$$

Note that Eq. B-9 differs slightly from Eq. III-1 in Section III of this report. The fraction  $\frac{1}{2}$  placed in front of  $\beta_2$  in Eq. III-1 signifies that  $\beta_2$  there is meant to represent acceleration, positive or negative, in the quadratic model for sea level change. If using Eq. B-9, the form that appears in most texts and commercial computing algorithms, be aware that acceleration is twice the value of the coefficient  $b_2$  returned as an estimate of  $\beta_2$  in those algorithms.

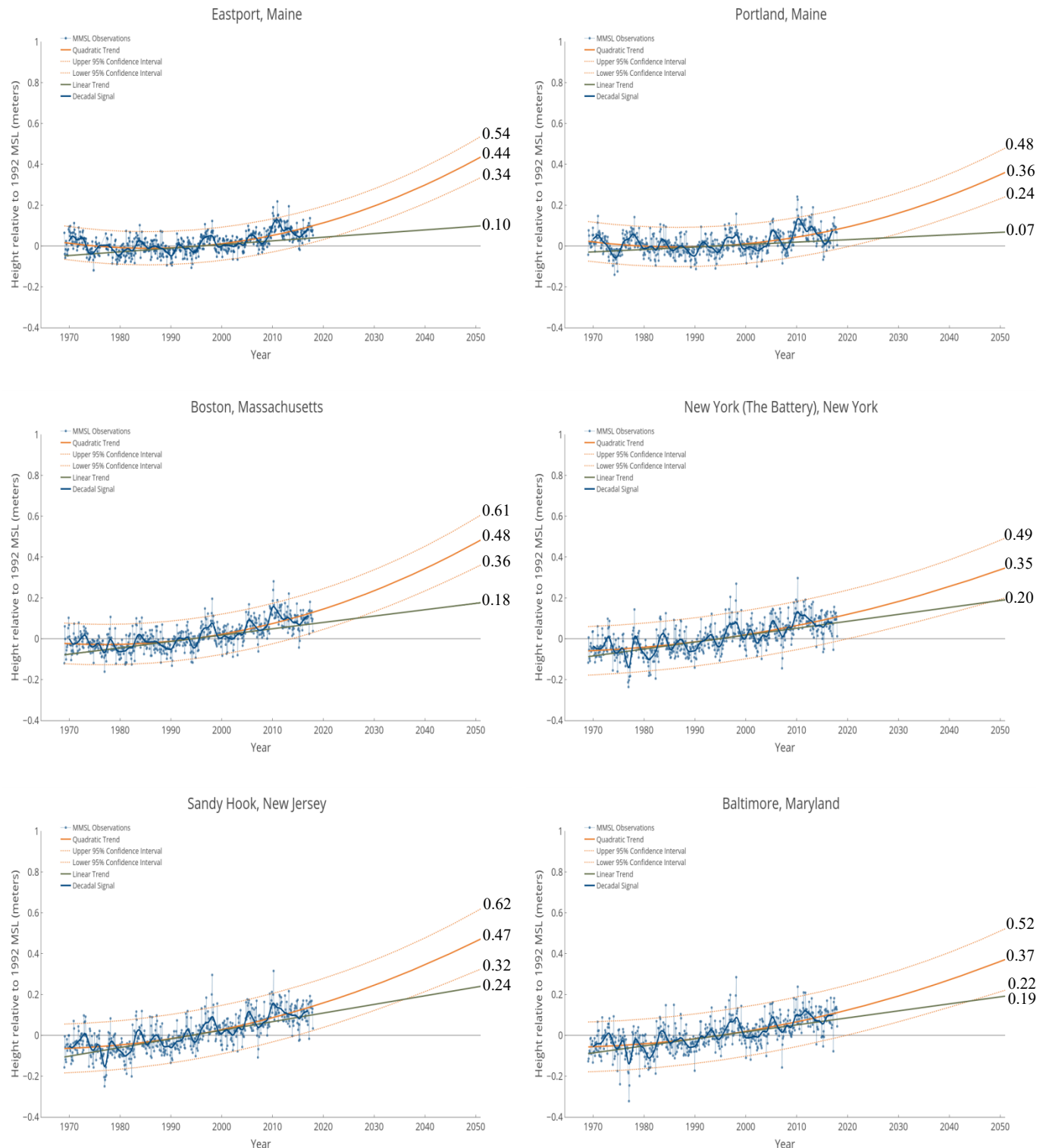
The MATLAB function *polyfit* was used here to find estimates of  $\beta_1$  and  $\beta_2$  after centering and applying a scaling transformation to the input data to improve the numerical properties of both the polynomial and the fitting algorithm. The function *polyval* further provides error estimates and predictions using the output from *polyfit*.

A confidence interval can be calculated on the acceleration estimate but it would have limited value in the present application. If high confidence in an underlying linear trend in sea level rise long-term appears misplaced, it is more so for an underlying non-linear trend whose variation over time is even more apparent. Among assumptions that apply in parametric statistics, the parent population being sampled is expected to follow a normal distribution with fixed mean and standard deviation. A normal distribution governing heights at a fixed time  $X_0$  in Eqs. B-7 and B-8 is a reasonable assumption but less so for parameters  $\beta_1$  and  $\beta_2$  where the sampled population is often not a stationary one, especially if it is subject to change driven by environmental factors. For this reason confidence intervals on estimated sea level rise rate ( $b_1$ ) and acceleration ( $2b_2$ ) are not included in this report.

In the near-term, estimates  $b_1$  and  $2b_2$  can be useful guides by themselves concerning trends in rise rate and acceleration when the temporal context for change is understood. As illustrated in the two graphs in Fig. B-2, the decadal signal begins and ends with roughly the same neutral phase, which helps to explain why the quadratic trends are similar – each projecting about a half-meter of rise by 2050 – even though the height confidence intervals for the quadratic trend projection based on the shorter series of observations quickly become unreasonable. It can be seen that even a slight addition of data beyond 1994 brings about a different ending phase for the decadal signal with implications regarding the accompanying quadratic trend projection to be expected.

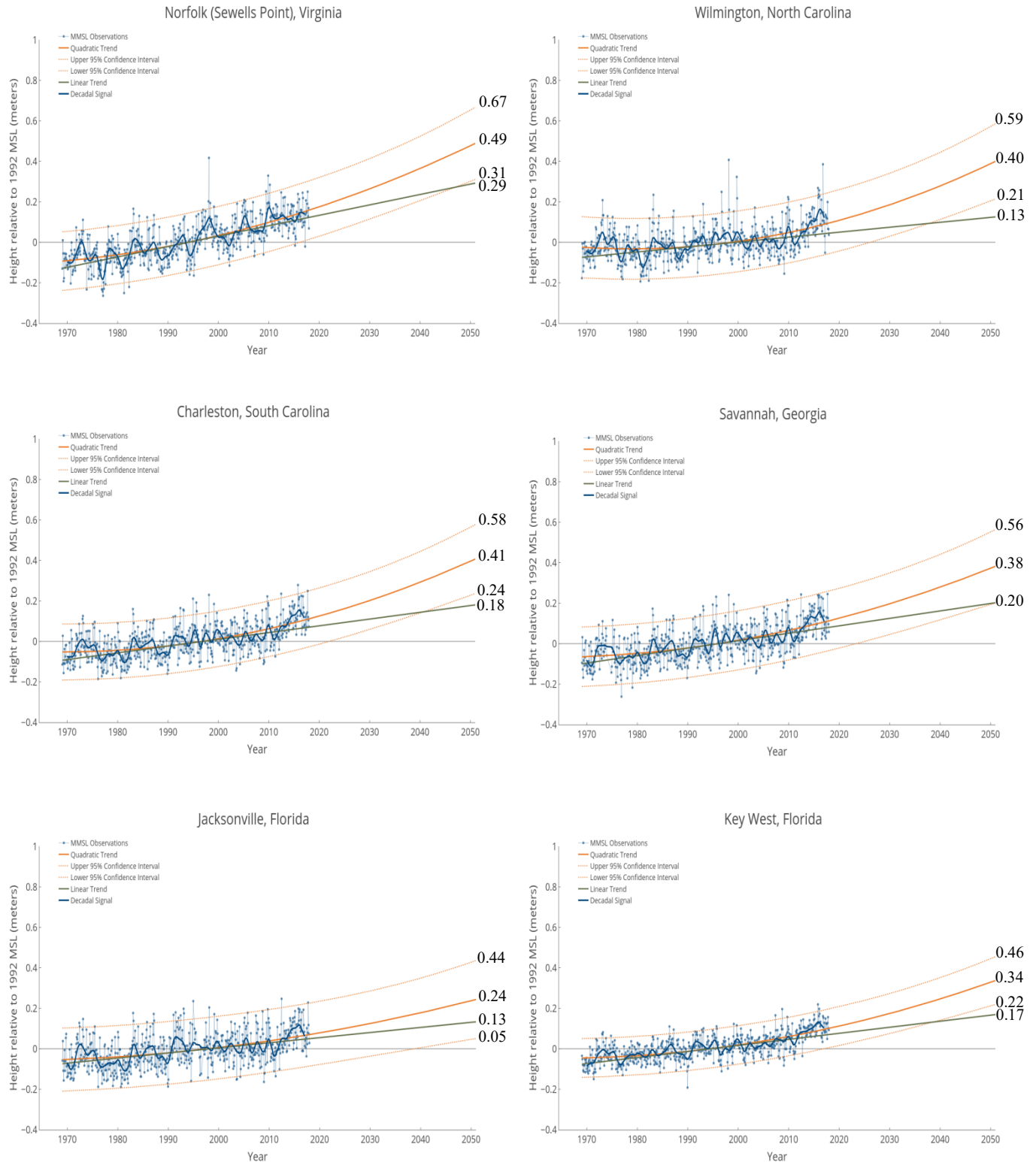
## Appendix C – Linear and Quadratic Trends with Year 2050 Projections

### U.S. EAST COAST 1969-2017



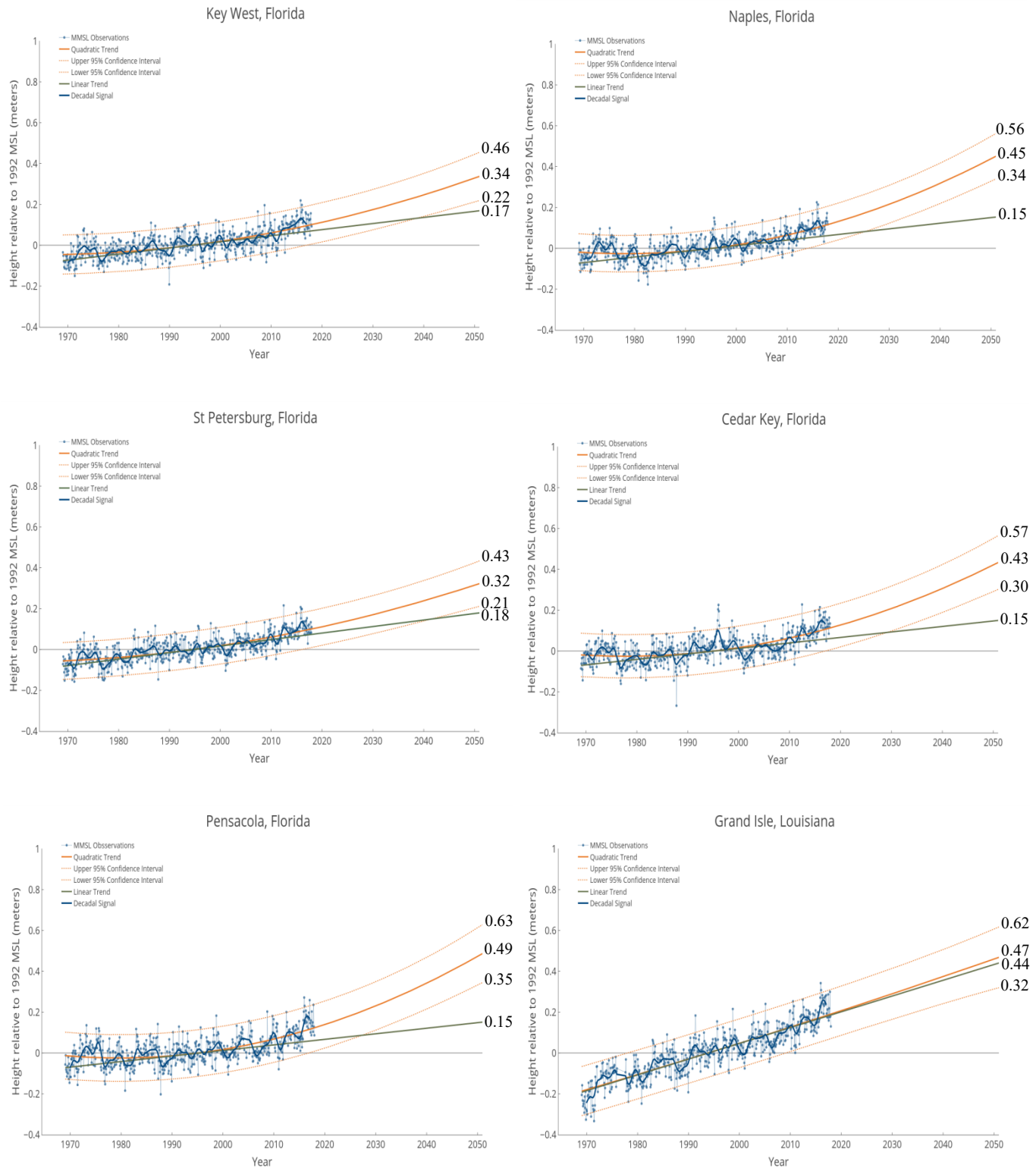
## Appendix C – Linear and Quadratic Trends with Year 2050 Projections

### U.S. EAST COAST 1969-2017



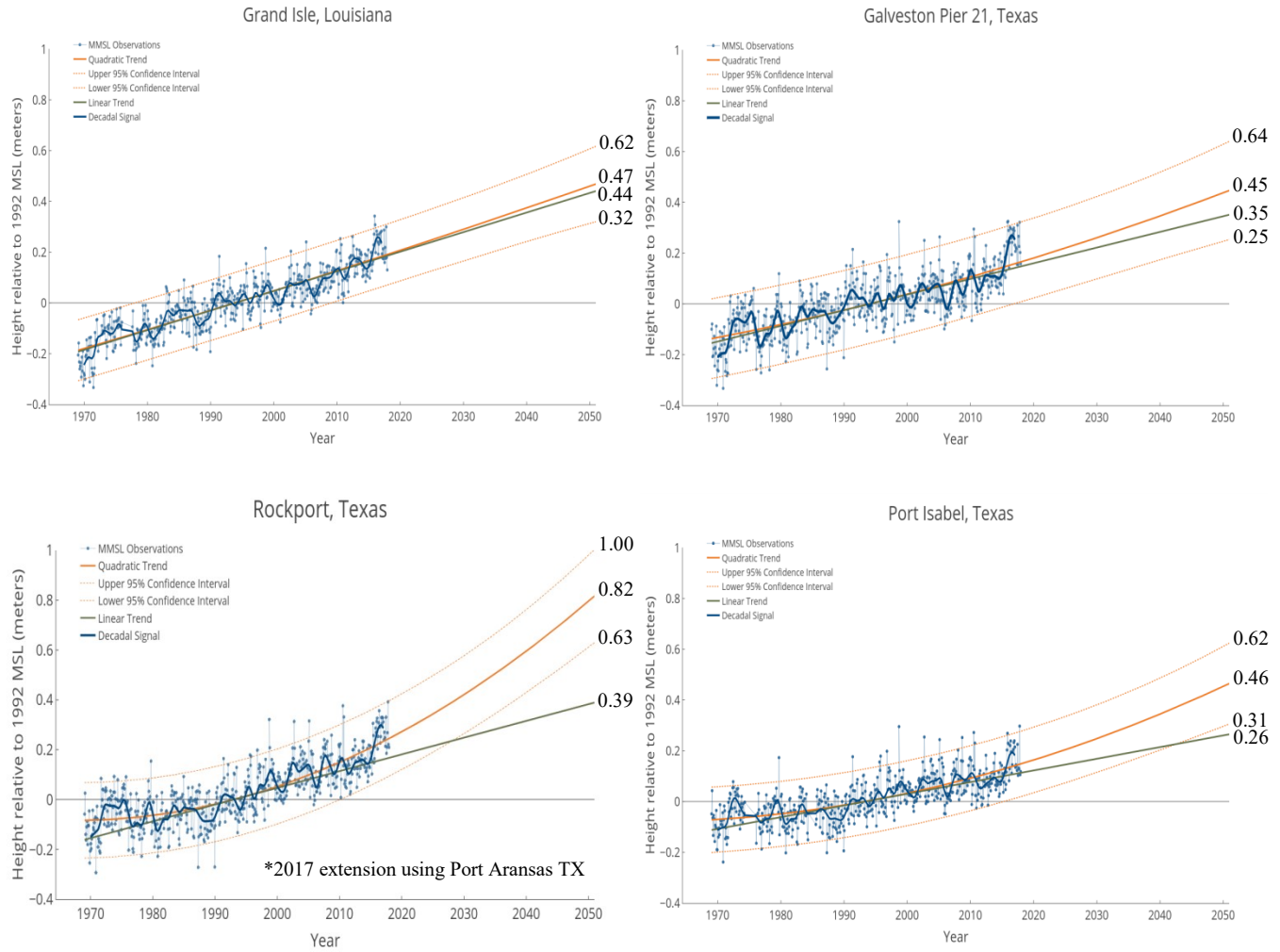
## Appendix C – Linear and Quadratic Trends with Year 2050 Projections

### U.S. GULF COAST 1969-2017



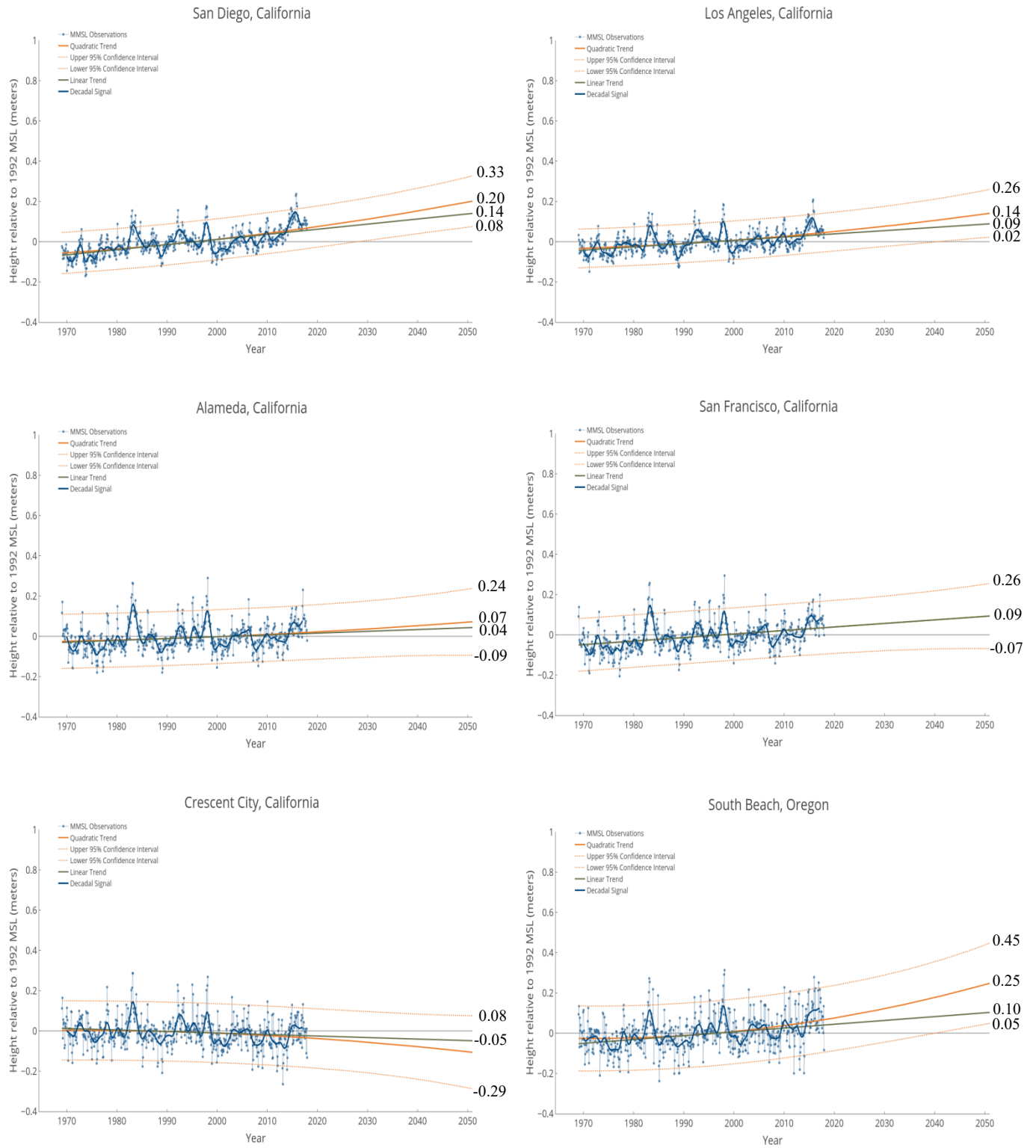
## Appendix C – Linear and Quadratic Trends with Year 2050 Projections

### U.S. GULF COAST 1969-2017



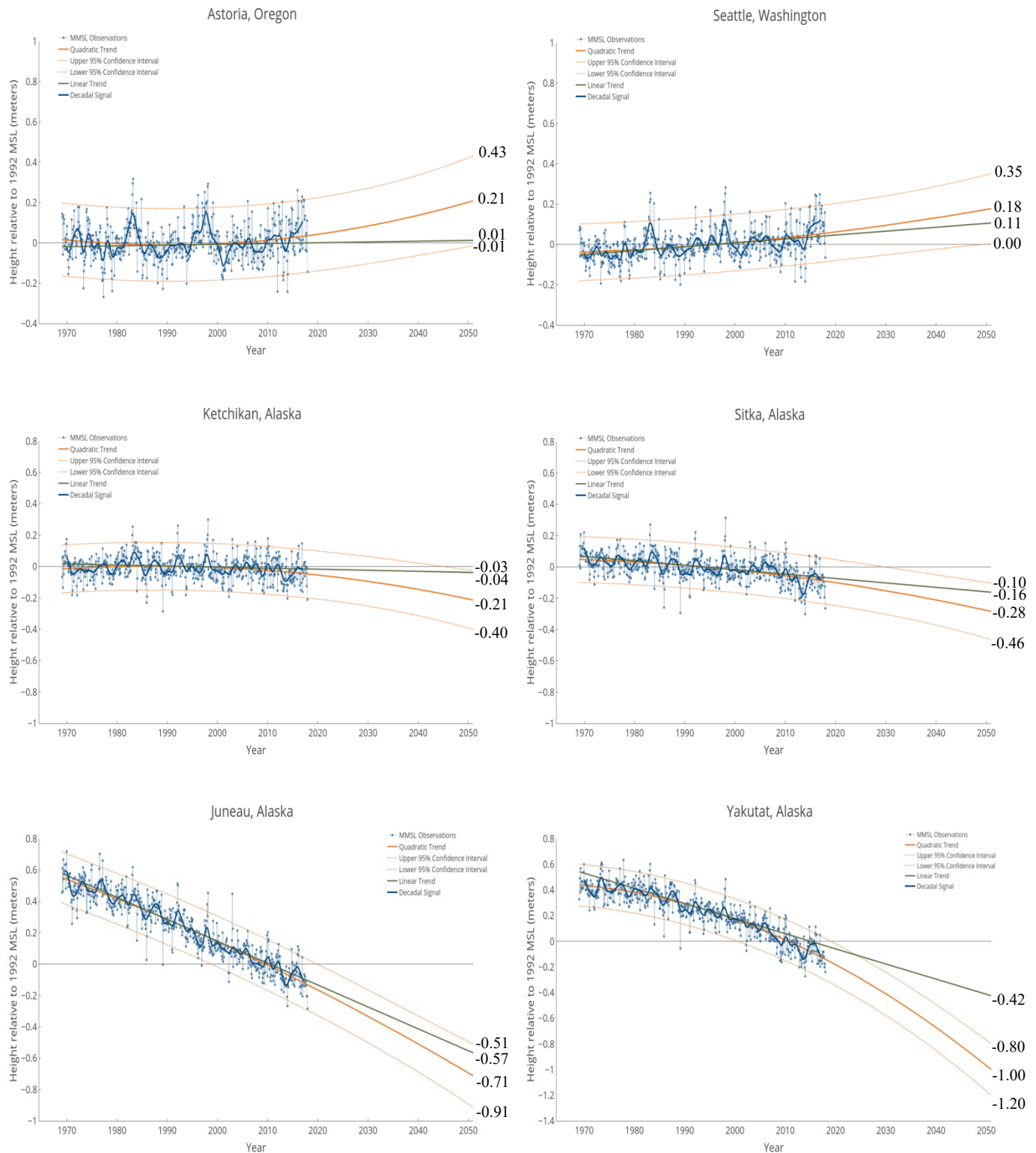
## Appendix C – Linear and Quadratic Trends with Year 2050 Projections

### U.S. WEST COAST 1969-2017



## Appendix C – Linear and Quadratic Trends with Year 2050 Projections

### U.S. WEST COAST



## APPENDIX D: Q-mode Factor Analysis

Q-mode factor analysis is one of a number of computational procedures for interpreting multivariate data using eigenvector methods. Several of these procedures are related but bear different names, including empirical orthogonal functions (EOF), principal components analysis (PCA), principal coordinates analysis, and R-mode factor analysis.

To begin, factor analysis requires a collection of observations (measurements) of a fixed number of variables  $m$ , made on a fixed number of objects  $n$ , forming an  $n \times m$  data matrix where  $n > m$ . Variables can consist of any type of repeated measurement that may, or may not, have the same units as another variable in the analysis being performed. In the present study, the variables are the fourteen RSL measurements in a sea level history where all units are either mm/year or mm/year<sup>2</sup>. The ‘objects’ are the geographic locations where the measurements were made.

Matrix Operations: Eigenvector methods, as used in most multivariate procedures, require a square-symmetric matrix – a matrix  $[X]$  having the same number of rows and columns with correspondingly identical off-diagonal elements  $x_{ij} = x_{ji}$ . Given an  $n \times m$  matrix  $[X]$ , this can be achieved by pre-multiplying it by its transpose to form a square-symmetric  $m \times m$  matrix,

$$[R] = [X]'[X] \quad (\text{D-1})$$

If  $[X]$  is first scaled so that its column elements sum to zero,  $[R]$  is a *variance-covariance* matrix; if further scaled, or *standardized*, so that elements in each column sum to zero with unit standard deviation, then  $[R]$  becomes a *correlation* matrix – one showing the correlation between variables that are all weighted equally. Using vector representation, each row of  $[R]$  in either form can be treated as a vector in  $m$ -dimensional variable space. This is the starting point for R-mode factor analysis which seeks to model the relationship between variables.

If  $[X]$  is instead post-multiplied by its transpose,

$$[Q] = [X][X]' \quad (\text{D-2})$$

where  $[Q]$  is a square-symmetric  $n \times n$  matrix. Instead of treating  $[Q]$  as a variance-covariance equivalent, a *similarity* metric known as cosine  $\theta$  is often used for the purpose of understanding the relationship between objects rather than variables. After first standardizing the objects by dividing the elements  $x_{k=1,n}$  in each row of  $[X]$  by the root sum of squares for that row, the compositional relationship between objects can be derived as

$$\text{cosine } \theta_{ij} = \frac{\sum_{k=1}^m x_{ik} x_{jk}}{\sqrt{\sum_{k=1}^m x_{ik}^2 \sum_{k=1}^m x_{jk}^2}} \quad (\text{D-3})$$

where  $\theta_{ij}$  expresses the similarity between object  $i$  and object  $j$  by recognizing each object as a vector of unit length positioned in  $m$ -dimensional coordinate space with angle  $\theta_{ij}$  between vectors. If  $\theta_{ij} = 0^\circ$  the vectors coincide (cosine  $\theta = 1$ ) indicating identical variable composition;

when  $\theta_{ij} = 90^\circ$  the vectors are orthogonal (cosine  $\theta = 0$ ) indicating completely dissimilar variable composition. Note that, although there are only  $m$  summations in Eq. D-3, the cosine  $\theta$  matrix that results is of size  $n \times n$  with  $n > m$ .

Eigenvectors and Eigenvalues: Given a data set consisting of measurements on three variables, a 3-D plot of the measurement vectors on three right-angle coordinate axes can be visualized as defining an ellipsoid with major and minor axes positioned at angles to the coordinate axes. A linear combination of weighted original variables can be found that produce new vectors coinciding with the ellipsoid axes. These are the *eigenvectors* whose lengths may be determined from their corresponding *eigenvalues*. Eigenvectors are ranked according to the amount of variance accounted for when the original measurements are projected onto their axes in variable space. Given a large number of variables, it often happens that two or three eigenvectors alone can account for a high percentage of the total variance or ‘information’ in the data set. And while there is often correlation among the original variables, there is none between the variables projected onto orthonormal, mutually-independent eigenvector axes – axes called components in PCA and *compositional end-members* in Q-mode factor analysis.

Factor analysis basically differs from PCA by assuming the existence of a fixed number of underlying factors  $p$  (where  $p < m$ ) that explain most of the data variability observed. The factor analyst must then judge from independent information, or experience, whether to specify a two-factor solution or some other number for  $p$  in advance of the analysis.

In Q-mode analysis as performed here, the elements of an eigenvector obtained from the cosine  $\theta$  matrix previously described are *factor scores* that represent the composition of that factor and its position as an object in variable space. Q-mode scores are converted into *factor loadings* by multiplying each vector element by the square root of the corresponding eigenvalue<sup>1</sup>. At this point a decision can be made to *rotate* the first  $p$  factor axes about their origin, one pair at a time, so as to maximize the loadings on each retained factor axis while ignoring  $m-p$  others. The object vectors keep the same orientation with respect to each other throughout.

A procedure called *varimax* is described in text books on statistics that accomplishes factor rotation. Computing packages such as MATLAB provide the functions that perform matrix operations and obtain eigenvectors and eigenvalues.

An Example from the U.S. Gulf Coast: Given the RSL rise rates observed at nine U.S. Gulf Coast locations, rotated factor loadings from a Q-mode analysis specifying a three-factor solution ( $p = 3$ ) are shown in Figure D-1 below. The loadings in this case illustrate a situation in which there is effectively only one factor. The object (location) vectors have a very narrow spread and, as vectors of unit length, their position on the red circle of unit radius means they have zero loadings on a third factor perpendicular to the page but have high *commonality* with factors 1 and 2. However, a further rotation about the axis origin could align the vectors equally well with either factor 1 or factor 2 due to the narrow spread. Although narrow, the loadings vectors do suggest an order among locations with least compositional similarity between Cedar Key and the Grand Isle-Galveston-Port Isabel group of locations.

---

<sup>1</sup> It can be verified that, for an  $n \times n$  symmetric matrix derived from an  $n \times m$  matrix, no more than  $m$  eigenvalues obtained from the  $n \times n$  matrix will be non-zero.

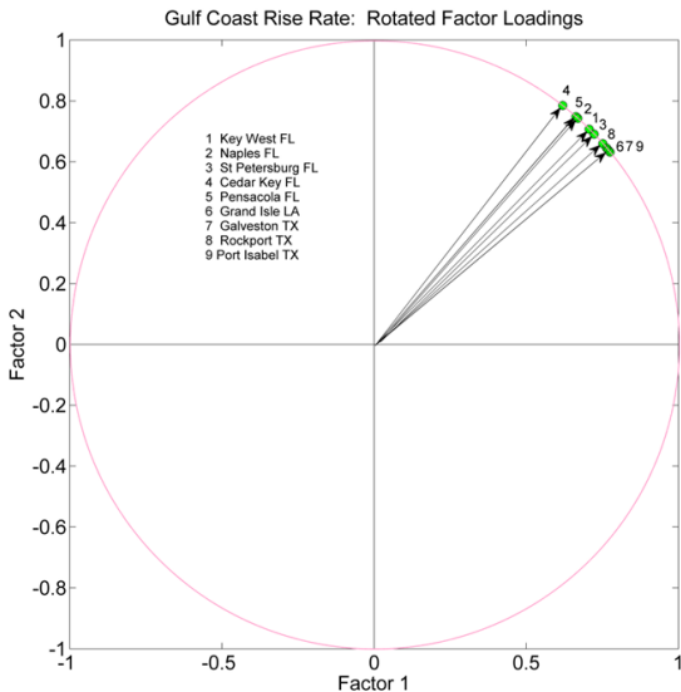


Figure D-1. Rotated loadings for factors 1-2 derived from RSL rise rate histories at U.S. Gulf Coast locations using MMSL observations from 1969 through the year 2017. A presumed third factor would be normal to the page.

**Objects as Mixtures:** In Q-mode factor analysis, the normalized object vectors can be regarded as mixtures of the  $p$  factors selected by the analyst. For example, in the position shown in Fig. D-1, object 3 (St Petersburg FL) can be seen as an almost 50:50 mixture of factors 1 and 2 based on object 3's loadings on these factors; i.e., from its vector orientation and its length equal to the root sum of squares of the loadings on each factor which are 50:50 in proportion (0.7 each, approximately). Here, both factor 1 and factor 2 are acting as hypothetical end-members that, in combination, have produced object 3. Without axis rotation, object 3 would have aligned closely with the factor 1 end-member – which would no longer be quite so hypothetical.